



universität
wien

DISSERTATION

Structural and functional studies of α -actinin

angestrebter akademischer Grad

Doktorin der Naturwissenschaften (Dr. rer.nat.)

Verfasserin:	Mag. Anita Paula Testa Salmazo
Matrikel-Nummer:	0549235
Dissertationsgebiet (lt. Studienblatt):	Molekulare Biologie
Betreuerin:	Dr. Kristina Djinović-Carugo

Wien, im 24.06.2009

Structural and functional studies of α -actinin

Dissertation

Vorgelegt am Institut für Biomolekulare Strukturchemie an der Universität Wien.

Verfasst von

Anita Paula Testa Salmazo

Betreut von

Dr. Kristina Djinović-Carugo

To my dearly loved... parents Gilberto and Regina, sisters Camila and Julia, niece
Yasmin, nephew Kauan and husband Roberto...

“Home is where we are.”

Acknowledgements

I would like to thank Kristina Djinović-Carugo for the opportunity, guidance, support, all interesting discussions and for recognizing my efforts.

The thesis examiners: Prof. Dr. Dieter Fürst, Prof. Dr. John Victor Small and Prof. Dr. Robert Konrat.

The PhD committee, for all instructive suggestions: Dr. Peggy Stolt-Bergner, Prof. Dr. Roland Foisner, Dr. Tim Clausen and Prof. Dr. John Victor Small.

Björn: for all scientific and personal help, for always thinking that everything is possible, even to have a protein crystal of human α -actinin full length. He is my hero!!!

Claudia: for the nice lab maintenance, help with the “get used to Austrian life” and German lessons.

Sofia: for the new friendship born in a good time, the help with crystallography and software, making our work environment less serious and for everything she did and still does to help me.

Eirini and Murad: the students that help me a lot with crystal hit optimizations. Their participation in this work made a big difference, no doubt.

The “diploma gang” for all time spent together and all help from German classes to science: Kerstin, Bettina, Maria, Ajda, Christian and Georg.

My PhD and post-doc colleagues: Bashir, Julius, Mads and Patrizia.

The NMR group: Prof. Georg Kontaxis, Karin L., Reby, Nico, Christoph, Martin, Martina, Conny, Sven, Leo, Gerald, and, in special, Bettina, Karin K. and Renate for the help with NMR data.

Werner König: the help with hardware.

Ursula Talhammer: the help with paperwork.

Larissa: my first steps in Europe were done under her assistance. I thank her for the accommodation, her kindly attention, the aid with the languages, the nice dinners with Hannes and Julian and off course, all help with and discussions about crystallography.

Inari and Petri Kursula: for being always there.

Brazilian friends in Vienna: Alisson, Catarina, Daniela, Fabio, Julia and Mariana. Being in the same situation, far away from home, the friendship becomes strong very fast and our hearts more solicitous.

Brazilian friends in Brazil: Alessandra, Leandro, Luciana, Silvia and Tarcila. The distance does not matter for real friendship.

My whole family: for all encouragement they give to keep me (here) going on and with their love, healing the homesickness periods.

A special acknowledgement to Roberto, my husband: the best companion, the best friend, my best smile, the best thing that happened to my life.

ABSTRACT

α -Actinin belongs to the spectrin superfamily of proteins involved in cytoskeletal network, bundling or cross-linking actin filaments. Human α -actinin isoforms are composed of an N-terminal actin-binding domain (ABD, formed by two calponin like domains), a central rod domain formed by four spectrin-like repeats (SR1, SR2, SR3 and SR4) and a C-terminal calmodulin-like domain (CaM, formed by four EF-hands). Its functional unit is an antiparallel homodimer leading to a molecular architecture that allows the protein to cross-link actin filaments. Four different α -actinin isoforms are present in human cells: isoforms 1 and 4 are calcium sensitive and found in non-muscle cells, while isoforms 2 and 3 are calcium insensitive and found in muscle cells.

The muscle isoforms are regulated by the phosphoinositide PiP2 that upon binding to α -actinin ABD triggers conformational changes and enhances α -actinin binding capacity to actin filaments and other muscle proteins. Molecular details on interaction between PiP2 and α -actinin and concomitant conformational changes are not clear, but it was proposed that while the PiP2 head interacts with the N-terminal (ABD), the PiP2 hydrophobic tail disturbs the interaction between juxtaposed N-terminal and C-terminal regions in the α -actinin antiparallel dimer, in particular the CaM domain and the neck region, which connects the ABD to the rod domain.

A number of efforts based on binding assays and structural studies have been carried out in order to elucidate α -actinin regulation at molecular level with the aim to better understand myofibrillogenesis and enhance insights into a number of diseases.

In this thesis, we have performed interaction studies between PDZ domain of ZASP and α -actinin dimer with the aim to understand whether the hydrophobic tail of phosphoinositides is able to modulate this interaction. However, under the conditions used no interaction between PDZ domain of ZASP and α -actinin dimer was observed.

In order to further characterize the interaction between α -actinin and PiP2, we have designed single-site mutants of residues implicated in binding to PiP2 polar head and analysed them together with the wild type (WT), with a range of biochemical and biophysical experiments including PiP stripes, circular dichroism (CD), differential scanning fluorimetry (DSF), nuclear magnetic resonance spectroscopy (NMR), isothermal titration calorimetry (ITC) and X-ray diffraction. The mutants were designed based on the PiP2 binding site proposed after analysis on the

structure of ABD of α -actinin isoform 3. Apart from experiments with PiP strips, the biochemical and biophysical experiments were carried out with ABD of α -actinin isoform 2 and the inositols triphosphate (IP3) and hexakisphosphate (IP6), which are phosphoinositides head with three and six phosphate groups respectively.

These studies one hand showed that the ABD does not undergo any structural rearrangement upon binding to IP3 or IP6 and on the other, suggested that arginine residue at position 192 could be an important player in the ABD:PiP2 interaction, which is characterized by a binding constant in the milli molar range. Structural studies of human ABD α -actinin isoform 2 did not show IP3 bound to the domain, probably because of weak binding affinity and revealed ABD in the close conformation, similar to that found in crystal structures of ABD isoforms 3 and 4.

In order to understand α -actinin molecular architecture and its structural mechanisms underlying its regulation, we carried out structural studies by single crystal diffraction and small angle X-ray scattering (SAXS) on full length α -actinin isoforms 1 and 2, α -actinin half dimers (ABD-SR1-SR2//SR3-SR4-CaM), as well as on *Entamoeba histolytica* α -actinin isoform 2, which has only two spectrin-like repeats. Since no crystal hits were initially obtained after extensive crystallization screens, the human full length muscle isoform 2 was mutated aiming to decrease the surface entropy of the protein. Additionally, WT and surface entropy mutant were submitted to protein reductive methylation. These approaches enhanced the propensity of the human α -actinin full length isoform 2 to crystallize, yielding crystals diffracting to a resolution of 4.5 Å.

Molecular architecture of α -actinin full length, half dimer constructs and *E. histolytica* α -actinin was characterized by SAXS. The analysis of the molecular envelope showed the expected protein shape and dimensions when compared with the determined structures of the individual domains (ABD, central rod domain and CaM), with CaM in close proximity of ABD domain in closed conformation.

ZUSAMMENFASSUNG

α -Aktinin gehört zur Superfamilie der Spektrinproteine, die am zytoskeletalen Netzwerk und an der Bündelung beziehungsweise Quervernetzung von Aktinfilamenten beteiligt sind. Humane α -Aktinin Isoformen setzen sich aus einer N-terminalen Aktin-Bindungsdomäne (ABD, bestehend aus zwei Calponin-artigen Domänen), einer zentralen Stab Domäne bestehend aus vier Spektrin-artigen Wiederholungen (SR1, SR2, SR3 und SR4) und einer C-terminalen Calmodulin-artigen Domäne (CaM, bestehend aus vier EF-hands) zusammen. Die funktionelle Einheit ist ein antiparalleles Homodimer, dessen molekularer Aufbau dem Protein das Quervernetzen von Aktinfilamenten ermöglicht. In menschlichen Zellen existieren vier α -Aktinin Isoformen: Isoform 1 und 4 sind Calcium-sensitiv und kommen in nicht-Muskelzellen vor, während die Isoformen 2 und 3 unempfindlich gegenüber Calcium sind und in Muskelzellen vorkommen.

Die Isoformen der Muskeln werden durch das Phosphoinositid PIP2 reguliert, das durch die Bindung an α -Aktinin eine Konformationsänderung bewirkt und die Bindungskapazitäten von α -Aktinin an andere Muskelproteine erhöht. Die molekularen Details der Interaktion zwischen PIP2 und α -Aktinin und der gleichzeitigen Konformationsänderung sind nicht geklärt, jedoch wird angenommen, dass, während der PIP2 Kopf mit dem N-Terminus interagiert (ABD), der hydrophobe Schwanz von PIP2 die Interaktion zwischen dem benachbarten N-Terminus und C-Terminus des antiparallelen α -Aktinin Dimers stört, speziell zwischen der CaM Domäne und der Neck Region, die die ABD mit der Stab Domäne verbindet.

Unter vielen Bemühungen wurde versucht, die Regulation dieses Prozesses zu verstehen, wodurch die Myofibrillogenese besser verstanden und erhöhte Einsicht in eine Reihe von Krankheiten erzielt werden könnte. Um der Frage bezüglich der α -Aktinin Regulation nachzugehen, wurden mehrere Bindungs- und Strukturstudien durchgeführt.

In dieser Dissertation wurden Interaktionsanalysen zwischen der PDZ Domäne von ZASP und dem α -Aktinin Dimer durchgeführt, um aufzuklären, ob der hydrophobe Schwanz des Phosphoinositids die Bindung verstärken kann. Unter den verwendeten Bedingungen wurde keine Interaktion beobachtet.

Zur weiteren Charakterisierung der Interaktion zwischen α -Aktinin und PIP2 wurden Konstrukte mit jeweils einer Punktmutation in den Aminosäurereste erstellt, die bei der Bindung an die polaren Köpfe von PIP2 eine Rolle spielen. Diese wurden

gemeinsam mit dem Wildtyp anhand einer Reihe biochemischer und biophysikalischer Experimente, einschließlich PIP Strips, zircularem Dichroismus (CD), Differenzialfluoreszenzanalyse (DSF), Kernspinresonanzspektroskopie (NMR), isotherme Titration (ITC) und Röntgenstreuung analysiert. Die Mutanten basierten auf den PIP2 Bindungsstellen, die nach der Analyse der Struktur von ABD Isoform 3 angenommen wurden. Abgesehen von den Experimenten mit den PIP Strips wurden die biochemischen und biophysikalischen Experimente mit ABD von α -Aktinin Isoform 2 und Inositoltriphosphat (IP3) und Hexakisphosphat (IP6) durchgeführt, wobei es sich um Phosphoinositid Köpfe mit drei beziehungsweise sechs Phosphatgruppen handelt.

In Strukturanalysen von humanem α -Aktinin Isoform 2 ABD war IP3 nicht an die Domäne gebunden, wahrscheinlich auf Grund geringer Bindungsaffinität, und zeigten ABD in geschlossener Konformation, entsprechend den Kristallstrukturen von ABD Isoformen 3 und 4.

Um den molekulare Aufbau von α -Aktinin und den strukturellen Mechanismus, der seiner Regulation zu Grunde liegt zu verstehen, wurden Strukturanalysen von Einzelkristallen und Kleinwinkelstreuung (SAXS) an vollständigem α -Aktinin Isoform 1 und 2, dem halben Dimer (ABD-SR1-SR2//SR3-SR4-CaM), als auch an *Entamoeba histolytica* α -Aktinin Isoform 2, das nur zwei Spektrin-artige Wiederholungen hat, durchgeführt. Alle Konstrukte wurden umfassenden Kristallisations-Screens unterzogen. Da anfangs keine Kristallisationstreffer erzielt werden konnten, wurde die vollständige menschliche Muskelisoform 2 mutiert, um die Oberflächenentropie des Proteins zu verringern. Zusätzlich wurden Wildtyp und Oberflächenentropie-Mutanten reduktiver Methylierung unterzogen. Diese Ansätze erhöhten die Wahrscheinlichkeit von humanem α -Aktinin Isoform 2 zu kristallisieren, und hatten Kristalle zum Resultat, die bei einer Auflösung von 4.5 Å streuten.

Der molekulare Aufbau des vollständiges α -Aktinin, der Konstrukte des halben Dimers und *E. histolytica* α -Aktinin, wurden durch SAXS charakterisiert. Die Analyse der molekularen Hülle zeigte die erwartete Proteinform und Größe, nachdem sie mit den aufgeklärten Strukturen der einzelnen Domänen (ABD, zentrale Stab Domäne und CaM) verglichen wurden, mit CaM in enger räumlicher Nähe zu ABD, das in geschlossener Konformation vorlag.

LIST OF ABBREVIATIONS

2Eh	full length <i>Entamoeba histolytica</i> α -actinin isoform 2
2AFL	full length human α -actinin isoform 2
2AFLY	truncated version of full length
6x His-tag	hexahistidine affinity purification tag
ABD	actin-binding domain
AFL	α -actinin full length
CaM	calmodulin-like domain
CD	circular dichroism
CH	calponin homology domain
DLS	dynamic light scattering
DsbA	disulfide oxidoreductase A affinity purification tag
DSF	differential scanning fluorimetry
ΔG	Gibbs energy
ΔH	enthalpy
ΔS	entropy
EDTA	ethylenediaminetetraacetic acid
EF-3/4	the last two EF - hands of CaM
EM	electronic microscopy
GST	glutathione S-transferase affinity purification tag
hd	half dimer (ABD_SR1_SR2//SR3_SR4_CaM)
HEPES	4-(2-hydroxyethyl)-1-piperazineethanesulfonic acid
IMAC	immobilized metal affinity chromatography
IP3	inositol triphosphate
IP6	inositol hexakisphosphate
IPTG	isopropyl β -D-1-thiogalactopyranoside
ITC	isothermal titration calorimetry
K_a	affinity constant
K_d	dissociation constant
KDa	kilodalton
LB	Luria Bertani bacterial broth
LPA	lysophosphatidic acid
mAU	milli absorbance unit

Met-K	protein sample after reductive methylation
MW	molecular weight
NMR	nuclear magnetic resonance
Nonidet	nonylphenylethylenglycol
OD	optical density
pb	pair base
PCR	polymerase chain reaction
PDB	protein data bank
PDZ	acronym combining the first letters of three proteins, which were first discovered to share the domain (Post synaptic density protein, Drosophila disc large tumour suppressor and Zonula occludens-1 protein)
PEG	polyethylene glycol
PH	pleckstrin homology domain
PiP2	phosphatidylinositol (4, 5)-biphosphate
PiP3	phosphatidylinositol (3, 4, 5)-triphosphate
PIPES	piperazine-N,N'-bis(2-ethanesulfonic acid)
RFU	relative fluorescence unit
r.m.s.d.	Root mean square deviation
rpm	rounds per minute
SAXS	small angle X-ray scattering
SDS - PAGE	sodium dodecyl sulfate polyacrylamide gel electrophoresis
SEC	size exclusion chromatography
SER	surface entropy reduction
SR	spectrin-like repeats (SR1; SR2; SR3; SR4)
TES	N-Tris(hydroxymethyl)methyl-2-aminoethanesulfonic acid
TEV	tobacco etch virus protease
T _m	melting temperature
Tris	tris(hydroxymethyl)aminomethane
TrxA	thioredoxin A affinity purification tag
UV	ultraviolet light
v/v	volume/volume
ZASP	Z-band alternatively spliced PDZ-motif proteins
WT	wild type

Table of contents

ABSTRACT	xi
ZUSAMMENFASSUNG.....	xiii
LIST OF ABBREVIATIONS	xv
Table of contents	xvii
List of figures	xx
List of tables	xxii
1. INTRODUCTION	1
1.1 α -actinin	1
1.1.1 Cytoskeleton.....	2
1.1.2 Striated muscle.....	2
1.2 α -actinin molecular architecture	5
1.2.1 Actin-binding domain (ABD)	5
1.2.2 Central rod domain (SR).....	8
1.2.3 Calmodulin-like domain (CaM)	10
1.3 α -actinin regulation.....	12
1.4 α -actinin interactions	15
1.4.1 ZASP	16
2. AIM OF THE THESIS	18
3. MATERIALS AND METHODS.....	20
3.1 Constructs and nomenclature	20
3.2 DNA manipulation	20
3.2.1 DNA amplification (PCR) and colony PCR	20
3.2.1.1 α -actinin	21
3.2.1.2 PDZ domain of ZASP.....	21
3.2.2 DNA agarose gel electrophoresis.....	21
3.2.3 Restriction endonuclease reactions.....	21
3.2.4 DNA purification.....	21
3.2.6 Competent cells transformation.....	24
3.2.6.1 Co-transformation experiments.....	25
3.2.7 Selection of positive clones using antibiotics.....	25
3.2.8 Plasmid extraction in mini scale (miniprep)	25
3.2.9 DNA sequencing.....	25
3.3 Protein manipulation	26
3.3.1 Over-expression of recombinant proteins.....	26
3.3.1.1 Small scale overexpression	27
3.3.2 Purification of recombinant proteins	27

3.3.2.1	Purification of human α -actinin half dimer (hd).....	28
3.3.2.2	Co-purification experiments	28
3.3.2.3	Analytical size exclusion chromatography.....	28
3.3.3	Tag cleavage by Tobacco etch virus (TEV) protease	28
3.3.4	Protein dialysis	29
3.3.5	SDS-polyacrylamide gel electrophoresis (SDS-PAGE)	29
3.3.6	Protein concentration.....	29
3.3.7	Protein concentration determination	29
3.3.10	Differential scanning fluorimetry (DSF)	30
3.3.10.1	Binding of inositol hexakisphosphate (IP6) to ABD	30
3.3.11	Dynamic light scattering (DLS)	30
3.3.12	Protein reductive methylation	31
3.3.13	Surface entropy reduction (SER) mutations	31
3.3.14	Characterization of ABD mutants	32
3.3.14.1	Mutants	32
3.3.14.2	PiP strips.....	32
3.3.14.3	Isothermal titration calorimetry (ITC).....	33
3.3.14.4	Circular dichroism (CD).....	33
3.3.14.5	Nuclear magnetic resonance spectroscopy (NMR).....	33
3.3.15	Protein crystallization experiments	34
3.3.15.1	ABDY soaking and co-crystallization	35
3.3.16	Data collection.....	35
3.3.17	Structural determination, model building, refinement and validation.....	35
3.3.18	Small angle x-ray scattering (SAXS)	36
4.	RESULTS	37
4.1	Constructs, gene amplification and selection	37
4.1.1	α -actinin.....	37
4.1.2	PDZ domain of ZASP	39
4.2	Over-expression of recombinant proteins	39
4.2.1	Expression of AFL, 2Eh, hd, ABD and PDZ domain of ZASP	39
4.2.2	Co-expression systems for α -actinin.....	39
4.3	Differential scanning fluorimetry (DSF)	42
4.4	Purification of recombinant proteins.....	43
4.4.1	Purification of AFL, 2Eh, hd and ABD.....	43
4.4.2	Purification of a co-expression system: 2ABDa_SR1 + 2SR4_CaM	49
4.4.3	Co-purification experiments.....	50
4.4.3.1	α -actinin	50

4.4.3.2 hd + PDZ domain of ZASP	51
4.5 Dynamic light scattering (DLS).....	53
4.6 Crystallization trials and protein reductive methylation.....	53
4.7 Crystallization trials and protein surface entropy reduction (SER)	55
4.7.1 Cleavage of the flexible N-terminal of Δ 2AFL E310A/K311A (Δ 2AFLY)...	57
4.7.2 6x His - tag cleavage	58
4.8 Preliminary data collection of AFL E310A/K311A	59
4.9 Actin binding domain (ABD): WT versus mutant	60
4.9.1 Differential scanning fluorimetry (DSF).....	62
4.9.2 Circular dichroism (CD)	62
4.9.3 Nuclear magnetic resonance spectroscopy (NMR)	63
4.9.4 Isothermal titration calorimetry data (ITC)	64
4.9.5 Protein crystallization: ABDa versus ABDY	65
4.9.6 Data collection, processing and structure determination	66
4.10 Small angle X-ray scattering (SAXS): 2Eh, AFL and hd.....	69
5. DISCUSSION AND PERSPECTIVES	72
5.1 Cloning of α -actinin domains.....	72
5.2 Actin binding domain (2ABD)	73
5.3 Full length α -actinin.....	78
5.3.1 Entamoeba histolytica α -actinin (2Eh)	78
5.3.2 Human α -actinin isoform (2AFL).....	79
5.4 Protein-protein complex: α -actinin half dimer (hd) and PDZ domain of ZASP.	81
5.5 Other constructs.....	82
5.5.1 α -actinin domains complex.....	82
5.5.1.1 Co-expression.....	82
5.5.1.2 Co-purification.....	83
5.5.2 α -Actinin half dimer (hd)	84
5.5.3 Crystallization of other α -actinin constructs	84
5.6 Small angle X-ray scattering (SAXS): 2Eh, AFL and hd.....	84
6. CONCLUSIONS	86
6.1 Actin binding domain (2ABD)	86
6.2 Full length α -actinin.....	86
6.3 Protein-protein complex: α -actinin half dimer (hd) and PDZ domain of ZASP.	87
6.4 Final remark	87
7. REFERENCES	88
CURRICULUM VITAE	100

List of figures

Figure 1.1 Schematic view of the cytoskeleton in focal contacts	3
Figure 1.2 Schematic view of striated muscle.....	4
Figure 1.3 Schematic representation of human α -actinin antiparallel homodimer.....	5
Figure 1.4 Domain organization of human α -actinin ABD isoform 3	6
Figure 1.5 Actinin-binding sites (ABS) of α -actinin ABD	8
Figure 1.6 Rod domain structure	9
Figure 1.7 Structure of α -actinin EF-3/4.....	11
Figure 1.8 Schematic representation of the α -actinin regulation model	13
Figure 1.9 PiP2 proposed binding site within ABD of α -actinin isoform 3	14
Figure 1.10 Structure of PDZ domain of ZASP	17
Figure 3.1 Representation of the human α -actinin isoform 2 and <i>E. histolytica</i> α -actinin isoform 2	22
Figure 3.2 Different amino groups	31
Figure 4.1 PCR products of human α -actinin.....	37
Figure 4.2 PCR product of the PDZ domain	39
Figure 4.3 15% SDS-PAGE of small scale co-expression experiments of human α -actinin.....	40
Figure 4.4 Melting curves of DSF	42
Figure 4.5 Melting curves of DSF	43
Figure 4.6 Protein purification of 1AFL	44
Figure 4.7 Protein purification of 2AFL	45
Figure 4.8 Protein purification of 2Eh.....	46
Figure 4.9 Protein purification of hd.....	47
Figure 4.10 Protein purification of 2ABD.....	48
Figure 4.11 Purification of the 2ABDa_SR1 + 2SR4_CaM complex.....	49
Figure 4.12 15% SDS-PAGE of fractions obtained from the co-purification.....	50
Figure 4.13 Formation of 2hd (his-tagged) and PDZ (GST-tagged) complex	51
Figure 4.14 Analytical SEC of 2hd + PDZ.....	52
Figure 4.15 Crystal hits of 6x His - 2Eh Met-K.....	54
Figure 4.16 Crystal hits and further optimization hits of 6x His - 2AFL Met-K.....	55
Figure 4.17 Initial crystalline hits of the double-site mutant 6x His - Δ 2AFL E310A/K311A	56
Figure 4.18 Crystal hits of 6x His - Δ 2AFL Met-K	56

Figure 4.19 Crystal hits of 6x His - Δ 2AFLY Met-K	57
Figure 4.20 Crystal hits of Δ 2AFLY Met-K	58
Figure 4.21 Diffraction patterns of Δ 2AFL and Δ 2AFLY E310A/K311A Met-K.....	60
Figure 4.22 PiP strips binding assays for 2ABDa WT and the mutants	61
Figure 4.23 Stability of 2ABDa WT versus IP6 concentration.....	62
Figure 4.24 Near-UV CD spectra of 2ABDa WT and IP6.....	62
Figure 4.25 Part of the superposition HSQC spectra	63
Figure 4.26 ITC data acquired at 25 °C by titrating IP3 to 2ABDa WT and mutants .	64
Figure 4.27 Crystal hits of 2ABDY used for soaking in IP3 or IP6	65
Figure 4.28 Crystals of 2ABDY + IP3.....	66
Figure 4.29 Diffraction pattern of 2ABDY.....	67
Figure 4.30 Overall structure of 2ABDY refined at 1.8 Å.....	68
Figure 4.31 SAXS experimental X-ray scattering pattern	69
Figure 4.32 SAXS rigid body models	71
Figure 5.1 Schematic view of Bsal (green) and NcoI (red) compatible ends for cloning of human α -actinin inserts	72
Figure 5.2 Putative PiP2 binding residues of 2ABD	73
Figure 5.3 Alignment of the four human α -actinin isoforms.....	76
Figure 5.4 N-terminal secondary structure prediction of 2ABD	76
Figure 5.5 Structure superposition of human α -actinin ABD isoforms.....	78

List of tables

Table 3.1 Oligonucleotides and T _m (°C).....	23
Table 3.2 Expression plasmids and fused tags	24
Table 3.3 <i>E. coli</i> strains	25
Table 3.4 Antibiotics	26
Table 4.1 α -Actinin constructs designed for this project	38
Table 4.2 Co-transformation constructs and <i>E. coli</i> strains for over-expression experiments.....	41
Table 4.3 Optimal stable buffers resulted from DSF.....	43
Table 4.4 Protein yield per litre of culture	48
Table 4.5 DLS.....	53
Table 4.6 Merged scaling statistic of 6x His – Δ 2AFLY Met-K data sets	59
Table 4.7 Data collection and processing statistics of Δ 2AFLY Met-K	59
Table 4.8 Isothermal titration analysis of 2ABDa WT and mutants.....	64
Table 4.9 Data collection processing of 2ABDY	67
Table 4.10 SAXS χ -values for fitting of ab initio models to experimental data.....	70
Table 4.11 SAXS χ -values for fitting of rigid body modelling to experimental data rigid body modelling χ -values.	70

1. INTRODUCTION

1.1 α -actinin

α -Actinin is a ubiquitously conserved protein that cross-links actin filaments. It belongs to the spectrin superfamily of proteins, an important group of actin-binding proteins, which also encloses spectrin, utrophin and dystrophin. These proteins are involved in functions that requires cross-linking, bundling or binding to actin filaments. Phylogenetic analysis shows that this large functional variety within the family arose through alternative splicing and gene duplication of a common ancestral α -actinin gene (Baines, 2003; Broderick and Winder, 2005; Thomas et al., 1997; Viel, 1999; Virel and Backman, 2004, 2007).

Proteins from spectrin family are involved in several diseases, *e.g.* familial focal segmental glomerulosclerosis (FSGS), Duchenne muscular dystrophy (DMD) and hereditary spherocytosis [HS; reviewed by (Broderick and Winder, 2005; Kaplan et al., 2000)]; hepatitis C (Lan et al., 2003), among others.

α -Actinin isoforms have been characterized genetically and/or biochemically from a large variety of taxa, from protists to mammals (Arimura et al., 1988; Barstead et al., 1991; Beggs et al., 1992; Fyrberg et al., 1990; Honda et al., 1998; Noegel et al., 1987). Regarding expression patterns, biochemical characteristics, tissue and sub-cellular location, α -actinin proteins can be grouped into two different classes: non-muscle cytoskeletal isoforms (section 1.1.1) and muscle isoforms (section 1.1.2). The first ones are calcium sensitive while the latter are calcium insensitive (Blanchard et al., 1989; BurrIDGE and Feramisco, 1981; Otto, 1994).

Apart from its mechanical role involved in cell shape and locomotion by conferring both stability and plasticity to actin-based arrays (Xu et al., 1998), α -actinin plays several important roles in the cell, such as linking the cytoskeleton to different transmembrane proteins in a variety of junctions, regulating the activity of a number of receptors and being a scaffold to connect the cytoskeleton to diverse signalling pathways (Blanchard et al., 1989; MacArthur and North, 2004; Otey and Carpen, 2004; Virel and Backman, 2004).

1.1.1 Cytoskeleton

The cytoskeleton is a dynamic structure present in the cytoplasm of prokaryotic [reviewed by (Michie and Lowe, 2006; Shih and Rothfield, 2006)] and eukaryotic [reviewed by (Frixione, 2000)] cells, composed of highly organized filamentous systems. It plays important roles in living cells, being involved in establishing cell shape, locomotion, intracellular transport and cell division. Its structure is built up by three main types of protein filaments: actin filaments (microfilaments), intermediate filaments and microtubules. These filaments can be assembled in bundles or networks by several actin-binding proteins depending on their size and flexibility [reviewed by (Sjoblom et al., 2008a)].

One important actin-binding protein is α -actinin, the central focus of this thesis, which bundles actin filaments (Zamir and Geiger, 2001).

In cytoskeleton two α -actinin isoforms are found, the non-muscle isoforms 1 and 4, which are commonly associated with focal contacts (Figure 1.1) and stress fibers (Edlund et al., 2001; Otey and Carpen, 2004; Pavalko and Burridge, 1991). In migrating cells, their distribution differs since the α -actinin isoform 1 is more abundant in actin stress fibers, while the isoform 4 is more abundant in circular dorsal ruffles (Araki et al., 2000; Honda et al., 1998; Nikolopoulos et al., 2000).

1.1.2 Striated muscle

Muscle is the contractile tissue of vertebrates' body and can be found in two major types: smooth (visceral) and striated (cardiac and skeletal). The striated muscles are formed of fibres (Figure 1.2A), which in turn are built by myofibrils (Figure 1.2B), which themselves are formed of repeating units called sarcomeres [Figure 1.2C; reviewed by (Squire et al., 2005)].

The sarcomere is the contractile unit of the muscle composed of three filamentous systems: thin filaments (actin), thick filaments (myosin) and titin/nebulin filaments. Titin is a giant multidomain protein that spans half sarcomeres (Granzier and Labeit, 2007; Granzier and Labeit, 2005; Maruyama, 1997) and acts as a molecular ruler organizing the actin filaments by interacting with several sarcomeric proteins, including α -actinin (Trinick, 1996).

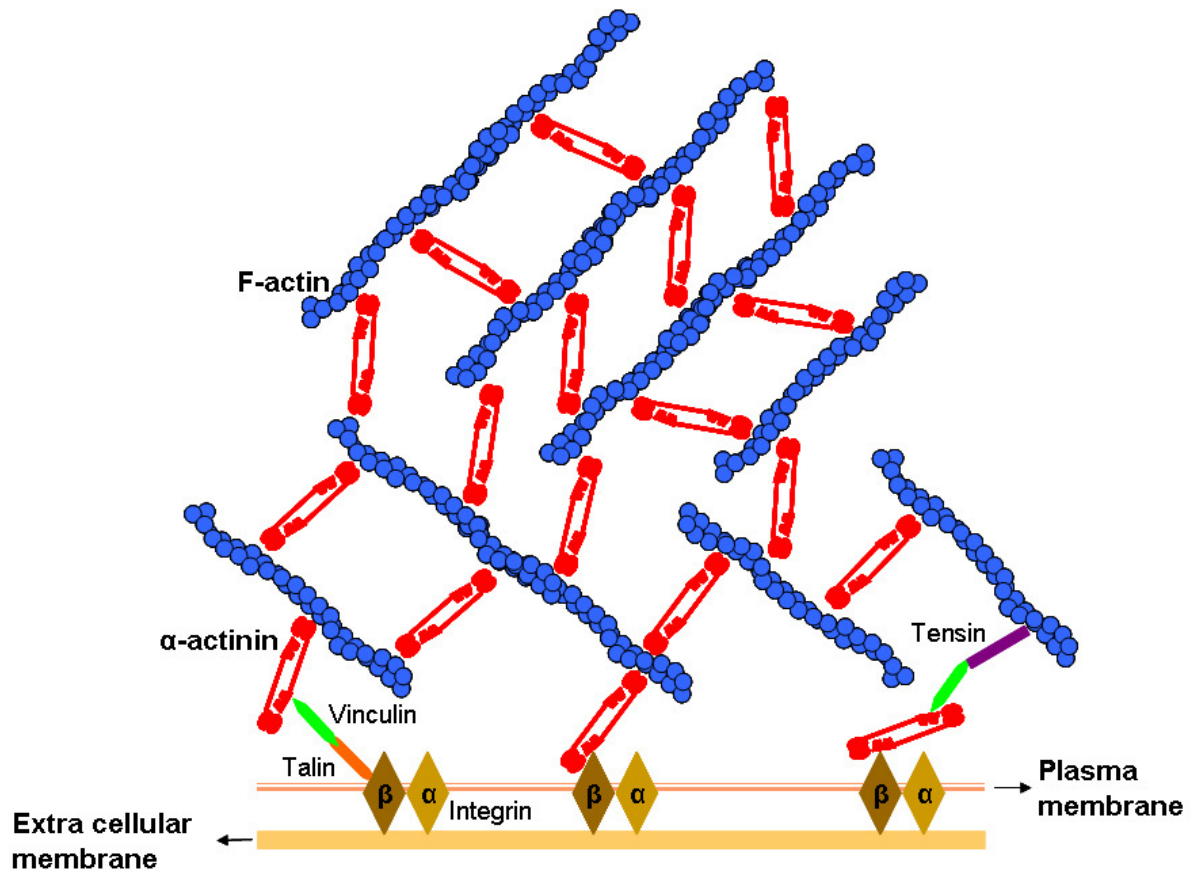


Figure 1.1 Schematic view of the cytoskeleton in focal contacts where α -actinin (red) links actin filaments (blue) to membrane associated proteins: vinculin (green), talin (orange), integrin (brown) and tensin (purple). Modified from (Sjoblom et al., 2008a).

The boundary between sarcomeres is the Z-disk (Figure 1.2D), a highly specialized structure that maintains the organization of the sarcomere and is responsible for the connection between two sarcomeres. It is a multi-protein complex where the most abundant component is α -actinin.

In Z-disk, α -actinin cross-links antiparallel actin filaments coming from adjacent sarcomeres, forming a lattice-like structure that stabilizes the muscle contractile apparatus and acts as a scaffold for many other proteins interaction [Figure 1.2D; (Clark et al., 2002; Masaki et al., 1967; Squire, 1997)].

Similarly to the non-muscle isoforms, α -actinin muscle isoforms 2 and 3 are distributed differently in muscle tissues. While the isoform 2 is the major isoform in the cardiac and oxidative skeletal muscle, the isoform 3 is largely expressed in glycolytic skeletal muscle fibers (Mills et al., 2001).

Fluorescence and photo-bleaching studies have shown that the integrity of sarcomeric α -actinin is important for formation, maintenance and dynamics of the Z-

disk since this protein is present during all stages of the myofibrillogenesis as well in the mature muscle (Stout et al., 2008; Wang et al., 2005).

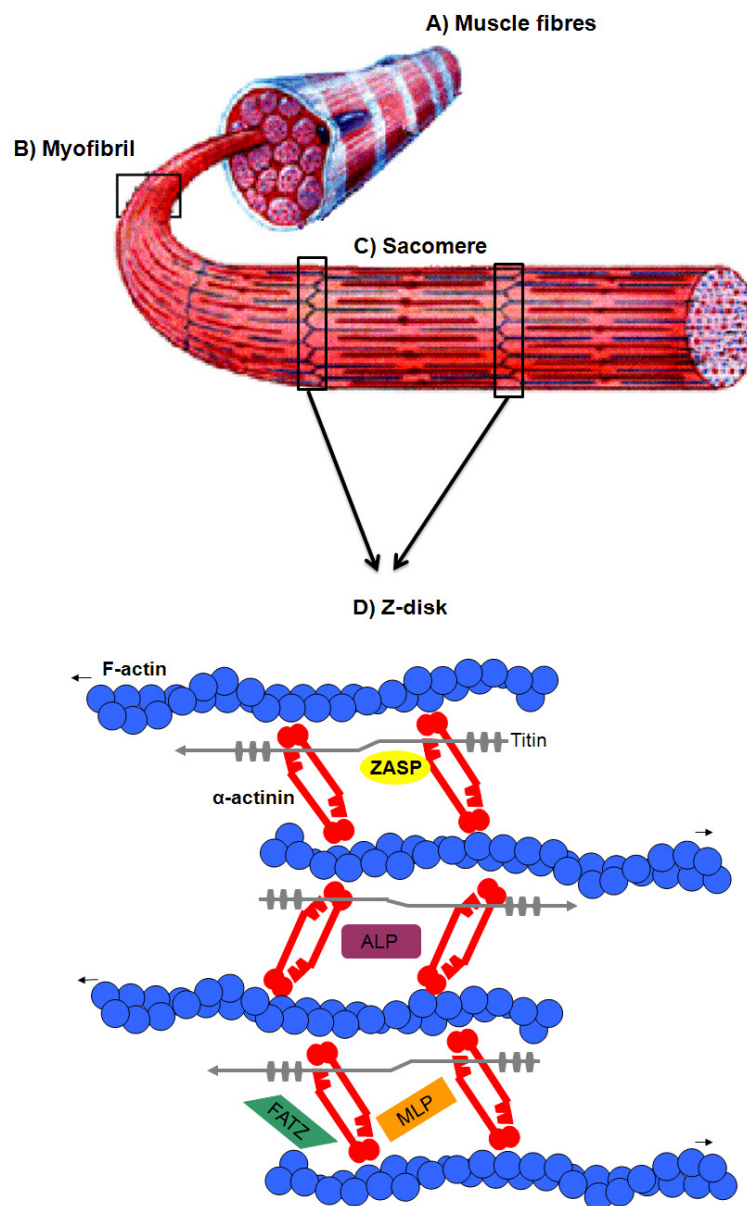


Figure 1.2 Schematic view of striated muscle. **A)** muscle fibre; **B)** myofibril; **C)** sarcomere; **D)** sarcomeric Z-disk where α -actinin (red) cross-links antiparallel actin filaments (blue) and interacts with titin (gray), ZASP (yellow), ALP (purple), MLP (orange), FATZ (green), among others. Modified from <http://www.ucl.ac.uk/~sjjgsca/MuscleSarcomere.gif>, (Clark et al., 2002) and (Sjoblom et al., 2008a).

1.2 α -actinin molecular architecture

All members of the spectrin superfamily have at their N-terminal a characteristic actin-binding domain (ABD), composed of two consecutive calponin homology domains (CH); followed by spectrin-like repeats (SR) and EF-hands.

The functional unit of α -actinin is an antiparallel homodimer, composed of an ABD, connected *via* a flexible neck region to four spectrin-like repeats (SR1-SR4), forming the central rod that is followed by a C-terminal calmodulin-like domain (CaM), formed by 4 EF-hands (Castresana and Saraste, 1995; Davison and Critchley, 1988; Trave et al., 1995). This molecular architecture results in the formation of a rod-shaped molecule with functional domains (ABD and CaM) at both ends (Figure 1.3), allowing the protein to cross-link actin filaments (Young and Gautel, 2000).

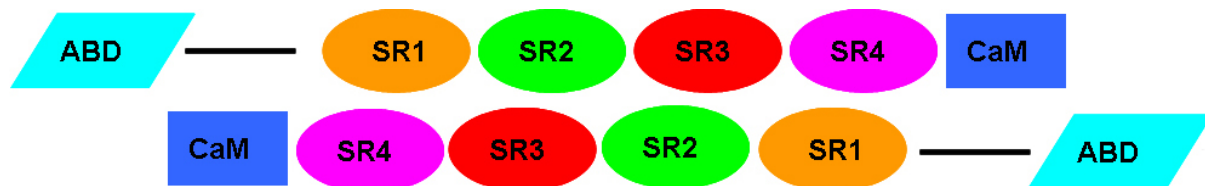


Figure 1.3 Schematic representation of human α -actinin antiparallel homodimer with its domains: ABD (light blue), SR1-SR4 (orange, green, red and pink respectively) and CaM (dark blue).

1.2.1 Actin-binding domain (ABD)

The ABD of α -actinin isoforms is the most conserved domain within the protein family, reflecting the evolutionary high conservation of its binding partner: actin (Sheterline et al., 1995). This domain consists of a tandem pair of type 1 and type 2 calponin homology domains (CH1, CH2), found in several actin-binding proteins, including most of the spectrin superfamily proteins and also in fimbrins, parvins/actopaxins/affixins (Gimona et al., 2002).

The crystal structures of ABD domains from numerous actin binding proteins have already been determined: *Arabidopsis thaliana* and *Schizosaccharomyces pombe* fimbrin (Goldsmith et al., 1997; Klein et al., 2004), utrophin (Keep et al., 1999), dystrophin (Norwood et al., 2000), human and mouse plectin (Garcia-Alvarez et al., 2003; Sevcik et al., 2004), as well as human α -actinin 1, 3, and 4 (Borrego-Diaz et al., 2006; Franzot et al., 2005; Lee et al., 2008). In all structures, the ABD adopts a closed conformation (Figure 1.4), except for *A. thaliana* fimbrin that has unique mutations at the CH1-CH2 interface [reviewed by (Sjoblom et al., 2008b)].

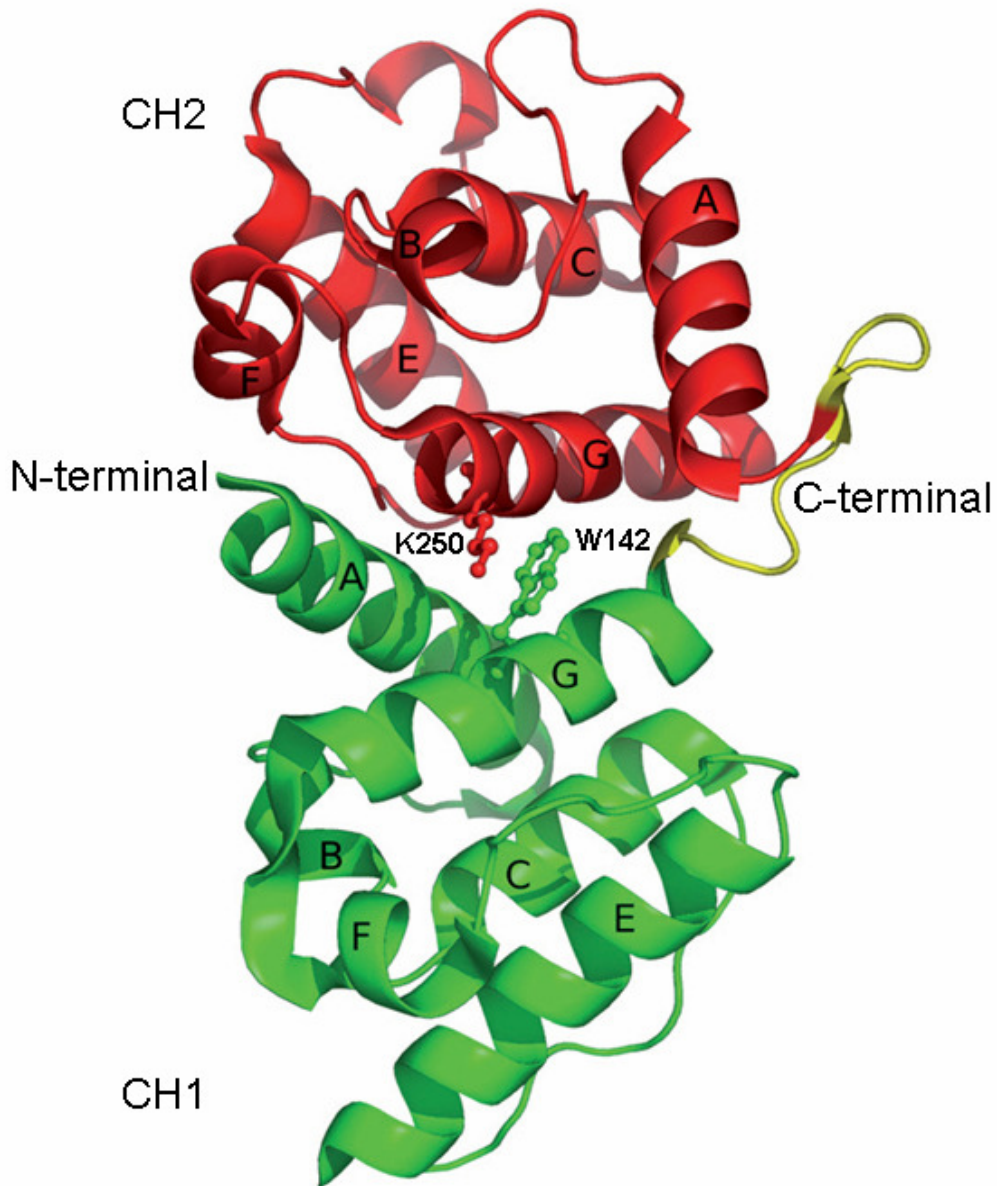


Figure 1.4 Domain organization of human α -actinin ABD isoform 3 in closed conformation [PDB entry WKU; (Franzot et al., 2005)]. CH1 is coloured in green, CH2 in red and the connecting linker in yellow. Highlighted with ball and sticks are the conserved residues, K250 and W142, which are important for the interaction between the CH domains. Modified from (Sjoblom et al., 2008a).

Each individual CH domain is composed of four principal helices (A, C, E and G) that form the core of the domain. Helices C and G are parallel to each other and are sandwiched between the N-terminal helix A and helix E.

The closed arrangement of CH1-CH2 in ABD is achieved in a similar manner in all ABD domains: helices A and G of CH1 pack against the C-terminal region of CH2 [helices F and G; Figure 1.4; reviewed by (Sjoblom et al., 2008a; Sjoblom et al., 2008b)]. The nature of the CH1-CH2 domain interface is semi polar, part is hydrophobic and part is polar contacts that stabilize the interaction between the two domains (Borrego-Diaz et al., 2006; Franzot et al., 2005).

A detailed analysis of the inter-domain interface and of the conservation of amino acid residues involved revealed a critical and highly conserved interaction between the tryptophan residue 128 at CH1 (W128 of helix G) and the lysine residue 236 at CH2 [K236 of helix G; numbers corresponding to human α -actinin isoform 1; (Banuelos et al., 1998; Borrego-Diaz et al., 2006)], which form hydrophobic interactions (Crowley and Golovin, 2005). In isoform 3, these residues correspond to W142 and K250, highlighted in Figure 1.4.

Interestingly, the crystal structure of human ABD α -actinin isoform 4 mutant K255E (K255 corresponds to the position 236 in isoform 1 and position 250 in isoform 3, Figure 1.4), involved in familial focal segmental glomerulosclerosis, displays the same closed conformation as observed in other ABD domains, suggesting that the compact conformation is a highly stable structure in typical ABD (Lee et al., 2008).

Mutational, cross-linking and NMR studies on ABD from different proteins have identified three actin binding sites [ABS1-3; (Bresnick et al., 1991; Bresnick et al., 1990; Corrado et al., 1994; Fabrizio et al., 1993; Gimona and Winder, 1998; Hemmings et al., 1992; Kuhlman et al., 1992; Levine et al., 1990, 1992; Way et al., 1992; Winder et al., 1995)]. These sites map to the N-terminal of CH1 at helix A (ABS1: residues 48-57), the C-terminal of CH1 at helix G (ABS2: residues 123-147) and to the interdomain linker flanked by the N-terminal α -helix of CH2 domain [ABS3: residues 153-172; numbers corresponding to human α -actinin isoform 3; Figure 1.5 (Franzot et al., 2005)].

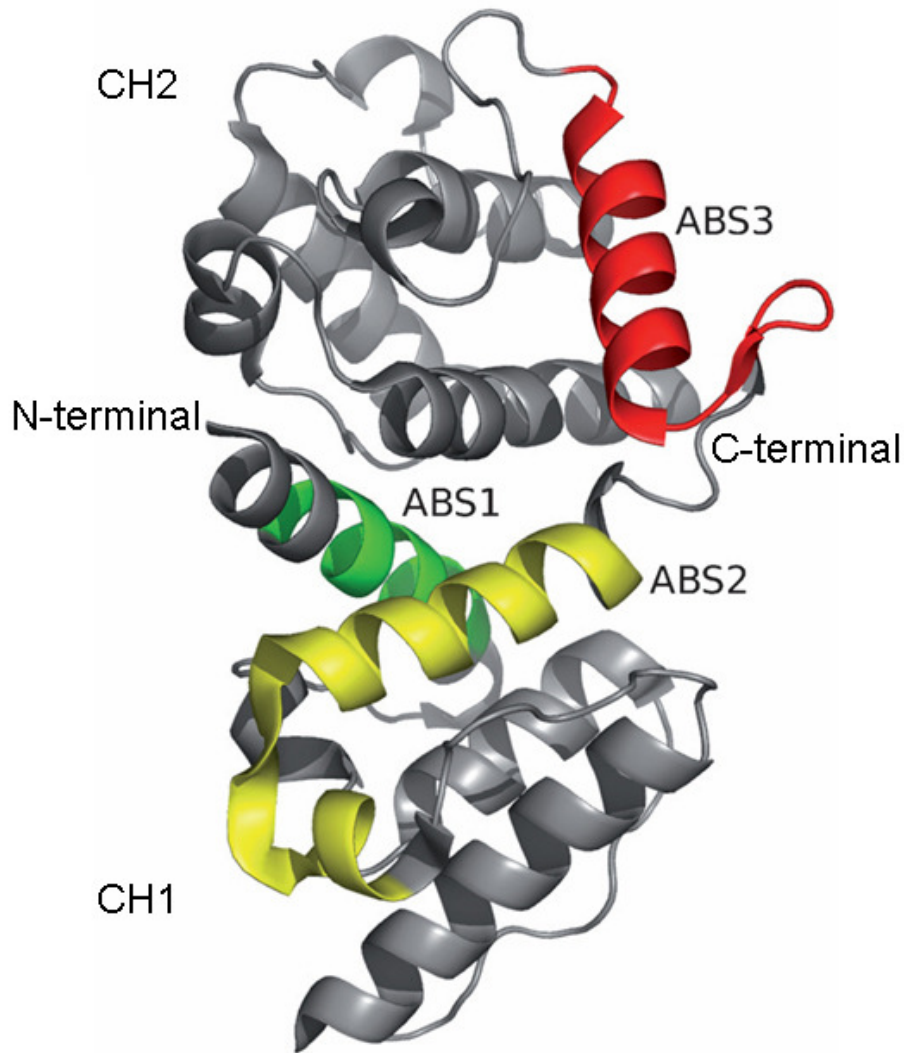


Figure 1.5 Actinin-binding sites (ABS) of α -actinin ABD. ABS1 is coloured in green, ABS2 in yellow and ABS3 in red. Modified from (Sjoblom et al., 2008a).

1.2.2 Central rod domain (SR)

The central rod region of a human α -actinin isoform is composed of four consecutive spectrin-like repeats (SR). However, the number of the repeats has changed during evolution and the central rod domain appears to be the least conserved region of the α -actinin. All known vertebrate α -actinin molecules contain four SR, while the fungus *S. pombe* and the parasite *Trichomonas vaginalis* have two SR (Wu et al., 2001) and five SR (Bricheux et al., 1998), respectively. The protozoan *Entamoeba histolytica* has one or two SR depending on which protein isoform (Virel et al., 2007; Virel and Backman, 2004, 2006).

The three-dimensional structure of a single spectrin-like repeat adopts a triple helix coiled-coil bundle. Such a structure of the repeating unit was predicted on the

basis of amino acid sequence analysis of spectrin (Speicher and Marchesi, 1984) and has been observed in a number of structures coming from the spectrin superfamily of proteins (Djinovic-Carugo et al., 1999; Grum et al., 1999; Kliche et al., 2001; Kusunoki et al., 2004a; Kusunoki et al., 2004b; Pascual et al., 1997; Yan et al., 1993; Ylanne et al., 2001a).

In the spectrin superfamily, the number of SR controls the specific distance between the domains at the N-terminal and C-terminal, and therefore, the length and flexibility of the cross-linker (Winder, 1997). In human α -actinin, the central rod domain forms an antiparallel homodimer (Ylanne et al., 2001a, b) with an overall length of 240 Å and width between 40-50 Å (Figure 1.6). The repeating units are connected by short linkers, providing structural rigidity to the subunit and to the dimer, a feature required for its primary function, bundling of actin filaments.

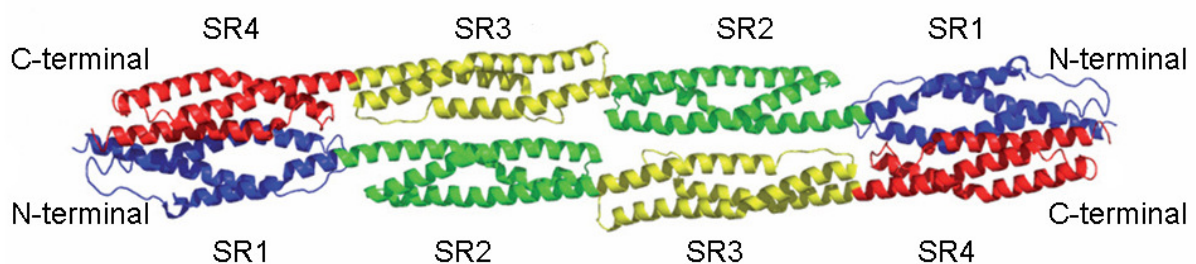


Figure 1.6 Rod domain structure [PDB entry 1HCI; (Ylanne et al., 2001b)], showing the dimer organization with the spectrin-like repeats coloured in blue for SR1, green for SR2, yellow for SR3 and red for SR4. Modified from (Sjoblom et al., 2008a).

On the contrary, structure determination of a repeat pair of α -spectrin in multiple crystal lattice conditions (Grum et al., 1999) and subsequent studies on different double and triple spectrin-like repeat constructs (Kusunoki et al., 2004a; Kusunoki et al., 2004b) revealed inherent flexibility between repeats, a characteristic long assumed from the flexible nature of the erythrocyte membranes (Winkelmann and Forget, 1993).

Intrinsic structural flexibility of the α -actinin dimer is required to carry out bundling of different arrays of actin filaments (Djinovic-Carugo et al., 1999; Ylanne et al., 2001a): while in skeletal and cardiac muscle, α -actinin cross-links antiparallel actin filaments coming from adjacent sarcomeres (Figure 1.2), in non-muscle and smooth muscle cells actin filaments are not part of an organized lattice, and can

therefore assume very diverse orientations (Figure 1.1). The built-in flexibility resides in the neck region of α -actinin, connecting the ABD to the central rod domain, consenting ABD to adopt variable orientations with respect to the main body of α -actinin.

A marked feature of the α -actinin central rod domain is its 90° twist along the long axis of the dimer. Analysis of the inter-subunit interface shows an extensive list of polar (42%) and non-polar (58%) contacts, burying about 11% of the solvent accessible area of the monomer (Ylanne et al., 2001a), in agreements with the high affinity of dimer formation in the pico molar range (Flood et al., 1995; Flood et al., 1997).

The electrostatic potential of the dimer interface surface shows a gradient from basic in SR1 to acidic in SR4, well conserved throughout the isoforms and species, leading to formation of aligned antiparallel dimer.

α -Actinin central rod surface is characterised by an extend acidic electrostatic potential, and was proposed to act as a docking scaffold, offering two binding sites at a time due to the internal symmetry of the rod domain (Ylanne et al., 2001a).

1.2.3 Calmodulin-like domain (CaM)

The C-terminal calmodulin-like domain (CaM) of α -actinin is composed of four EF-hand motifs, which exhibit functional divergence between α -actinin isoforms. The EF-hands of non-muscle isoforms (1 and 4) bind calcium, regulating in this way the actin-binding activity of the molecule, while the EF-hands of muscle isoforms lost this ability [α -actinin regulation details are presented in section 1.3; (Burridge and Feramisco, 1981; Fukami et al., 1992; Tang et al., 2001)].

EF-hands are helix-loop-helix motifs involved in binding intracellular calcium. Generally, EF-hands come in side-by-side pairs, forming a globular domain capable of coordinating up to two calcium (Ca^{2+}) ions (Lewit-Bentley and Rety, 2000). Ca^{2+} binding triggers a major conformational change of the globular domain from a closed state to an open one, causing a rearrangement of the α -helices and exposure of hydrophobic residues to the surface of the protein, allowing the protein to interact with specific targets (Ikura, 1996).

In a subset of EF-hand family of proteins, motifs have diverged to the extent that they have partially or entirely lost the capacity of taking Ca^{2+} (Nakayama and

Kretsinger, 1994), which can be observed in α -actinin muscle isoforms (2 and 3; section 1.3).

In striated muscle, for instance, the CaM domain of α -actinin muscle isoforms is involved in targeting the α -actinin to the Z-disk *via* binding to titin and other proteins (Young et al., 1998; Young and Gautel, 2000)]. The region of titin that binds to CaM domain of α -actinin consists of a series of repeated sequence motifs of about 45 residues, termed Z-repeats [more specifically Z-repeat 7; (Ohtsuka et al., 1997; Sorimachi et al., 1997)].

The structure of EF-3/4 of human α -actinin isoform 2 was determined in complex with the titin Z-repeat 7 by nuclear magnetic resonance spectroscopy [NMR (Atkinson et al., 2001)]. The Z-repeat 7 of titin binds to the groove formed by the two semi open lobes of the two EF hands (Figure 1.7). Upon complex formation Z-repeat 7 adopts an α -helical structure and binds with nano molar affinity to EF-3/4 (Au et al., 2004; Joseph et al., 2001).

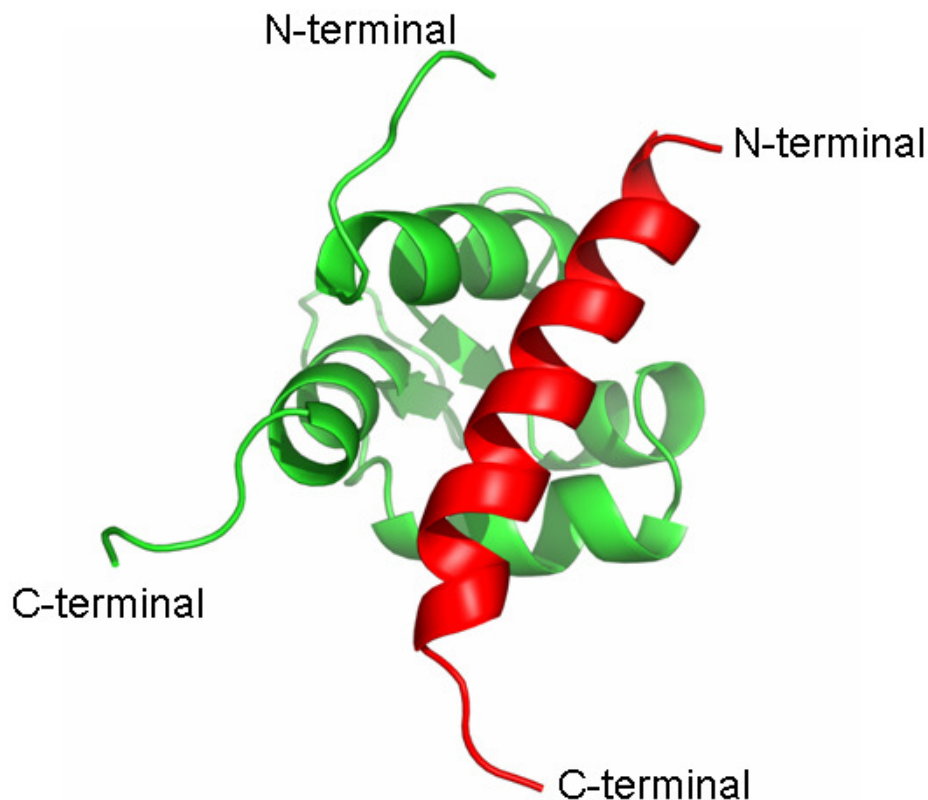


Figure 1.7 Structure of α -actinin EF-3/4 (green) in complex with titin Z-repeat 7 [red; PDB entry 1H8B; (Atkinson et al., 2001)].

1.3 α -actinin regulation

Four mechanisms of α -actinin regulation are known: binding of calcium (Ca^{2+}), binding of phosphatidylinositol, processing by proteases and phosphorylation by tyrosine kinases [reviewed by (Otey and Carpen, 2004)].

It has been shown that the binding of α -actinin to actin filaments can be regulated by calcium and/or phosphatidylinositol depending on the isoform. Non-muscle isoforms (1 and 4) are regulated by Ca^{2+} (Burrige and Feramisco, 1981), while muscle isoforms (2 and 3) are regulated by binding of the phosphoinositide phosphatidylinositol 4, 5-biphosphate [PIP₂; (Fukami et al., 1992)].

The actin binding properties of the non-muscle molecules are reduced or even abolished at calcium concentration higher than 10^{-7} M and pH 7.0 (Condeelis and Vahey, 1982; Fechheimer et al., 1982; Noegel et al., 1987; Witke et al., 1993). At lower concentrations the viscosity of F-actin is significantly increased by the α -actinin isoforms 1 and 4 (Blanchard et al., 1989; Otey and Carpen, 2004). The detailed mechanism of calcium and α -actinin interaction is still unknown.

The Ca^{2+} insensitivity of the muscle isoforms is determined by mutations on the Ca^{2+} coordinates within the CaM domain that diverges considerably from the classical consensus. Consequently, these isoforms lost the properties of Ca^{2+} binding (Beggs et al., 1992; Blanchard et al., 1989). It was speculated that during evolution of α -actinin the ancestral gene encoded a Ca^{2+} sensitive isoform, while the calcium insensitive isoforms arose with the development of the muscle tissue, where the actin binding regulation should be independent of the Ca^{2+} flux (Blanchard et al., 1989).

The current muscle isoforms regulation model proposed by Young and Gautel (2000) pictures the interaction between N-terminal and C-terminal of the two subunits. This model states that the CaM domain of one subunit interacts with the neck region, between the ABD and the first spectrin-like repeat (SR1) of the other subunit. This interaction prevents the binding of the protein to various partners. However, in the presence of the phosphoinositide PIP₂, conformational changes are triggered which release this interaction and make CaM domain free to bind to its partners (Figure 1.8) such as titin (Atkinson et al., 2001; Joseph et al., 2001; Young et al., 1998) and the PDZ domain of ZASP (Au et al., 2004; Faulkner et al., 1999). These conformational changes enhance the actin binding capacity of α -actinin (Young and Gautel, 2000).

How the phosphoinositide is able to release the interaction between the CaM domain and the neck is not known at molecular level. It is believed that its polar head group interacts with the ABD, while the tail interferes with the interaction between the CaM domain and the neck (Young and Gautel, 2000). The phosphate groups 4 and 5 of the phosphoinositide head group interact with the second calponin homology domain (CH2) of ABD (Fraley et al., 2003). The binding site within CH2 domain was mapped by immunoassays and site-directed mutagenesis (Fukami et al., 1996) to the amino acids 168-184 (numbers corresponding to the sequence of chicken skeletal muscle α -actinin isoform).

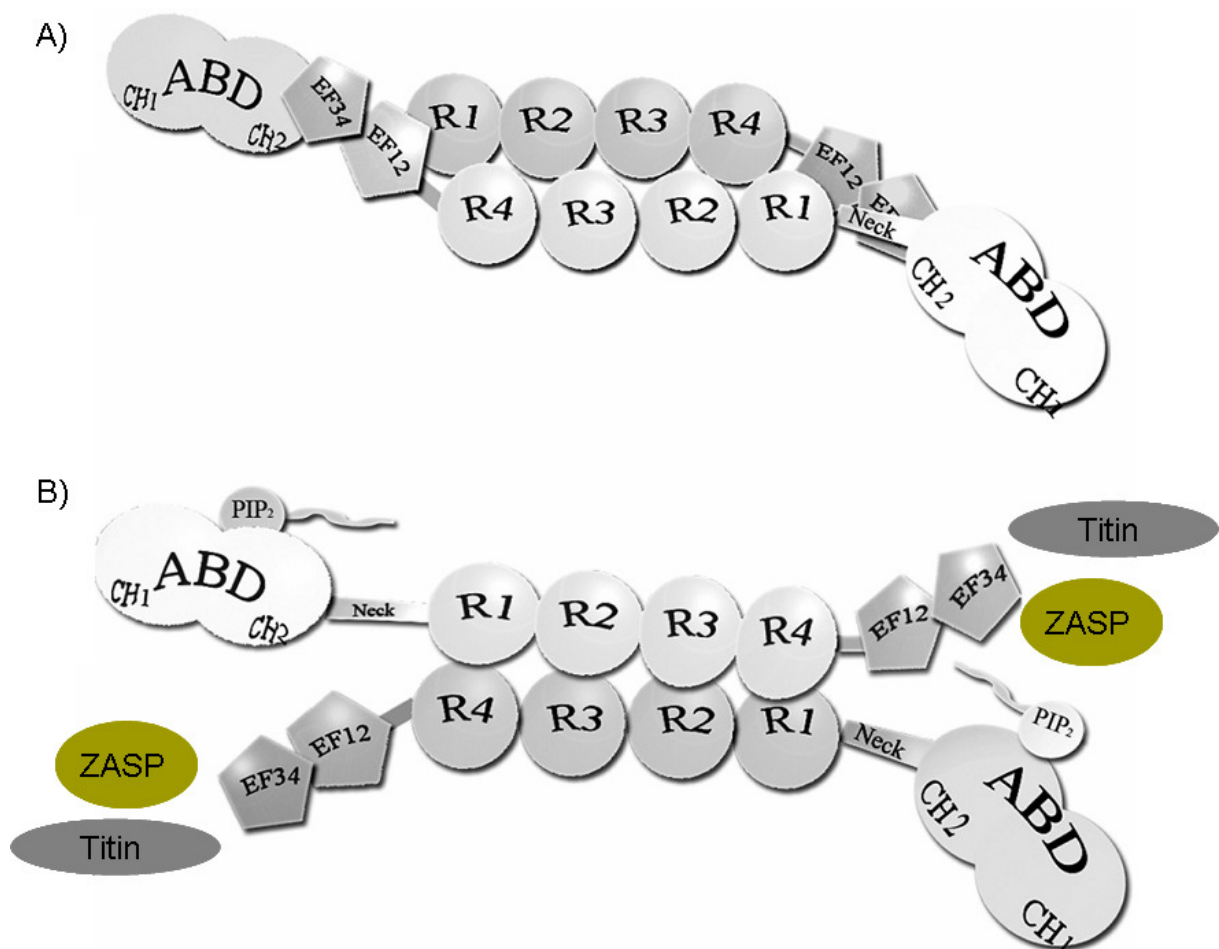


Figure 1.8 Schematic representation of the α -actinin regulation model. **A)** Inactive state: the CaM domain of one subunit interacts with the neck of the other subunit. **B)** Active state: upon binding of PIP_2 , conformational changes are triggered that releases the CaM domain to bind to its patterns, such as titin (dark gray) or ZASP (dark yellow). Modified from (Sjoblom et al., 2008a).

Subsequently, analysis of the three-dimensional crystal structure of the human ABD isoform 3 (Franzot et al., 2005) suggested that the most probable region for the binding of the phosphate group of the phosphoinositide PiP2 to the CH2 domain comprises the positively charged arginine residues R170, R176 and R199 (numbers corresponding to α -actinin isoform 3; Figure 1.9), which are present only in the CH2 domain of α -actinin muscle isoforms (Gimona et al., 2002). These residues follow the pattern observed in structures solved with others phosphoinositides head group bound to proteins and, moreover, their relative solvent accessibility of the polar side chain is suitable for binding (Franzot et al., 2005).

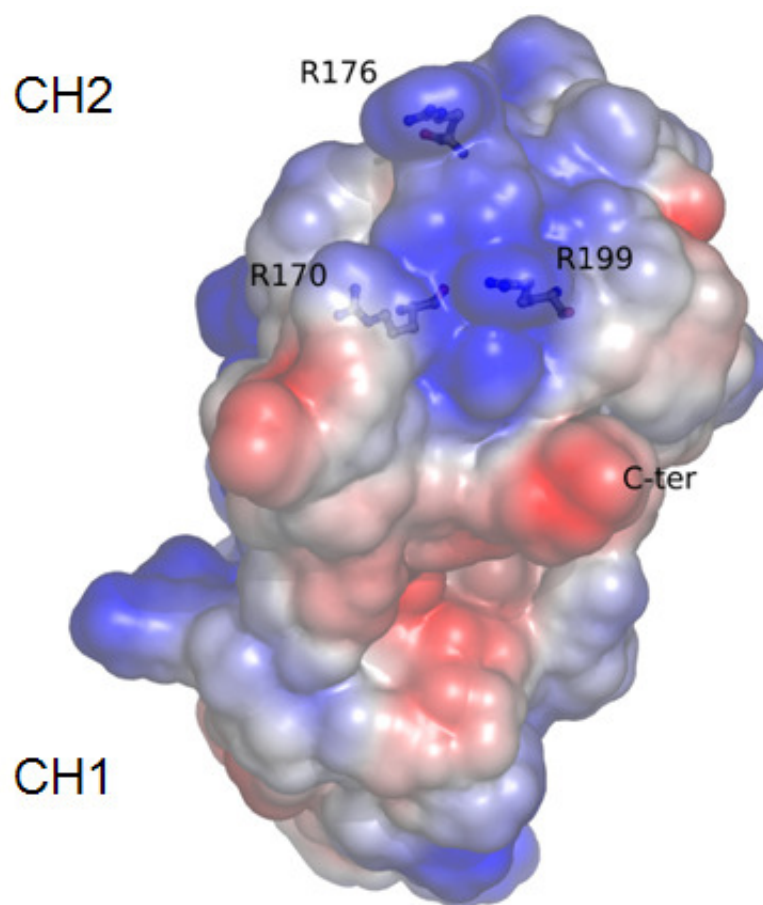


Figure 1.9 PiP2 proposed binding site within ABD of α -actinin isoform 3. Solvent accessible surface of ABD is coloured by electrostatic potential. Residues identified as putative PiP2 ligands are highlighted in sticks: R170, R176 and R199. Modified from (Sjoblom et al., 2008a).

Immunofluorescence assays showed the relationship between the phosphoinositide PiP2 synthesis and sarcomeric Z-disk, suggesting that the requirement of PiP2 for the activation of α -actinin is necessary during the Z-disk formation in developing muscle (Young and Gautel, 2000).

However, there are some controversies about the regulation of α -actinin by phosphoinositides. Not only PiP2 is involved in the regulation of α -actinin, as described above, but also the phosphatidylinositol 3, 4, 5-triphosphate (PiP3). It has been shown that in non-muscle cells, the binding of PiP2 or PiP3 decreases the actin binding capacity of α -actinin (Corgan et al., 2004; Fraley et al., 2003; Full et al., 2007; Greenwood et al., 2000). It remains an opened question awaiting elucidations.

As already mentioned, apart from these processes of regulation described: Ca^{2+} and PiP binding, two other regulatory mechanisms have been identified: processing by proteases and phosphorylation by tyrosine kinases (Otey and Carpen, 2004).

The proteolytic process is carried out by calpain, which cleaves proteins involved in integrin mediated adhesions and actin-based membrane protrusions during cell migration (Franco et al., 2004). Calpains are regulated not only by calcium, depending on the protease isoform (Lebart and Benyamin, 2006), but also by phosphoinositides PiP2 and PiP3, which in turn modulate autolysis of calpain and proteolysis of α -actinin by calpain (Saido et al., 1992). Sprague et al. (2008) have shown that the susceptibility of α -actinin to calpain isoform 1 cleavage is decreased by PiP2 and increased by PiP3, while the cleavage by calpain isoform 2 is not influenced by PiP2. The same group also mapped the calpain isoform 2 cleavage site in presence of PiP3 to the final helix of the CH2 domain of α -actinin [after the tyrosine residue 246 (Y246) in chicken gizzard α -actinin; (Sprague et al., 2008)].

Tyrosine phosphorylation regulation is mediated by an integrin-activated tyrosine kinase focal adhesion kinase (FAK), a regulator of adhesion plaques and cell motility. FAK phosphorylates the ABD domain of α -actinin on the Y12 of the non-muscle human isoform, reducing its affinity to actin filaments (Izaguirre et al., 2001) and suggesting α -actinin as a target for signalling pathways, which regulate cell adhesion. It was proposed that the decrease of affinity for actin filaments changes the mechanical properties of the cytoskeleton, leading to enhanced cell motility (Izaguirre et al., 2001).

1.4 α -actinin interactions

In addition to interaction with actin filaments, α -actinin can interact with many cytoskeletal and regulatory proteins, acting as a multivalent platform for several protein-protein interactions (Djinovic-Carugo et al., 2002; MacArthur and North, 2004;

Otey and Carpen, 2004). A comprehensive overview of the functional categories that demonstrate α -actinin versatility involved in structural, signalling and metabolic roles can be found in others reviews (Clark et al., 2002; Djinovic-Carugo et al., 2002; Ervasti, 2003; Faulkner et al., 2001; MacArthur and North, 2004; Otey and Carpen, 2004; Sjoblom et al., 2008a).

1.4.1 ZASP

An important binding partner of α -actinin muscle isoform is the sarcomeric protein ZASP (**Z**-band **A**lternatively **S**pliced **P**DZ-motif protein), found in striated muscle with different variants derived from alternative splicing (Faulkner et al., 1999). ZASP is a human orthologue of cypher (mouse) and several cardiac and muscle diseases are associated to the Cypher/ZASP family of proteins [reviewed by (Sheikh et al., 2007)].

ZASP is composed of an N-terminal PDZ domain, which is the only common domain within the family. ZASP variants present different numbers of LIM domains, while ZASP itself has none, being therefore a truncated form of PDZ/LIM proteins (Faulkner et al., 1999).

PDZ domains are protein-protein interaction modules composed of 80-120 residues (Xia et al., 1997), consisting mainly of six β -strand (β A- β F) and two α -helices (α A and α B), folded into a β sandwich. C-terminal residues of PDZ partners bind to the groove formed between α B and β B [reviewed by (Hung and Sheng, 2002)].

PDZ domains can interact with other proteins in four different manners: binding to C-terminal (Kornau et al., 1995; Sato et al., 1995), to internal peptides (Shieh and Zhu, 1996), to PDZ domains (Brenman et al., 1996) or to LIM domains (Cuppen et al., 1998) of their partners. The binding specificity is determined by the interaction between the first residue of the helix α B and the side chain of the C-terminal ligand, at position 2. According to the type of interactions between the PDZ and ligand, PDZ domains can belong to three different classes, namely 1, 2 and 3 [reviewed by (Hung and Sheng, 2002)]. The class 1 PDZ domains interact *via* hydrogen bonds to their ligand, the class 2 domains bind to their partners *via* hydrophobic interactions and the class 3 domains have a preference for negatively charged residues to perform the interaction.

Experiments have shown that the interaction between ZASP and α -actinin has been mapped to the PDZ domain of ZASP and C-terminal (EF-3/4) of α -actinin isoform 2, more specifically to EF-3/4, suggesting that ZASP and titin bind to α -actinin around the same region (Faulkner et al., 1999; Zhou et al., 2001).

The structure of PDZ domain of ZASP was determined by NMR (Au et al., 2004) and revealed a typical class 1 PDZ domain (Figure 1.10). The same study also showed that the affinity between PDZ and the EF-3/4 of α -actinin is relatively weak (micro molar range) in comparison with other PDZ domains and their binding partners. Moreover, it was shown that ZASP and titin have distinct binding sites within the α -actinin C-terminal, rendering it possible for the two proteins to interact with α -actinin at the same time (Au et al., 2004).

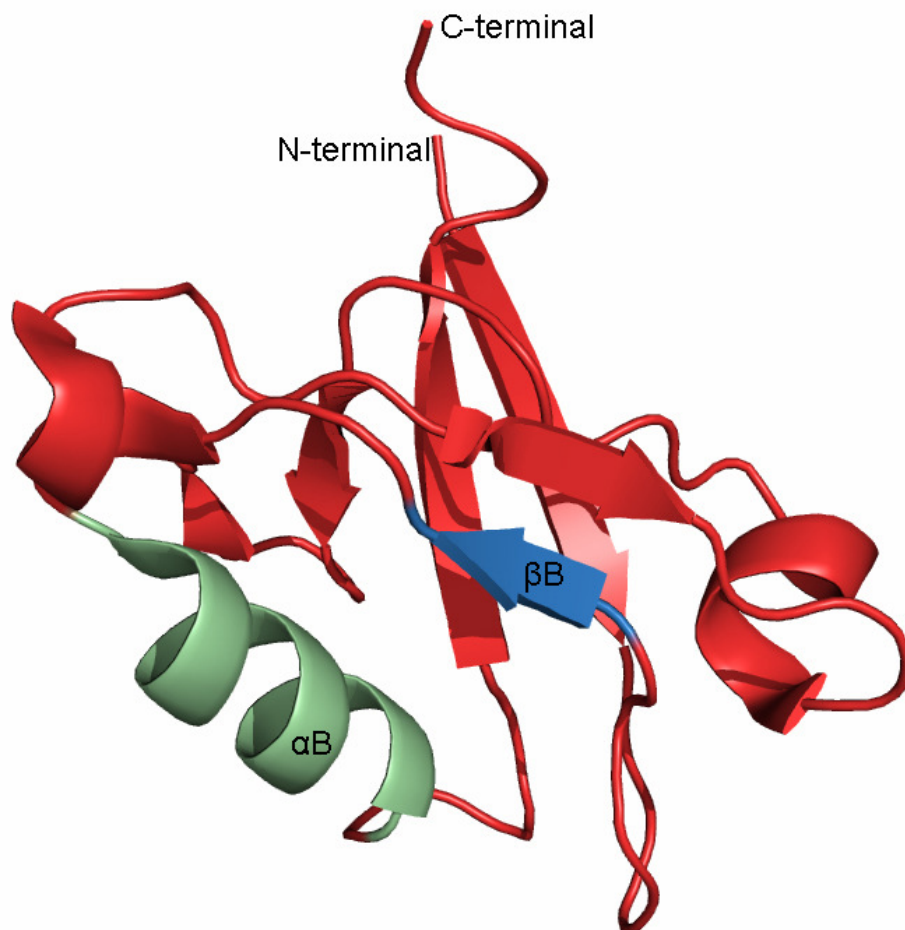


Figure 1.10 Structure of PDZ domain of ZASP [PDB entry 1RGW; (Au et al., 2004)]. The binding between PDZ and C-terminal partners is localized in the groove between α B (pale green) and β B (pale blue).

2. AIM OF THE THESIS

Understanding the regulation of α -actinin's interaction with actin filaments and several other binding partners is very important for comprehension of its functions in Z-disk of striated muscle. The current model was suggested by Young and Gautel [section 1.3; (Young and Gautel, 2000)] who proposed that PiP2 regulates the binding of α -actinin muscle isoforms to actin filaments, titin (Atkinson et al., 2001; Joseph et al., 2001; Young et al., 1998) and ZASP (Au et al., 2004; Faulkner et al., 1999). The interaction between α -actinin and PiP2 has not yet been characterised at molecular detail, but it is believed that while the polar head interacts with the α -actinin ABD, its hydrophobic tail interferes with the interaction of between CaM-like domain of one and the neck region of the juxtaposed α -actinin in the antiparallel dimer, releasing the functional domains ABD and CaM to interact with their binding partners.

Although a body of structural data is available on individual domains of α -actinin (ABD, central rod domain and EF-3/4 of CaM; section 1.2), no structural information so far exists on the entire molecule or its smaller functional units, *e.g.* on half dimer or on the complex of the actin-binding domain and first spectrin-like repeat (ABD_SR1) bound to CaM domain or EF-3/4. The aim of this work is to generate structural information to address questions concerning α -actinin structure and regulation by employing a combination of biochemical, biophysical and structural studies.

Specific aims are:

1- Interaction studies

- ✓ Analysis of the influence of the phosphoinositides on the interaction of α -actinin isoform 2 and PDZ domain of ZASP in the context of α -actinin antiparallel dimer;
- ✓ Validation of the proposed PiP2 binding site of α -actinin muscle isoform (Franzot et al., 2005) through binding studies of ABD and mutants of residues implicated in binding to inositol triphosphate (IP3) or inositol hexakisphosphate (IP6), which are the soluble heads of phosphoinositides.

2- Structural studies

- ✓ Validation of the proposed PiP2 binding site on ABD (Franzot et al., 2005) through X-ray diffraction studies of ABD in complex with IP3 or IP6;
- ✓ Generation of high resolution structural information on α -actinin isoforms 1 and 2 full length (AFL), half of the dimer (ABD_SR1_SR2//SR3_SR4_CaM; hd) and smaller functional units through single crystal X-ray diffraction analysis in order to understand α -actinin architecture at molecular detail;
- ✓ Generation of high resolution structural information on *Entamoeba histolytica* α -actinin isoform 2 full length (2Eh; smaller version of human isoforms with two spectrin repeats) through single crystal X-ray diffraction analysis to understand α -actinin architecture at molecular detail;
- ✓ Generation of molecular models based on SAXS-derived molecular envelope of human α -actinin isoforms 1 and 2, and *E. histolytica* α -actinin isoform 2 to gain understanding of α -actinin molecular architecture.

3. MATERIALS AND METHODS

3.1 Constructs and nomenclature

The constructs designed for this study are showed in Figure 3.1. For human α -actinin constructs the residues are numbered according to the sequence of human α -actinin isoform 2 (Figure 3.1A – I). Constructs for human α -actinin isoform 1 were based on the sequence alignment between the two isoforms (1 and 2). The full length human α -actinin isoforms 1 and 2 (1AFL, 2AFL) and the half dimer (1hd, 2hd) were cloned into pET8c and kindly supplied by the group of Dr. Jari Yläanne (University of Jyväskylä).

Regarding the nomenclature, numbers in front of the construct abbreviations denote the corresponding α -actinin isoform (1 = non-muscle isoform or 2 = muscle isoform). Constructs with the suffix **Y** start at tyrosine residue 19 (Y19) and those with the suffix **a** start at the beginning of the actin binding domain (ABD, A35).

For *Entamoeba histolytica* α -actinin isoform 2 (2Eh), only the full length construct was used (Figure 3.1J) and it was cloned into pET19b by our collaborators, the group of Dr. Lars Backman (University of Umeå).

3.2 DNA manipulation

3.2.1 DNA amplification (PCR) and colony PCR

The PCR reaction was prepared to a final volume of 20 μ l: 1.25 mM MgCl₂, 0.25 mM dNTP's, 2.5 units of Taq Polymerase, 1x PCR buffer (10 mM Tris-HCl pH 8.0, 50 mM KCl, 0.08% Nonidet P-40), 10 pmol of each oligonucleotide (forward/reverse) and 10 to 20 ng DNA template. The cycles of individual PCR reactions were optimized according to the length of the amplification product and the oligonucleotides melting temperature (T_m; Table 3.1).

For colony PCR (used to identify positive clones) the reaction was similar to the DNA amplification described above, however, the template used was the mixture containing a dilution of a colony in 100 μ l Milli-Q water. This mixture was incubated at 95° C during 5 min, centrifuged to precipitate the debris (5000 g, 5 min, at room temperature) and 1 μ l of the supernatant was used as template for the colony PCR reaction.

3.2.1.1 α -actinin

The α -actinin target fragments were amplified by PCR using the full length fragment cloned into pET8c (by Dr. Jari Yläanne) as template. For all constructs specific oligonucleotides were designed including the restriction sites for Bsal (forward) and KpnI (reverse; Table 3.1).

3.2.1.2 PDZ domain of ZASP

The PDZ domain was amplified by PCR using the ZASP full length fragment cloned into pUC vector (by the group of Dr. Georgine Faulkner; ICGEB; Italy) as a template. Specific oligonucleotides were designed including the restriction sites for NcoI (forward) and KpnI (reverse; Table 3.1)

3.2.2 DNA agarose gel electrophoresis

DNA samples were resolved by DNA agarose gel in concentrations ranging from 0.7% (w/v) to 1% (w/v) in 1x TAE buffer (40 mM Trizma, 4.7% acetic acid, 50 mM EDTA pH 8.0) and 1.5 μ g/ml ethidium bromide (Sigma). The electrophoresis was carried out at 80 V and the DNA was then visualized under ultraviolet (UV) light.

3.2.3 Restriction endonuclease reactions

Expression plasmids and PCR fragments were submitted to restriction endonuclease reaction, according to their restriction sites. The plasmids were digested by NcoI – KpnI, human α -actinin DNA fragments were digested by Bsal – KpnI and the PDZ domain of ZASP was digested by NcoI – KpnI (Table 3.1). Restriction enzymes and buffers were purchased from New England BioLabs and the reaction was performed following the manufacturer's instructions.

3.2.4 DNA purification

The linearized plasmids and PCR fragments were purified from the agarose gel using the QIAGEN QIAquick Gel Extraction Kit according to the manufacturer's instructions.

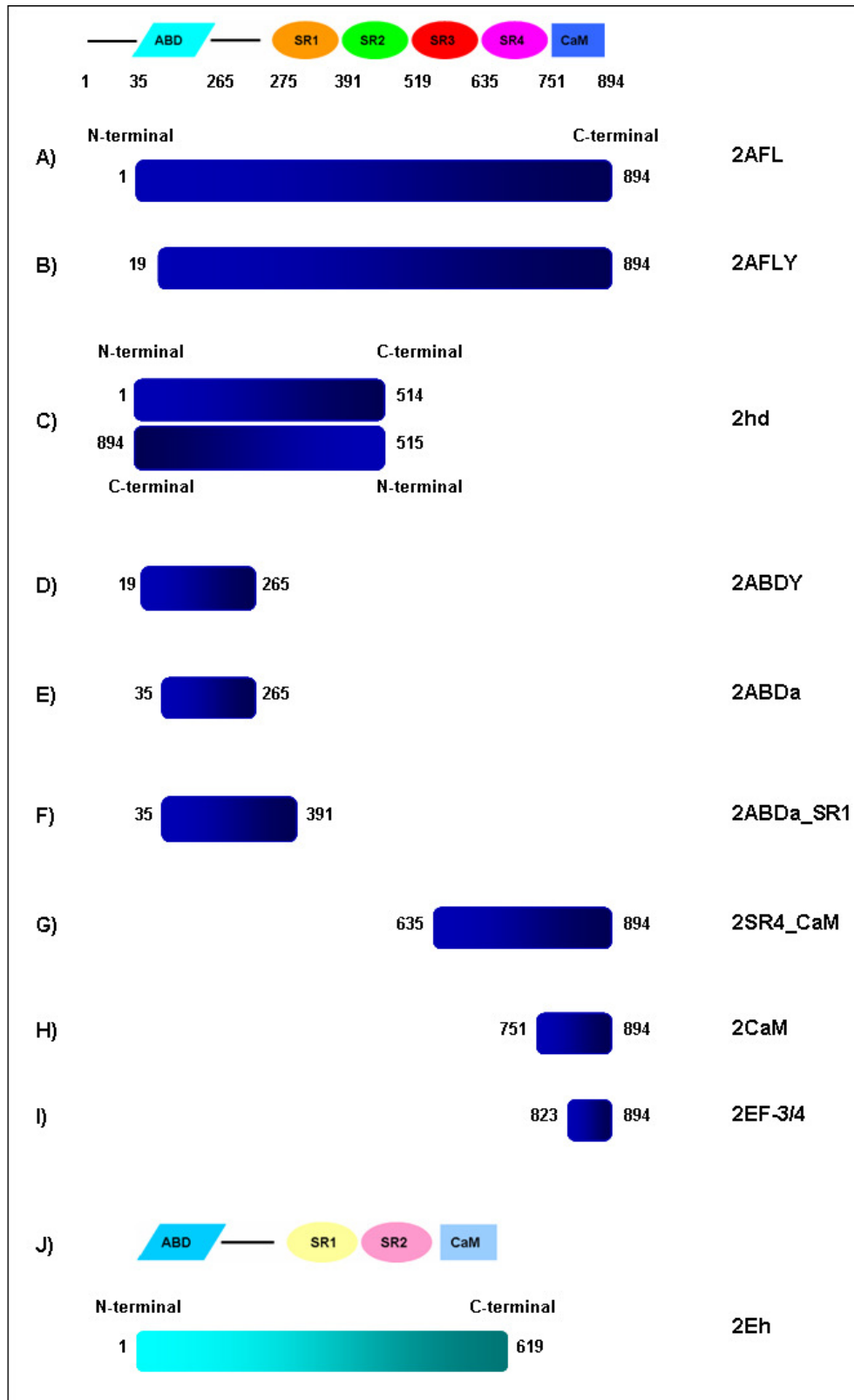


Figure 3.1 Representation of the human α -actinin isoform 2 and *E. histolytica* α -actinin isoform 2 constructs used in this study for protein expression. The constructs of human α -actinin isoform 1 were designed based on the sequence alignment between these two isoforms (1 and 2). **A)** 2AFL, **B)** 2AFLY, **C)** 2hd, **D)** 2ABDY, **E)** 2ABDa, **F)** 2ABDa_SR1, **G)** 2SR4_CaM, **H)** 2CaM, **I)** 2EF-3/4, **J)** 2Eh.

Table 3.1 Oligonucleotides and T_m (°C). Restriction sites are highlighted in red for NcoI, in green for BsaI and in purple for KpnI.

FRAGMENT	OLIGONUCLEOTIDES (5' to 3')	T _m (°C)
1ABDa_SR1_FOR 1ABDa_SR1_REV	AATTTGGTCTCCCATGGCCTGGGAGAAGCAGCAG AAAAGGTACCCTTATTATTAATTCAGCAACCACTCCTCATAGC	75.5 66.9
2ABDa_SR1_FOR 2ABDa_SR1_REV	AATTTGGTCTCCCATGGGCTGGGAGAAGCAGCAG AAAAGGTACCCTTATTATTAATTGAGCAACCACTCCTCGTAAC	75.5 66.5
1SR4_CaM_FOR 1SR4_CaM_REV	CATGCCATGGCCACAATGAGAGGCTACGCAAGC AAAAGGTACCCTAGAGGTCACCTCTCGCCG	71.9 65.2
2SR4_CaM_FOR 2SR4_CaM_REV	AATTTGGTCTCCCATGGGCAACGAGCGTCTGAGGCGCC AAAAGGTACCCTCACAGATCGCTCTCCCCG	82.2 67.4
1CAM_FOR 1CAM_REV	AATTTGGTCTCCCATGGAGCCAGGAGCAGATGAATGAGTTC AAAAGGTACCCTAGAGGTCACCTCTCGCCG	82.1 65.2
2CAM_FOR 2CAM_REV	AATTTGGTCTCCCATGGACCCAGGAGCAGATGAATGAGTTC AAAAGGTACCCTCACAGATCGCTCTCCCCG	82.1 67.4
1EF-3/4_FOR 1EF-3/4_REV	AATTTGGTCTCCCATGGCCGACACAGATACAGCAGACC AAAAGGTACCCTAGAGGTCACCTCTCGCCG	83.2 65.2
2EF-3/4_FOR 2EF-3/4_REV	AATTTGGTCTCCCATGGACACCGACACTGCCGAGCAGG AAAAGGTACCCTCACAGATCGCTCTCCCCG	87.2 67.4
2ABDa_FOR 2ABDa_REV	AATTTGGTCTCCCATGGGCTGGGAGAAGCAGCAG AAAAGGTACCCTTATTAAGCCGCTGTCTCGGCC	75.5 75.8
2ABDY_FOR 2ABDY_REV	AATTTGGTCTCCCATGGGCTACATGATCCAGGAGGAGG AAAAGGTACCCTTATTAAGCCGCTGTCTCGGCC	82.7 75.8
2AFly_FOR 2AFly_REV	AATTTGGTCTCCCATGGGCTACATGATCCAGGAGGAGG AAAAGGTACCCTCACAGATCGCTCTCCCCG	82.7 67.4
Δ2ABDa R163E_FOR Δ2ABDa R163E_REV	GGTCTGCTGCTTTGGTGTCAg ^{gaa} AAAACCTGCTCCTTATAGAAAT ATTTCTATAAGGAGCAGTTTTt ^{tc} CTGACACCAAAGCAGCAGACC	81 81
Δ2ABDa R169E_FOR Δ2ABDa R169E_REV	CAGAGGAAAACCTGCTCCTTATga ^{AAATGTGAACATT} CAGAACCTTC GAAGTTCTGAATGTTc ^{ATAAGGAGCAGTTTT} CCTCTG	78 78
Δ2ABDa R192E_FOR Δ2ABDa R192E_REV	GGACTCTGTGCCCTCATCCACga ^{ACACCCGGCCTGACCTCATTGAC} GTCAATGAGGTCAGGCCGGTg ^{tc} GTGGATGAGGGCACAGAGTCC	86 86
Δ2AFL E23A/ E24A/ E25A_FOR Δ2AFL E23A/ E24A/ E25A_REV	GATGAGTACATGATCCAGg ^{cgggcgcg} TGGGACCGGACCTGCTC GAGCAGGTCGCGGTCCCc ^{gcccgcgc} CTGGATCATGTACTCATC	94.1 94.1
Δ2AFL E149A/E150A_FOW Δ2AFL E149A/E150A_REV	CTATTCAGGATATTTGCGTTg ^{cgggcg} ACATCTGCCAAAGAAGGTC ACCTTCTTTGGCAGATGTc ^{gcccgc} AACCGAAATATCCTGAATAG	84.6 84.6
Δ2AFL E260A/Q261A/E263A_FOW Δ2AFL E260A/Q261A/E263A_REV	GCTTTTGGGGCGCGg ^{cgggcg} GCCg ^{cg} ACAGCGGCTAACAGG CCTGTTAGCCGCTGTc ^{gcccgc} CGCGCCCGCAAAGC	98.3 98.3
Δ2AFL E310A/ K311A_FOR Δ2AFL E310A/ K311A_REV	CTGGAGAACCGACTCCCg ^{cgggcg} ACCATGCAAGCCATGCAG CTGCATGGCTTGCATGGTc ^{gcccgc} GGGAGTCCGGTTCTCCAG	94.1 94.1
PDZ_FOR PDZ_REV	CATGCCATGGCTTACAGTGTGACCCTG TTGGTACCCTTACTTTGATTTCTGCAGGGTG	76 71.9

3.2.5 Cloning into expression plasmids

The expression plasmids used in this study were based on the pETM expression system. These vectors were designed to produce a fused tag at the N-terminal region of the protein. The tags can be polyhistidine-tag (6x His-tag), glutathione S-transferase-tag (GST) or other proteins, such as *E. coli* thioredoxin A (TrxA) and disulfide oxidoreductase A (DsbA), fused to the target protein to improve its solubility. The match between tag and vector is listed in Table 3.2.

After the restriction endonuclease reaction, linearized plasmids and target fragments were submitted to ligation reaction with the T4 ligase enzyme and buffer purchased from Fermentas. The reaction followed the manufacturer's instructions.

Table 3.2 Expression plasmids and fused tags expressed with the proteins.

PLASMID	N-TERMINAL TAG
pETM13	No tag
pETM11	6x His-tag
pETM13 GST	6x His-tag + GST-tag
pETM20	6x His-tag + TrxA
pETM13dsbAGSHISTEV	6x His-tag + DsbA

3.2.6 Competent cells transformation

The ligation products were transformed into chemical competent strain *Escherichia coli* DH5 α (cloning strain; Table 3.3). The transformation was done by the heating shock method where 10 μ l of the ligation mixture were added to 50 μ l of competent cells. After 20 min of incubation on ice, these cells were subsequently heated shock at 42° C during 30 sec and cooled on ice for another 5 min. After this thermal shock, 400 μ l of Luria Broth (LB, Sigma) were added and the resulting mixture incubated at 37° C and 120 rpm for 1 h, to allow the cells to recover from the shock.

The same protocol was used to transform positively selected plasmids into expression strains: *E. coli* BL21 (DE3), BL21 (DE3) pLysS, BL21 (DE3) Rosetta pLysS and BL21 (DE3) Star (Table 3.3).

Table 3.3 *E. coli* strains and their genetic background [Stratagene, Novagen, (Hanahan, 1983)].

<i>E. coli</i> STRAINS	GENOTYPE
DH5 α	supE44 Δ lacU169 (Φ 80 lacZ Δ M15) hsdR17 recA1 endA1 gyrA96 thi-1 relA1
BL21 (DE3)	<i>E. coli</i> B F ⁻ ompT hsdS _B (r _B ⁻ m _B ⁻) gal dcm λ (DE3)
BL21 (DE3) pLysS	<i>E. coli</i> B F ⁻ ompT hsdS _B (r _B ⁻ m _B ⁻) gal dcm λ (DE3) pLysS (Cm ^R)
BL21 (DE3) Rosetta pLysS	<i>E. coli</i> B F ⁻ ompT hsdS _B (r _B ⁻ m _B ⁻) gal dcm lacY1 λ (DE3) pLysS pRARE ² (Cm ^R)
BL21 (DE3) Star	<i>E. coli</i> B F ⁻ ompT hsdS _B (r _B ⁻ m _B ⁻) gal dcm λ (DE3) rne131

3.2.6.1 Co-transformation experiments

Plasmids containing the human α -actinin N-terminal (ABD_SR1, Construct A, Table 4.2) and C-terminal (CaM or EF-3/4, Construct B, Table 4.2) fragments desired for a complex formation (positively selected by antibiotics, colony PCR and DNA sequencing) were mixed together in a concentration ratio of 1:1 and transformed into expression strains for further co-expression experiments and protein-protein complex formation.

3.2.7 Selection of positive clones using antibiotics

The transformation products were plated into LB-agar medium (LB + 1.5% agar) containing the appropriated antibiotic: ampicillin (100 μ g/ml), kanamycin (100 μ g/ml) or chloramphenicol (34 μ g/ml), depending on the plasmid and the *E. coli* strain in study (Table 3.4). The plate was incubated over night at 37° C.

3.2.8 Plasmid extraction in mini scale (miniprep)

After the selection of positive clones by antibiotics and colony PCR, these colonies were submitted to miniprep using the QIAprep Spin Miniprep Kit (QIAGEN) according to the manufacturer's instructions.

3.2.9 DNA sequencing

The extracted plasmids from *E. coli* DH5 α were sent to DNA sequencing at VBC-Biotech Service GmbH, Vienna, Austria. The oligonucleotides used for sequencing were complementary to T7 promoter or T7 terminator.

Table 3.4 Antibiotics used for selection of positive clones.

ANTIBIOTIC	STRAINS AND PLASMIDS
Ampicillin	<i>E. coli</i> DH5 α , BL21 (DE3) and BL21 (DE3) Star transformed with pETM20, pET8C and pET19b
Kanamycin	<i>E. coli</i> DH5 α , BL21 (DE3) and BL21 (DE3) Star transformed with pETM11, pETM13, pETM13 GST and pETM13dsbAGSHISTEV
Ampicillin + Kanamycin (for co-transformation assays)	<i>E. coli</i> BL21 (DE3) and BL21 (DE3) Star transformed with pETM20 + pETM11, pETM13, pETM13 GST and pETM13dsbAGSHISTEV
Ampicillin + Kanamycin + Chloramphenicol (for co-transformation assays)	<i>E. coli</i> BL21 (DE3) pLysS, BL21 (DE3) Rosetta pLysS transformed with pETM20 + pETM11, pETM13, pETM13 GST and pETM13dsbAGSHISTEV
Kanamycin + Chloramphenicol	<i>E. coli</i> BL21 (DE3) pLysS, BL21 (DE3) Rosetta pLysS transformed with pETM11, pETM13, pETM13 GST and pETM13dsbAGSHISTEV
Ampicillin + Chloramphenicol	<i>E. coli</i> BL21 (DE3) pLysS, BL21 (DE3) Rosetta pLysS transformed with pETM20, pET8C and pET19b

3.3 Protein manipulation

3.3.1 Over-expression of recombinant proteins

After checking the sequence identity of the cloned inserts, the plasmids were then transformed into expression strains and plated into LB-agar with appropriated antibiotics.

A single colony was used for LB pre-culture. The pre-culture of the target protein grown over night at 37° C and 120 rpm was diluted in fresh LB containing the appropriated antibiotics. For small scale over-expression experiments, 0.4 ml of pre-culture was diluted in 10 ml LB while for large scale; 8 ml of pre-culture was diluted in 1 l LB, always with appropriated antibiotics.

The fresh culture grew at 37° C and 120 rpm until it reached an optical density OD₆₀₀ between 0.6 and 0.8. The proteins were subsequently induced by adding 0.5 μ M IPTG (Sigma). Protein induction lasted 4 h for experiments performed at 37° C or over night for experiments performed at 20° C. After this period the culture was harvested by centrifugation (6.000 rpm, 15 min, at 4° C).

3.3.1.1 Small scale overexpression

Lysis of the induced cells derived from the small scale over-expression experiments was done using the Bug buster Protein Extraction Reagent (Novagen), following the manufacturer's instructions.

3.3.2 Purification of recombinant proteins

In order to obtain pure protein the induced cells were resuspended in lysis buffer (20 ml lysis buffer per litre of culture: 20 mM Tris-HCl pH 7.6, 150 mM NaCl, 10 mM imidazole, supplied with protease inhibitor if necessary; Complete Mini EDTA-Free, Roche) and then disrupted by 10 min sonication on ice with 40% maximum energy output (Bandelin Sonoplus). The cell lysate was clarified by centrifugation (20.000 rpm, 30 min, at 4° C).

The supernatant resulting from the centrifuged lysate was submitted to three different protein purification steps including gravity flow IMAC, ion exchange and size exclusion chromatography (SEC).

The resin Ni sepharose 6 Fast Flow (GE Healthcare Life Sciences) charged with 0.1 M NiSO₄ was used for gravity flow IMAC. The cell lysate supernatant was poured into a gravity His-trap column (Bio-Rad) previously equilibrated with the lysis buffer. After the supernatant had passed through the column, 6 column volumes of the same buffer was used to wash it. Then, the protein was eluted from the column by the IMAC elution buffer (20 mM Tris-HCl pH 7.6, 150 mM NaCl, 300 mM imidazole).

The next protein purification step was the ion exchange chromatography using a Resource Q column (Amershan Biosciences) and an Äkta purifier system (GE Healthcare Life Sciences). The column was equilibrated with buffer A (50 mM Tris-HCl pH 7.6, 50 mM NaCl) and the protein was eluted from the column with buffer B (50 mM Tris-HCl pH 7.6, 2 M NaCl) in a linear gradient.

The last purification step by size exclusion chromatography was also performed in an Äkta purifier system (GE Healthcare Life Sciences) using Superdex200 or Superdex75 HiLoad 26/60 columns [depending on the molecular weight (MW) of the molecule; Amershan Biosciences] equilibrated with appropriated buffer (section 4.3).

3.3.2.1 Purification of human α -actinin half dimer (hd)

The purification of human α -actinin hd is considerably different from that of the other constructs. The dimer is formed (Figure 4.9A) during the protein expression and purified very tightly, with high level of purity, during the gravity flow IMAC since half of the molecule is His-tagged (6x His – SR3_SR4_CaM, ~40 kDa), while the other half remains not tagged (ABD_SR1_SR2, ~60 kDa).

3.3.2.2 Co-purification experiments

The induced cells containing the α -actinin target inserts for complex formation were broken together by sonication and after centrifugation the supernatant was submitted to gravity flow IMAC.

To form the complex of 2hd and PDZ domain of ZASP cells with both recombinant proteins over-expressed were mixed and broken together by sonication. After centrifugation the supernatant was submitted to gravity flow IMAC followed by size exclusion chromatography using the column Superdex200 HiLoad 26/60 (Amershan Biosciences), equilibrated with 20 mM Tris-HCl pH 7.6, 150 mM NaCl.

3.3.2.3 Analytical size exclusion chromatography

Analytical size exclusion chromatography was employed in order to analyse the formation of the α -actinin 2hd and the PDZ domain complex in the presence and absence of lysophosphatidic acid (LPA). An analytical Superdex200 10/300 GL column (Amershan Biosciences) was used, previously equilibrated with 20 mM Tris-HCl pH 7.6, 150 mM NaCl.

As a control, the two proteins were mixed in a molar ratio of 1:1 incubated 1 h at 4° C and centrifuged (18.000 rpm, 15 min, at 4° C) before analytical size exclusion chromatography. To verify whether LPA would enhance the complex formation, LPA was added to the protein-protein sample in a molar ratio between 2hd, PDZ and LPA of 1:1:1, 1:1:3 and 1:1:5.

3.3.3 Tag cleavage by Tobacco etch virus (TEV) protease

In order to cleave the tag from the protein, TEV protease was added to the target protein sample, which has been purified once by gravity flow IMAC, in an OD₂₈₀ ratio 1:50. This mixture was dialyzed over night against TEV cleavage buffer (50 mM Tris-HCl pH 7.5, 50 mM NaCl, 1 mM EDTA, 2 mM β -mercaptoethanol) at 4°

C. After cleavage, the sample was resubmitted to gravity flow IMAC, to eliminate any uncleaved protein, TEV and free tag. The cleaved target protein was subsequently submitted to further purification steps.

3.3.4 Protein dialysis

Protein dialysis was carried out in Spectra/Por Dialysis Membrane Tubing with molecular weight cut off (MWCO) between 12.000 Da and 14.000 Da (Spectrum laboratories Inc.) against appropriated buffer.

3.3.5 SDS-polyacrylamide gel electrophoresis (SDS-PAGE)

Protein samples were analysed under denaturing conditions in polyacrylamide gel according to their MW. The protocol followed Laemmli's method (Laemmli, 1970). The protein bands were visualized by coomassie blue staining.

3.3.6 Protein concentration

Concentration of the protein was done by centrifugation using Centriprep centrifugal filters devices with regenerated cellulose membranes and cut off of 50, 30 or 10 (Millipore), depending on the size of the molecule. The protocol followed the manufacturer's instructions.

3.3.7 Protein concentration determination

The protein concentration was determined by spectroscopy, measuring the absorbance of the protein by UV at 280 nm (OD_{280} ; Nanophotometer, IMPLLEN). The protein concentration was calculated by the equation:

$$\text{Protein concentration (mg/ml)} = OD_{280} \times \text{dilution} / \text{extinction coefficient (g/l)}$$

The extinction coefficient (ϵ) was calculated based on the primary sequence of each construct by the ProtParam tool found in the ExPASy proteomics website (<http://www.expasy.ch/>).

3.3.9 Protein storage

Purified proteins were stored by flash-freezing in liquid nitrogen and subsequently kept at - 80° C.

3.3.10 Differential scanning fluorimetry (DSF)

DSF was employed to screen an optimal buffer for protein stability. The temperature of the protein unfolding is monitored *via* the rise in the dye SYPRO Orange (Invitrogen) fluorescence signal while binding to hydrophobic patches of the protein that become accessible during the heating process (20° C to 95° C). The more stable a protein in a given condition is, the later it will start to unfold and the higher the melting temperature (T_m) will be (Ericsson et al., 2006).

Screens with 24 different conditions of buffers, in different range of pH and ion strength were prepared in a 96-well plate with 4x repetition to avoid pipetting errors.

The reaction was performed in a final volume of 25 μ l: 12.5 μ l buffer, 5 μ l protein (~1 mg/ml) and 7.5 μ l dye diluted 1/1000. The experiments were carried out in several Real-Time PCR machines with filters calibrated to absorb signals from the SYPRO Orange dye: Mx3005 Real-Time QPCR System (Stratagene), Mastercycler *eprealplex* (Eppendorf) and iQ5 multicolour Real-Time PCR Detection System (Bio-Rad).

3.3.10.1 Binding of inositol hexakisphosphate (IP6) to ABD

DSF was also applied to study the binding of inositol hexakisphosphate (IP6) to 2ABDa WT. The measurements were performed with different concentrations of IP6 diluted in 20 mM PIPES pH 7.5, 100 mM NaCl. The IP6 concentrations ranged from 0.02 mM to 1.5 mM and the final reaction volume was set to 15 μ l: 7.5 μ l protein (~60 μ M) and 4.5 μ l dye diluted 1/1000.

3.3.11 Dynamic light scattering (DLS)

DLS was used to evaluate the purity of a given protein sample before setting up crystallization trials. In this technique the hydrodynamic diameter of particles in solution is measured under a monochromatic light (laser) beam. The particles in Brownian motion in solution cause fluctuations in the scattered light intensity according to their composition. Protein solution in different oligomerization states (aggregates, monomers, dimers, etc) scatter light in a variety of intensities measured by a detector placed at a 90° angle to the incident laser light. Sample purity can therefore be measured according to its population (Borgstahl, 2007). It is believed that monodisperse samples (> 80%) are more likely to crystallize (D'Arcy, 1994).

DLS measurements were made in a DynaPro-801 instrument (Protein Solutions Inc.) at 22° C with 100 acquisitions taken at 1 s intervals each one. Data analysis was performed using the Dynamics V6 software (Protein Solutions Inc.).

3.3.12 Protein reductive methylation

Protein reductive methylation is a chemical modification method employed to alter the crystallization properties of the protein. This chemical modification generates changes in the surface charges of the protein that could enhance the crystal packing potential of the protein during the crystallization process. This change of surface charges occurs because primary free amino groups found in lysine residues (K) or in the N-terminal of the protein can be changed to secondary amino groups or tertiary amino groups (Figure 3.2).

The methylation protocol was established by Thomas S. Walter and co-workers (Walter et al., 2006). However, all samples submitted to methylation were previously purified (section 3.13) and subsequently dialyzed against the methylation buffer (50 mM HEPES pH 7.5, 250 mM NaCl). After the methylation process, the samples were re-purified through size exclusion chromatography with the appropriated buffer (section 4.3).

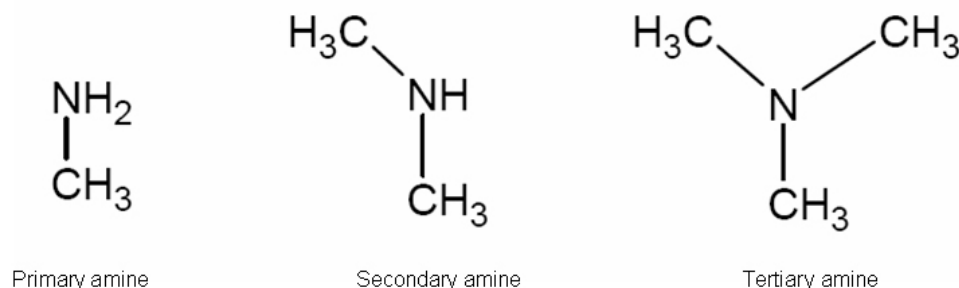


Figure 3.2 Different amino groups: primary (found in K or N-terminal region of proteins), secondary and tertiary.

3.3.13 Surface entropy reduction (SER) mutations

SER is a method that can enhance the crystallizability of a protein by reducing the phase transition energy barrier. This reduction occurs when cluster of surface residues with high conformational entropy are mutated to residues with lower ones, e.g. mutation of glutamate (E), lysine (K) or arginine (Q) to alanine [A;(Derewenda, 2004a)].

Since α -actinin is a recalcitrant protein to crystallization, the 2AFL construct was submitted to SER mutations. The choice of clusters to be mutated was done using the web service <http://nihserver.mbi.ucla.edu/SER/> which takes into account the entropy of the residues within a continuous stretch, predicted secondary structure and sequence conservation (Goldschmidt et al., 2007).

The website generated double-site and triple-site mutation clusters. The mutations were done using the Site-directed Mutagenesis Kit (Qiagen) and specific oligonucleotides (Table 3.1) following the manufacturer's instructions. The mutation sites were validated by DNA sequencing.

3.3.14 Characterization of ABD mutants

3.3.14.1 Mutants

Single-site mutants were designed to validate the proposed phosphatidylinositol (4, 5)-biphosphate (PiP₂) binding site within the ABD of α -actinin (Franzot et al., 2005). It has been suggested that this binding site is formed by arginine residues R163, R169 and R192 (numbering according to human α -actinin isoform 2).

The single R residues were mutated to glutamate (E) using the Site-directed Mutagenesis Kit (Qiagen) and specific oligonucleotides (Table 3.1) following the manufacturer's instructions. The mutation site was validated by DNA sequencing.

3.3.14.2 PiP strips

In order to study the binding of α -actinin 2ABDa WT and its mutants to different types of phosphoinositide [phosphatidylinositol (PtdIns), phosphatidylinositol 3-phosphate (PtdIns(3)P), phosphatidylinositol 4-phosphate (PtdIns(4)P), phosphatidylinositol 5-phosphate (PtdIns(5)P), phosphatidylinositol 3,5-biphosphate (PtdIns(3,5)P₂), phosphatidylinositol 4,5-biphosphate (PtdIns(4,5)P₂), phosphatidylinositol 3,4-biphosphate (PtdIns(3,4)P₂), phosphatidylinositol 3,4,5-triphosphate (PtdIns(3,4,5)P₃)], the proteins were submitted to PiP strips membrane binding method. The negative control was the protein chlorite dismutase (kindly provided by Julius Kostan). PiP strips were purchased from Echelon Biosciences Inc. and the protocol was according to the manufacturer's instructions.

3.3.14.3 Isothermal titration calorimetry (ITC)

ITC was used to study the binding of α -actinin 2ABDa WT and mutants to inositol triphosphate (IP3; Sigma). It is a technique used to study molecular interactions and can provide information such as stoichiometry (n), binding affinity (K_a), heat of binding (ΔH), entropy (ΔS), free energy (ΔG) and dissociation constant (K_d ; which is the inverse of the K_a). The principle of ITC is based on measurements of the heat released or absorbed when a protein is titrated with a hypothetical ligand. Its signal depends on the protein and ligand concentrations, the cell volume, the injected volume and the values of n , K_a and ΔH (Lewis and Murphy, 2005).

Titration of 2.5 mM IP3 into solutions of 266 μ M 2ABDa WT, 116 μ M Δ 2ABDa R169E and 379 μ M Δ 2ABDa R192E was carried out at 25° C in a VP-ITC Microcalorimeter (MicroCal). The IP3 was titrated using a 250 μ l rotating syringe into a sample cell containing the given sample. One initial injection of 2 μ l was followed by 29 injections of 10 μ l.

IP3 was dissolved to suitable concentration into the buffer used for protein dialysis (20 mM Na citrate pH 7.0, 100 mM NaCl) and all samples were degassed prior the experiment.

Data analysis was performed using the ORIGIN version 7 software (MicroCal) by peak integration and the binding data were fitted to the "one sites" model.

3.3.14.4 Circular dichroism (CD)

Near-UV CD was performed to gain information about conformational changes of 2ABDa WT upon binding of IP6 [Sigma; reviewed by (Kelly and Price, 2000)]. CD measurements were carried out on an Applied Photophysics PiStar-180 spectrometer, using a 1 mm path length quartz cell (Hella). Near-UV CD signals between 240nm and 360nm were measured for 2ABDa WT and 2ABDa WT with a tenfold excess of IP6 in 20 mM PIPES pH 7.5, 100 mM NaCl. Data was collected at 25° C, with a step size of 1 nm.

3.3.14.5 Nuclear magnetic resonance spectroscopy (NMR)

In order to study the binding of 2ABDa WT to IP3, the sample was submitted to 2D-NMR and selective T1 measurement. The experiments were carried out and analysed by Dr. Bettina Schweng (Department of Biomolecular Structural Chemistry, University of Vienna).

A) ^{15}N – labelling of ABD

To carry out the 2D-NMR experiments, the protein was ^{15}N -labelled using the following protocol: a pre-culture with *E. coli* (DE3) Rosetta pLysS carrying the ABDa WT insert cloned into pETM11 was grown in LB medium over night at 37° C. 8 ml of this pre-culture were diluted in 1 l of M9 minimal medium [6 g Na_2HPO_4 , 3 g KH_2PO_4 , 0.5 g NaCl diluted in 1 l Milli-Q water, followed by autoclaving. Prior to use, 2 ml of 1 M MgSO_4 and 20 ml of 20% D-glucose- $^{13}\text{C}_6$ (ISOTEC) were added] containing 1 g ammonium- ^{15}N chloride, 98 + atom% ^{15}N ($^{15}\text{NH}_4\text{Cl}$; ISOTEC) and appropriate antibiotics (Table 3.3). When an OD_{600} around 0.6 was reached, the temperature was decreased from 37° C to 20° C and the protein was induced over night by 0.5 μM IPTG.

B) Two-dimensional NMR

2D-NMR experiments were performed with 1 mM 2ABDa WT ^{15}N -labelled and IP3 in different concentration ratios, ranging from 1:1 to 1:6. Experiments were performed at 25° C in a Varian Unity 800 MHz spectrometer (Varian).

C) Selective T1 measurement

Selective T1 measurement was applied to study IP3 and non-labelled 2ABDa WT binding and the experiments were performed at 25° C in a Varian Unity 600 MHz spectrometer (Varian). In this experiment 100 μM IP3 were added to 10 μM 2ABDa WT and the measurement done.

3.3.15 Protein crystallization experiments

Pure protein solutions at different concentrations were submitted to crystallization trials with or without N-terminal 6x His-tag. Concentrations used were evaluated using the Pre-Crystallization Test kit (PCT, Hampton Research) following the manufacturer's instructions. Initial crystallization conditions were screened at 22° C using commercial screens such as Grid screen, PEG/Ion screen, Index 1-2 and Crystal screen 1-2 from Hampton Research; JBS 1-10 from JenaBioscience; Wizard 1-2 and Cryo1-2 from Emerald Biostructures; JSCG+ Suite and PACT Suite from QIAGEN. These initial screenings were performed by robot assisted nano-drop vapour diffusion (Cartesian, Zinsser Analytic or Phoenix, Rigaku) in drops formed with condition and protein solutions ratio of 1:1 and 1:2 (v/v).

The optimization of crystallization conditions was performed manually with sitting or hanging drop vapour diffusion methods at different temperatures (22 °C, 14 °C and 4 °C) and by grid screen, altering the buffer pH and precipitant concentration. Drops had volume ratio mother liquor to protein solution of 1:1 or 1:2, depending on the construct. Crystal hits were obtained in times varying from a few days to several months, also depending on the construct.

Once the best crystallization condition was found, the additive screen (Hampton Research) was used following the manufacturer's instructions.

3.3.15.1 ABDY soaking and co-crystallization

In order to check the PIP2 binding site within α -actinin ABD, diffraction-quality crystals from 2ABDY were soaked with IP3 or IP6. Co-crystallization experiments with IP3 were also attempted.

Soaking was done adding different concentrations of IP3 or IP6 to the cryo-solution. The cryo-solution was obtained adding PEG [25% to 30% (v/v)] to the mother liquor and the MW of the PEG was dependent on the mother liquor. The concentration of IP3 or IP6 used ranged from 10 mM to 15 mM (final concentration). Different soaking times ranged from 1 to 40 min.

The co-crystallization was done by adding 5 mM of IP3 to the protein sample (10 mg/ml). The mixture was incubated (at 30 °C, 30 min) and centrifuged (20.000 rpm, 20 min, at 4 °C). Subsequently, it was submitted to crystallization trials.

3.3.16 Data collection

Crystals used for data collection were soaked briefly in cryo-solution and then flash-frozen in liquid nitrogen or directly in the cryostream. Data were collected at 100 K using an ADSC Q315 detector at the ESRF beamline ID23-1 and the MAR225 detector at the ESRF beamline ID23-2.

The X-ray Detector Software program package [XDS; (Kabsch, 1993)] was used for processing the collected data. The diffraction images were displayed and the pictures were made by the ADXV software.

3.3.17 Structural determination, model building, refinement and validation

All ABD structures were solved by the molecular replacement (MR) method (Rossmann, 1990; Rossmann and Blow, 1962) using the program MOLREP (Vagin

and Teplyakov, 1997) , part of the Collaborative Computational Project No. 4 (CCP4). The model used as search model was the structure of human α -actinin ABD isoform 3 [PDB entry 1WKU; (Franzot et al., 2005)], excluding the water molecules.

Refinement of the structures was performed using REFMAC5 (Murshudov et al., 1997), also from CCP4. Model building was done using the program Crystallographic Object-Oriented Toolkit [Coot; (Emsley and Cowtan, 2004)].

Structure validation was done using the MolProbity web service <http://molprobity.biochem.duke.edu/> (Davis et al., 2004) and the molecule was visualized using the PyMOL molecular viewer software (DeLano Scientific LLC).

3.3.18 Small angle x-ray scattering (SAXS)

SAXS was used to study conformational changes in the N-terminal or C-terminal regions of α -actinin in the presence of Ca^{2+} ions. The scattering patterns of α -actinin 2Eh, human AFL and hd of both isoforms (1 and 2) were measured at solute concentrations ranging from 0.5 mg/ml to 6.0 mg/ml. Isoform 1 and Eh2 constructs were purified in standard buffer in the presence and absence of 2 mM CaCl_2 , while the constructs for isoform 2 were purified only with standard buffer (20 mM Tris-HCl pH 7.6, 150 mM NaCl). Sample purity was verified by DLS before the SAXS measurements.

Data were collected on beamline X33 at the DORIS storage ring of DESY (Hamburg) using a MAR345 image plate detector and analysed by the collaborators, Dr. Dmitri Svergun and Dr. Peter Konarev (EMBL-Hamburg outstation). The forward scattering $I(0)$ and the radius of gyration (R_g) were evaluated using the Guinier approximation, by the program GNOM (Svergun, 1992). The low resolution shape analysis of the SAXS data was done *ab initio* using the program DAMMIN (Svergun, 1999).

The low resolution molecular envelope was fit with the structure of individual domains by rigid body modelling using the software BUNCH (Petoukhov and Svergun, 2005).

4. RESULTS

4.1 Constructs, gene amplification and selection

4.1.1 α -actinin

DNA fragments for the constructs listed in Table 4.1 were amplified by PCR, except for human α -actinin full length (AFL) and half dimer (hd), kindly provided by Dr. Jari Yläne. Isoform 2 of *Entamoeba histolytica* α -actinin (2Eh) was cloned by the collaborators (Dr. Lars Backman).

The PCR products were of expected sizes (Figure 4.1) and were cloned into expression vectors listed in Table 4.1. Positive clones were subsequently selected through colony PCR and DNA sequencing.

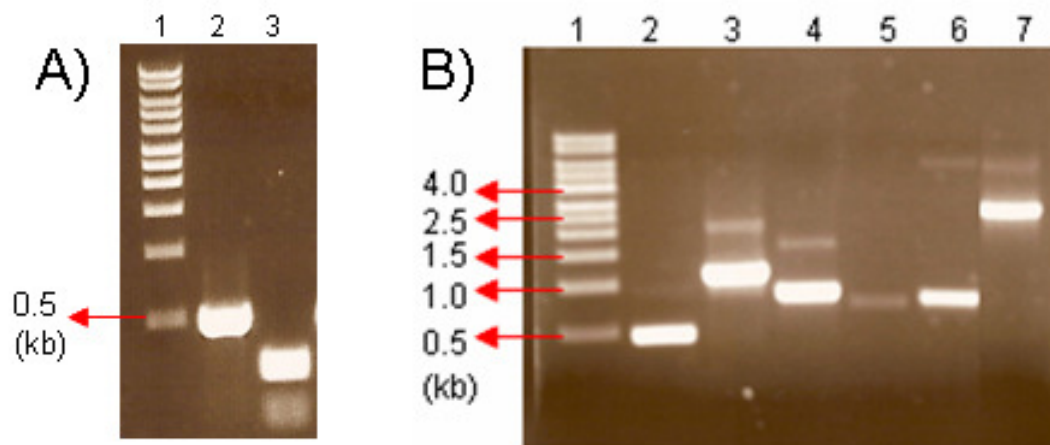


Figure 4.1 PCR products of human α -actinin obtained using the full length construct as a template and specific oligonucleotides (Table 3.1). DNA samples were resolved by 1% agarose gel. **A)** Column 1- DNA marker (kb), 2- CaM (435 pb) and 3- EF-3/4 (218 pb). **B)** Column 1- DNA marker (kb), 2- CaM (435 pb), 3- ABDa_SR1 (1070 pb), 4- SR4_CaM (800 pb), 5- 2ABDa (800 pb), 6- 2ABDY (780 pb) and 7- Δ 2AFLY (2600 pb).

Table 4.1 α -Actinin constructs designed for this project, expression vectors used for cloning and respective protein molecular weight (MW). Numbers in front of constructs abbreviations refer to α -actinin isoform in context (human isoforms: 1 = non-muscle or 2 = muscle). **Y** means that the construct starts at tyrosine residue 19 and **a**; the construct starts at the ABD.

Construct	Vector	MW (kDa)
1, 2ABDa_SR1	pETM13dsbAGSHISTEV	61
2SR4_CaM	pETM13dsbAGSHISTEV	50
1, 2ABDa_SR1	pETM20	57
1SR4_CaM	pETM20	46
1, 2CaM	pETM20	33
1, 2CaM	pETM13 GST	43
1, 2EF-3/4	pETM13 GST	34
1SR4_CaM	pETM13 GST	46
1, 2SR4_CaM	pETM13	30
1, 2CaM	pETM13	17
1, 2EF-3/4	pETM13	8
2SR4_CaM	pETM11	32
2ABDa_SR1	pETM11	43
2CaM	pETM11	18
2ABDa	pETM20	42
2ABDa	pETM13 GST	52
2ABDa	pETM11	27
Δ 2ABDa R169E	pETM11	27
Δ 2ABDa R192E	pETM11	27
2ABDY	pETM11	31
Δ 2AFL E23/ E24/ E25A	pET8C	105
Δ 2AFL E310/ K311A	pET8C	105
Δ 2AFLY (E310/ K311A)	pETM11	103
1, 2AFL (WT)	pET8C	105
1, 2hd (ABD_SR1_SR2//SR3_SR4_CaM)	pET8C	60 + 40
2Eh	pET19b	73.5

4.1.2 PDZ domain of ZASP

PDZ domain fragment was amplified by PCR (Figure 4.2) and cloned into expression vectors such as pETM13 GST and pETM13dsbAGSHISTEV (Table 3.2). Positive clones were then selected through colony PCR and DNA sequencing.

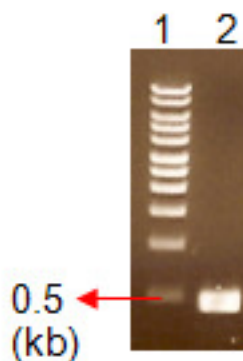


Figure 4.2 PCR product of the PDZ domain obtained using ZASP full length as a template and specific oligonucleotides (Table 3.1). DNA sample was resolved by 1% agarose gel. Column 1- DNA marker (kb) and 2- PDZ (430 pb).

4.2 Over-expression of recombinant proteins

4.2.1 Expression of AFL, 2Eh, hd, ABD and PDZ domain of ZASP

Over-expression of proteins AFL, 2Eh, hd, ABD (Figure 3.1) and PDZ was checked by SDS-PAGE. Since they were in the soluble fraction of the cell lysate they were submitted to purification steps.

4.2.2 Co-expression systems for α -actinin

With the objective of obtaining the complex of different domains of α -actinin (ABD_SR1 with CaM or EF-3/4; Figure 3.1), plasmids containing the α -actinin desired inserts were co-transformed in different *E. coli* strains (Table 4.2). The protein overexpression was checked by SDS-PAGE (Figure 4.3).

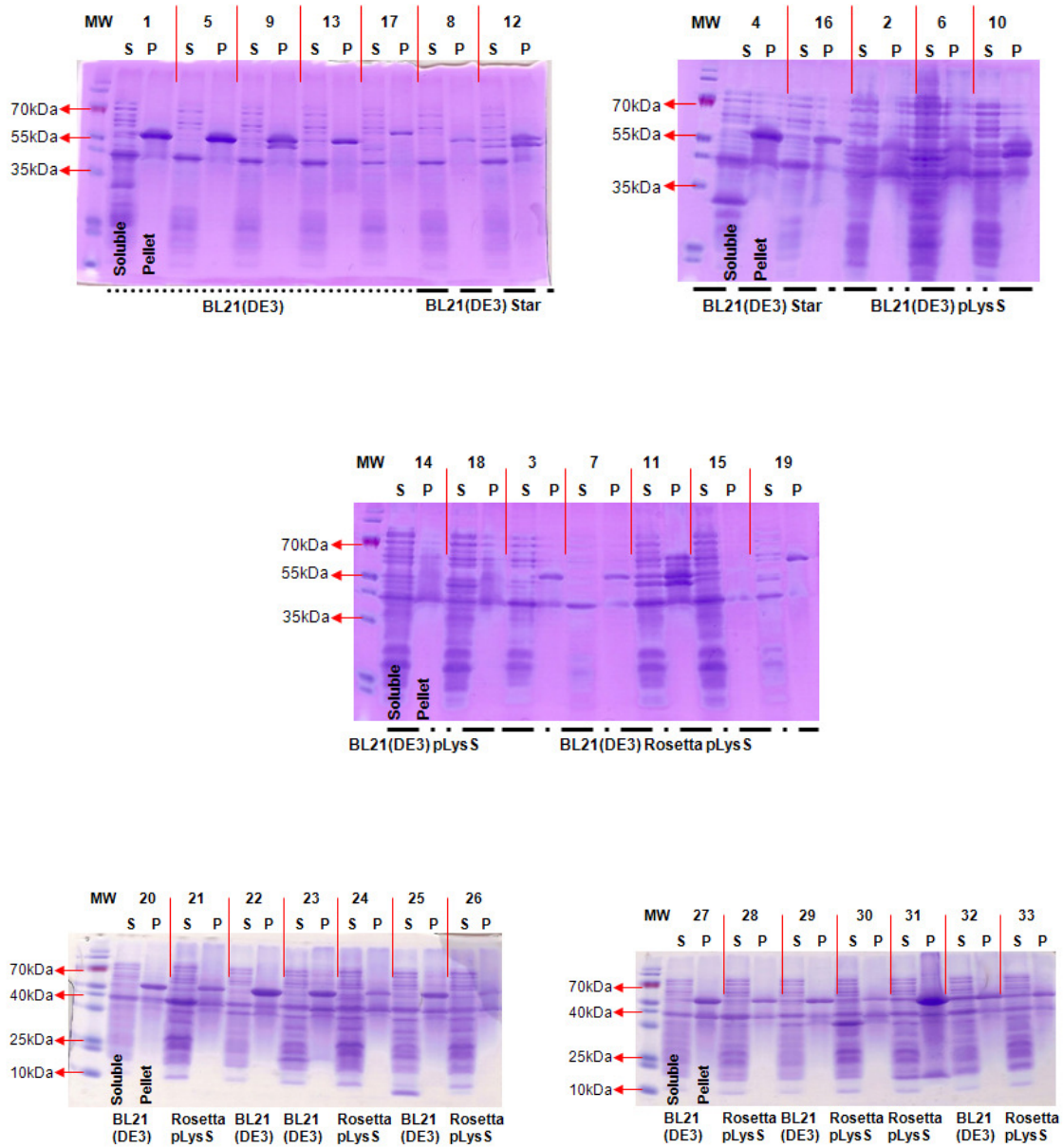


Figure 4.3 15% SDS-PAGE of small scale co-expression experiments of human α -actinin ABD_a_SR1 + SR4_CaM or CaM or EF-3/4 of both isoforms (1 and 2) at 37° C. Different constructs and *E. coli* strains are described at Table 4.2. The strains are also indicated under the gel. **S** is an abbreviation to soluble fraction of cell lysate, while **P** stands for pellet (insoluble fraction of the cell lysate).

Table 4.2 Co-transformation constructs and *E. coli* strains for over-expression experiments. Last column named “Figure 4.3” relates the co-expression results showed at Figure 4.3 to their respective constructs and strain.

Construct A	Construct B	Strains	Figure 4.3
1ABDa_SR1 pETM20 (His-tag + TrxA) 57kDa	1SR4_CaM pETM13 (GST-tag) 45kDa	BL21 (DE3)	1
		BL21 (DE3) pLysS	2
		BL21 (DE3) Rosetta pLysS	3
		BL21 (DE3) Star	4
	1SR4_CaM pETM13 (no tag) 30kDa	BL21 (DE3)	5
		BL21 (DE3) pLysS	6
		BL21 (DE3) Rosetta pLysS	7
		BL21 (DE3) Star	8
	1CaM 42kDa pETM13 (GST- tag)	BL21 (DE3)	20
		BL21 (DE3) Rosetta pLysS	21
	1EF-3/4 34kDa pETM13 (GST- tag)	BL21 (DE3)	22
	1CaM 16kDa pETM13 (no tag)	BL21 (DE3)	23
		BL21 (DE3) Rosetta pLysS	24
	1EF-3/4 8kDa pETM13 (no tag)	BL21 (DE3)	25
BL21 (DE3) Rosetta pLysS		26	
2ABDa_SR1 pETM20 (His-tag + TrxA) 57kDa	2SR4_CaM pETM13 (His-tag + DsbA) 50kDa	BL21 (DE3)	9
		BL21 (DE3) pLysS	10
		BL21 (DE3) Rosetta pLysS	11
		BL21 (DE3) Star	12
	2SR4_CaM pETM13 (no tag) 30kDa	BL21 (DE3)	13
		BL21 (DE3) pLysS	14
		BL21 (DE3) Rosetta pLysS	15
		BL21 (DE3) Star	16
	2CaM 42kDa pETM13 (GST- tag)	BL21 (DE3)	27
		BL21 (DE3) Rosetta pLysS	28
	2EF-3/4 34kDa pETM13 (GST- tag)	BL21 (DE3)	29
		BL21 (DE3) Rosetta pLysS	30
		BL21 (DE3) Rosetta pLysS	31
	2EF-3/4 8kDa pETM13 (no tag)	BL21 (DE3)	32
		BL21 (DE3) Rosetta pLysS	33
	1SR4_CaM pETM20 (His-tag + TrxA) 46kDa	1ABDa_SR1 pETM13 (His-tag + DsbA) 61kDa	BL21 (DE3)
BL21 (DE3) pLysS			18
BL21 (DE3) Rosetta pLysS			19

4.3 Differential scanning fluorimetry (DSF)

DSF was carried out to find the optimal stable buffer for protein purification, in attempt to enhance the probability to obtain protein crystals. The initial protein buffer was 20 mM Tris-HCl pH 7.6, 150 mM NaCl and this was not the optimal buffer suggested by this technique for any of the tested proteins (Table 4.3). The melting curves for the constructs are shown in Figures 4.4 and 4.5.

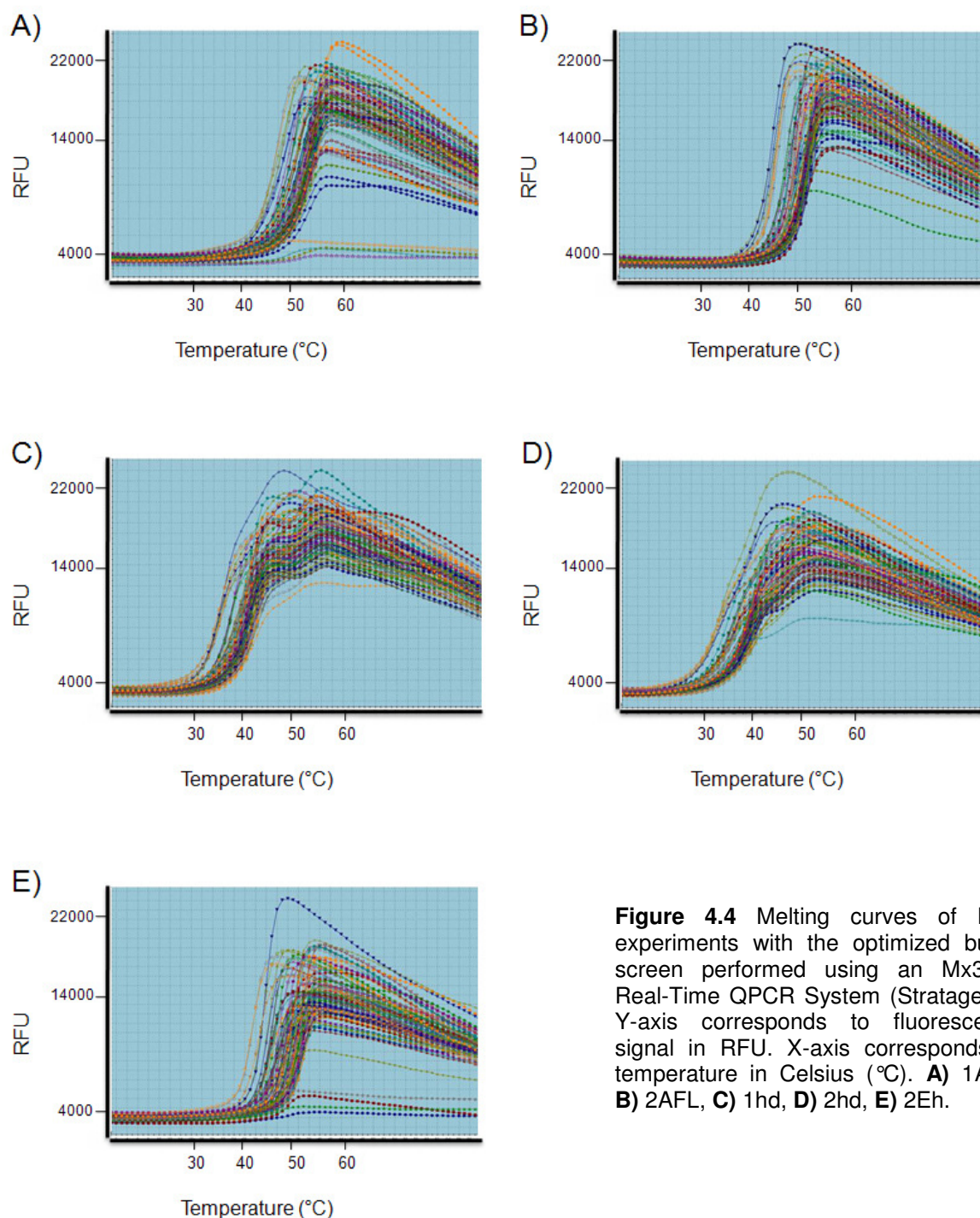


Figure 4.4 Melting curves of DSF experiments with the optimized buffer screen performed using an Mx3005 Real-Time QPCR System (Stratagene). Y-axis corresponds to fluorescence signal in RFU. X-axis corresponds to temperature in Celsius (°C). **A) 1AFL**, **B) 2AFL**, **C) 1hd**, **D) 2hd**, **E) 2Eh**.

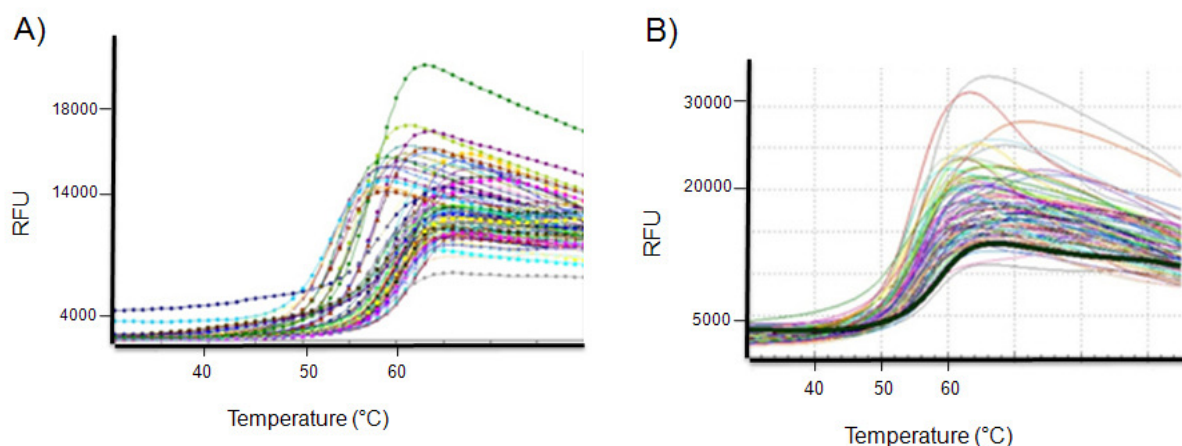


Figure 4.5 Melting curves of DSF with the optimized buffer screen. Y-axis corresponds to fluorescence signal in RFU. X-axis corresponds to temperature in Celsius (°C). **A)** 2ABDa performed using a Mastercycler eprealplex (Eppendorf), **B)** Δ 2AFLY performed in an iQ5 multicolour Real-Time PCR Detection System (Bio-Rad).

Table 4.3 Optimal stable buffers resulted from DSF and the difference (Δ) in melting temperature (T_m) between initial and optimal buffers.

Protein	Optimal buffer	ΔT_m (°C)
1AFL	20 mM TES pH 8.0, 150 mM NaCl	3
2AFL	20 mM Na cacodylate pH 6.5, 150 mM NaCl	5
Δ 2AFLY	20 mM HEPES pH 8.0, 150 mM NaCl	6
1hd	20 mM Na cacodylate pH 6.5, 150 mM NaCl	4
2hd	20 mM PIPES pH 7.5, 150 mM NaCl	4
2ABDa	20 mM PIPES pH 7.5, 150 mM NaCl	8
2Eh	20 mM Na cacodylate pH 6.5, 150 mM NaCl, 2 mM CaCl_2	2

4.4 Purification of recombinant proteins

4.4.1 Purification of AFL, 2Eh, hd and ABD

Three steps of protein purification were carried out for AFL, 2AFLY and 2Eh (Figure 3.1) including gravity flow IMAC, ion exchange and size exclusion chromatography. In the case of hd, 2ABDa and 2ABDY (Figure 3.1) two-step purification protocol including gravity flow IMAC and size exclusion chromatography was sufficient to achieve high purity.

Figures 4.6, 4.7, 4.8, 4.9 and 4.10 show the high levels of purity achieved after purification. In the case of AFL, hd or ABD purification, only the chromatograms of one construct [2AFL or 2AFL(Y); 2ABDa or 2ABDY] or one isoform (1hd or 2hd) are

shown, since the constructs or isoforms present similar elution volume and purity. Purification yields are described in Table 4.4.

Size exclusion chromatography for each protein was performed with the optimal buffer suggested by DSF (Table 4.3).

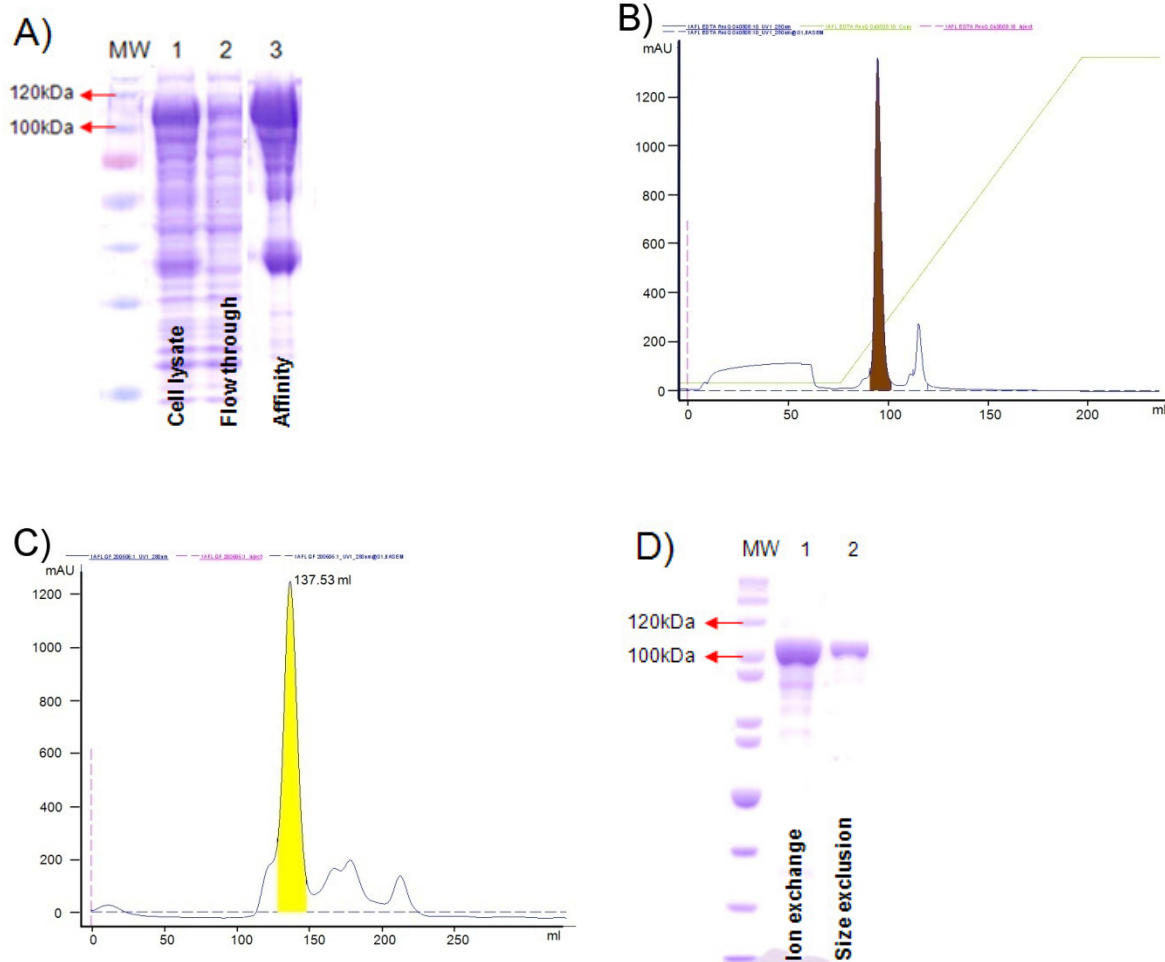


Figure 4.6 Protein purification of 1AFL. **A)** 12% SDS-PAGE of fractions obtained from the gravity flow IMAC. Columns 1- cell lysate, 2- flow through, 3 - elution fraction. **B)** Ion exchange chromatography of 1AFL carried out in a Resource Q column. **C)** SEC of 1AFL carried out in a Superdex200 HiLoad 26/60 column equilibrated with 20 mM TES pH 8.0, 150 mM NaCl. **D)** 12% SDS-PAGE of 1AFL pooled fractions obtained from ion exchange chromatography and SEC. Columns: 1- pool fractions corresponding to the peak of ion exchange chromatography, highlighted in brown (B), 2- pool fractions corresponding to the peak of SEC, highlighted in yellow (D).

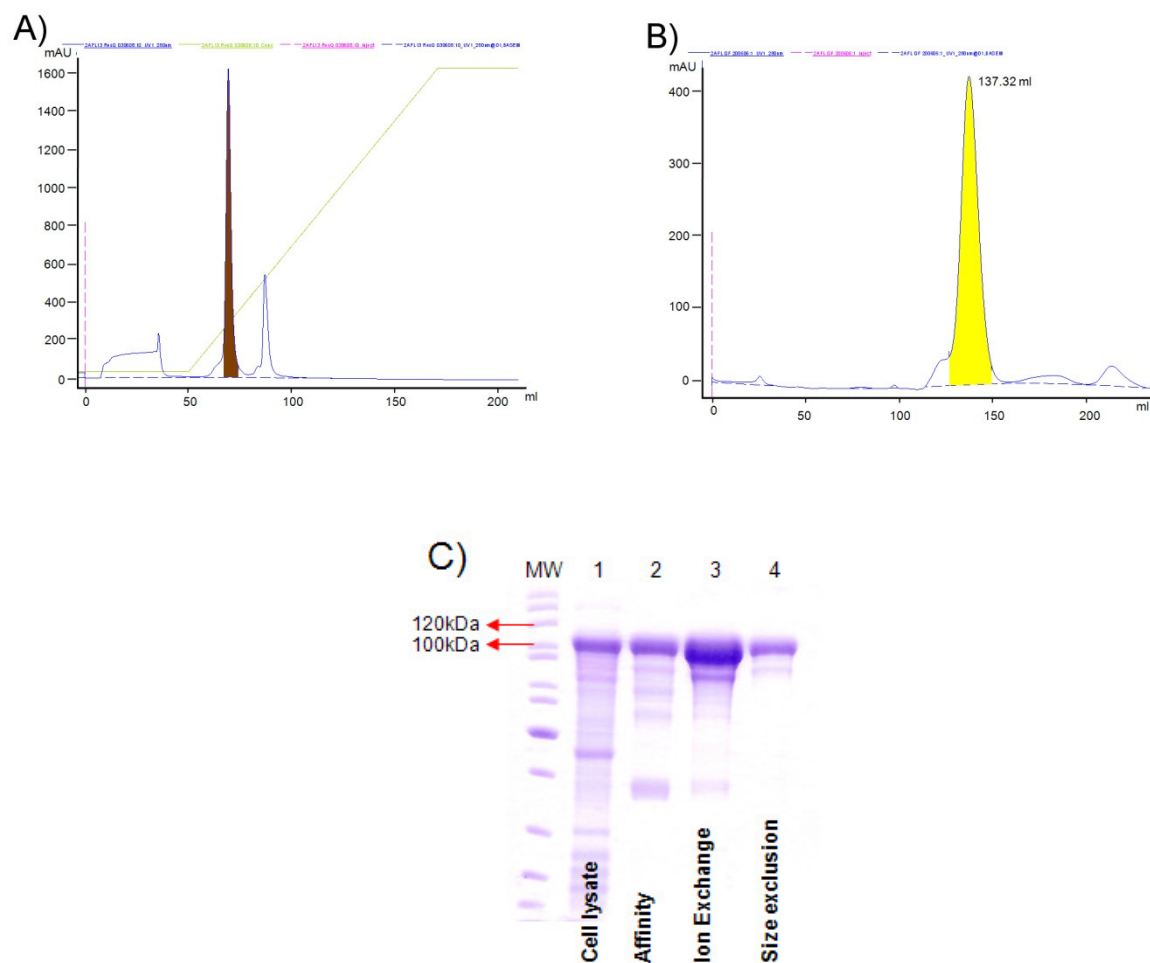


Figure 4.7 Protein purification of 2AFL (Figure 3.1). The pictures shown are for 2AFL to illustrate how the molecule behaves independent of the construct (2AFL or Δ 2AFLY), with similar elution volumes and purity. **A)** Ion exchange chromatography of 2AFL carried out in a Resource Q column. **B)** SEC of 2AFL carried out in a Superdex200 HiLoad 26/60 column equilibrated with buffers: 2AFL = 20 mM Na cacodylate pH 6.5, 150 mM NaCl; Δ 2AFLY = 20 mM HEPES pH 8.0, 150 mM NaCl. **C)** 12% SDS-PAGE of 2AFL pooled fractions obtained from gravity flow IMAC, ion exchange chromatography and SEC. Columns: 1- cell lysate, 2- pooled fractions obtained from gravity flow IMAC, 3- pooled fractions corresponding to the peak of ion exchange chromatography, highlighted in brown (A), 4- pooled fractions corresponding to the peak of SEC, highlighted in yellow (B).

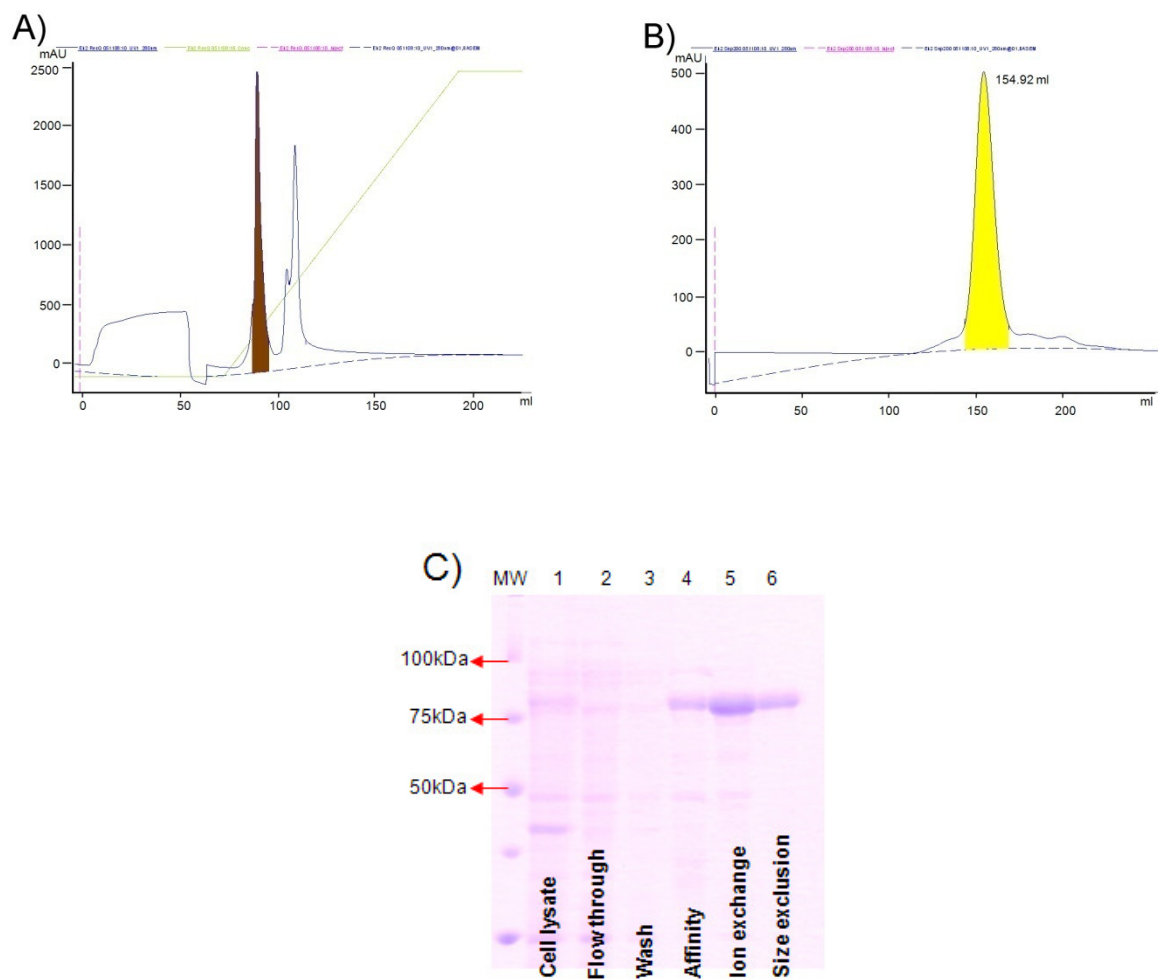


Figure 4.8 Protein purification of 2Eh (Figure 3.1). **A)** Ion exchange chromatography of 2Eh carried out in a Resource Q column. **B)** SEC of 2Eh carried out in a Superdex200 HiLoad 26/60 equilibrated with 20 mM Na cacodylate pH 6.5, 150 mM NaCl, 2 mM CaCl₂. **C)** 12% SDS-PAGE of 2Eh of pooled fractions obtained from gravity flow IMAC, ion exchange chromatography and SEC. Columns: 1- cell lysate, 2- flow through, 3- washing step, 4- pooled fractions obtained from gravity flow IMAC, 5- pooled fractions corresponding to the peak of ion exchange chromatography, highlighted in brown (A), 6- pooled fractions corresponding to the peak of SEC, highlighted in yellow (B).

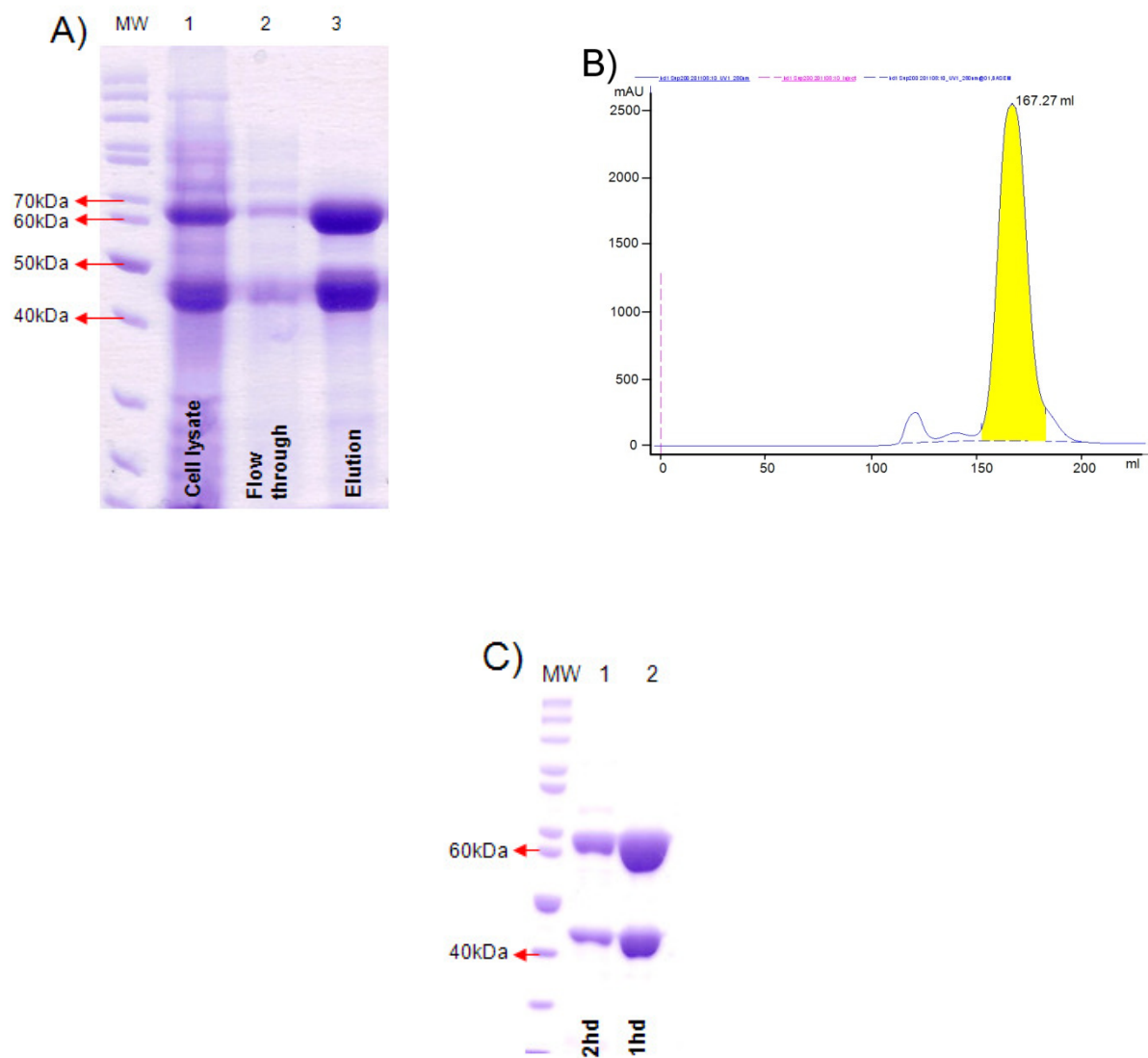


Figure 4.9 Protein purification of hd (Figure 3.1). The pictures shown are for 2hd to illustrate how the hd molecule behaves independent of the isoform (1hd or 2hd), since they present similar elution volume and purity. **A)** 12% SDS-PAGE of 2hd pooled fractions obtained from the gravity flow IMAC. Columns 1- cell lysate, 2- flow through and 3- elution fraction. **B)** SEC of 2hd carried out in a Superdex200 HiLoad 26/60 column equilibrated with buffers: 1hd = 20 mM Na cacodylate pH 6.5, 150 mM NaCl; 2hd = 20 mM PIPES pH 7.5, 150 mM NaCl. **C)** 12% SDS-PAGE of pooled fractions obtained from SEC. Columns: 1- pooled fractions corresponding to the peak of 2hd SEC, highlighted in yellow (B), 2- pooled fractions obtained from SEC of 1hd (chromatogram not shown).

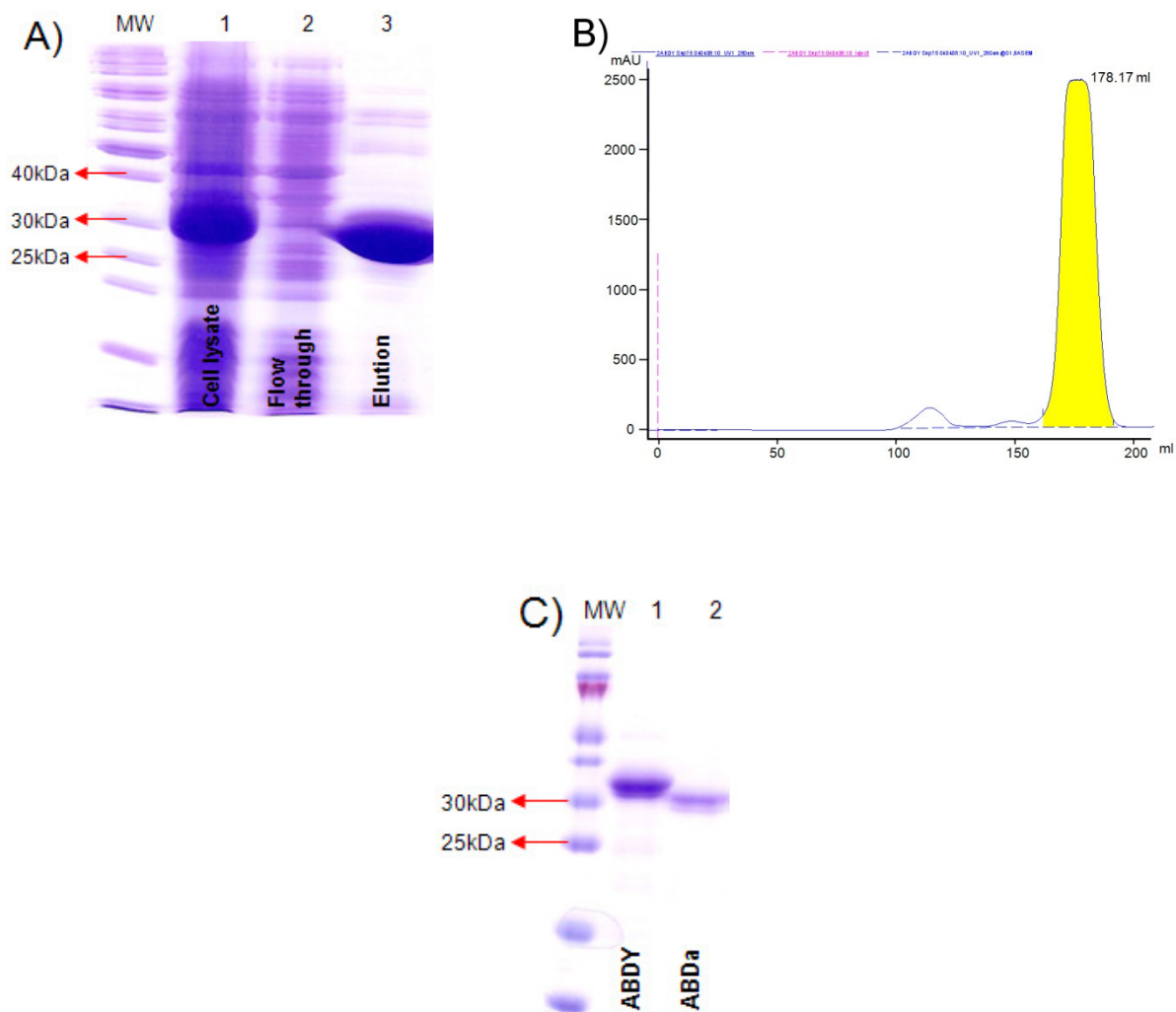


Figure 4.10 Protein purification of 2ABD. **A)** 15% SDS-PAGE of 2ABDY pooled fractions obtained from the gravity flow IMAC. Columns 1- cell lysate, 2- flow through and 3- elution fraction. **B)** SEC of 2ABDY just to show how the ABD molecule behaves, independent of the construct (2ABDa or 2ABDY; Figure 3.1). This chromatography was carried out in a Superdex75 HiLoad 26/60 column equilibrated with 20 mM PIPES pH 7.5, 150 mM NaCl, for both constructs. **C)** 15% SDS-PAGE of pooled fractions obtained from SEC. Columns 1- pooled fractions corresponding to the peak of 2ABDY size exclusion chromatography, highlighted in yellow (B), 2- SEC elution of 2ABDa (chromatogram not shown).

Table 4.4 Protein yield per litre of culture.

Protein	Yield/l (mg)
1AFL	6
2AFL (Y)	4
2ABDa	12
2ABDY	20
1hd	6
2hd	4
2Eh	3

4.4.2 Purification of a co-expression system: 2ABDa_SR1 + 2SR4_CaM

The most promising complex obtained from co-transformation experiments [Sample 15 in Figure 4.3: 2ABDa_SR1 (His-tagged) + 2SR4_CaM (not tagged)] was induced over night at 20°C. After this period the supernatant of the cell lysate was submitted to gravity flow IMAC and size exclusion chromatography. The low purity and low concentration of the eluted complex were assessed by SDS-PAGE (Figure 4.11).

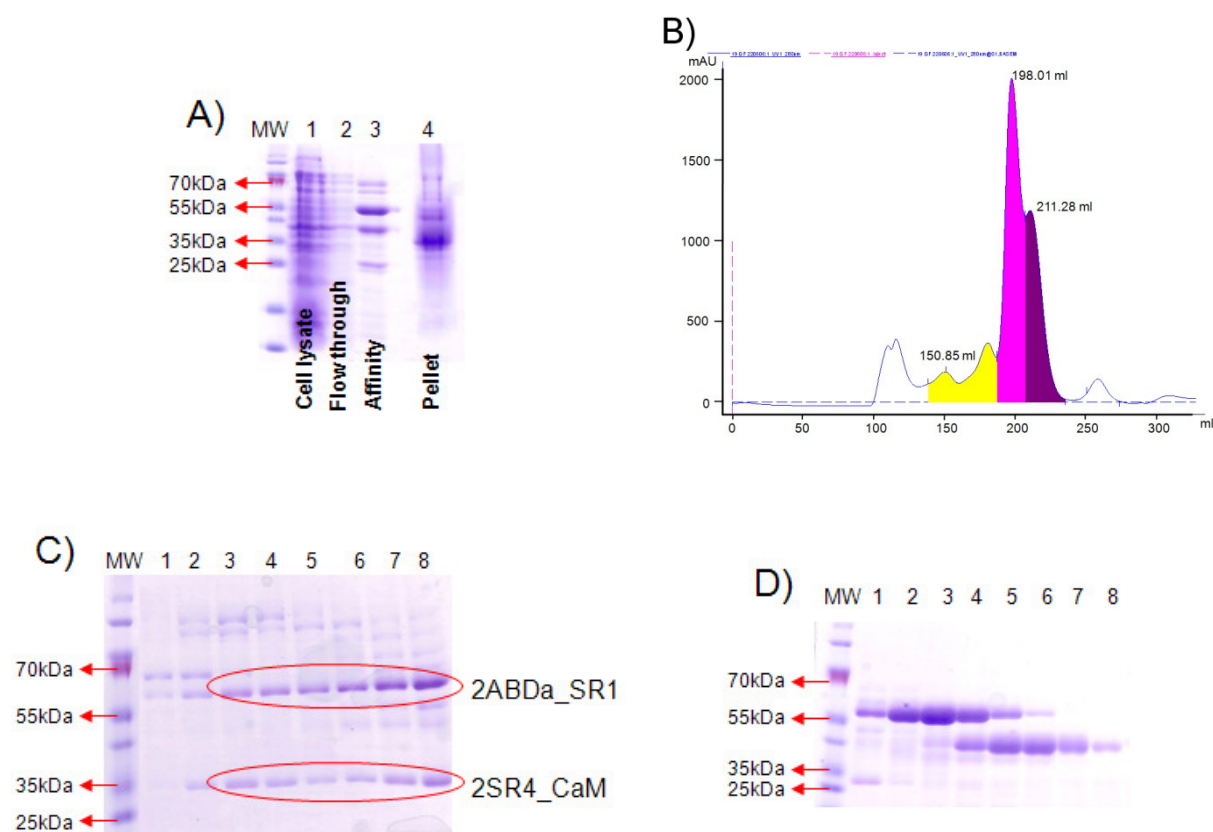


Figure 4.11 Purification of the 2ABDa_SR1 + 2SR4_CaM complex. **A)** 15% SDS-PAGE of pooled fractions obtained from the gravity flow IMAC. Columns 1- cell lysate, 2- flow through, 3- elution fraction and 4- insoluble portion of the cell lysate (pellet). **B)** SEC carried out in a Superdex200 HiLoad 26/60 column equilibrated with 20mM Tris-HCl pH 7.6, 150mM NaCl. **C)** 15% SDS-PAGE of fractions obtained from SEC. All columns correspond to the peak highlighted in yellow (B). **D)** 15% SDS-PAGE of fractions obtained from SEC. Columns 1, 2 and 3- fractions of the peak highlighted in pink (B); 4, 5, 6, 7, and 8- fractions of the peak highlighted in purple (B).

4.4.3 Co-purification experiments

4.4.3.1 α -actinin

A second approach used to try to obtain a complex of different α -actinin domains was co-purification of the desired components of the complex. Cells of individual components (ABD_SR1; EF-3/4; CaM) were broken together after protein induction and the supernatant of the cell lysate was submitted to gravity flow IMAC. In Figure 4.12 it is possible to see that co-purification experiments did not result in correct complex formation due to degradation, insolubility and/or shortage in production of one of the components.

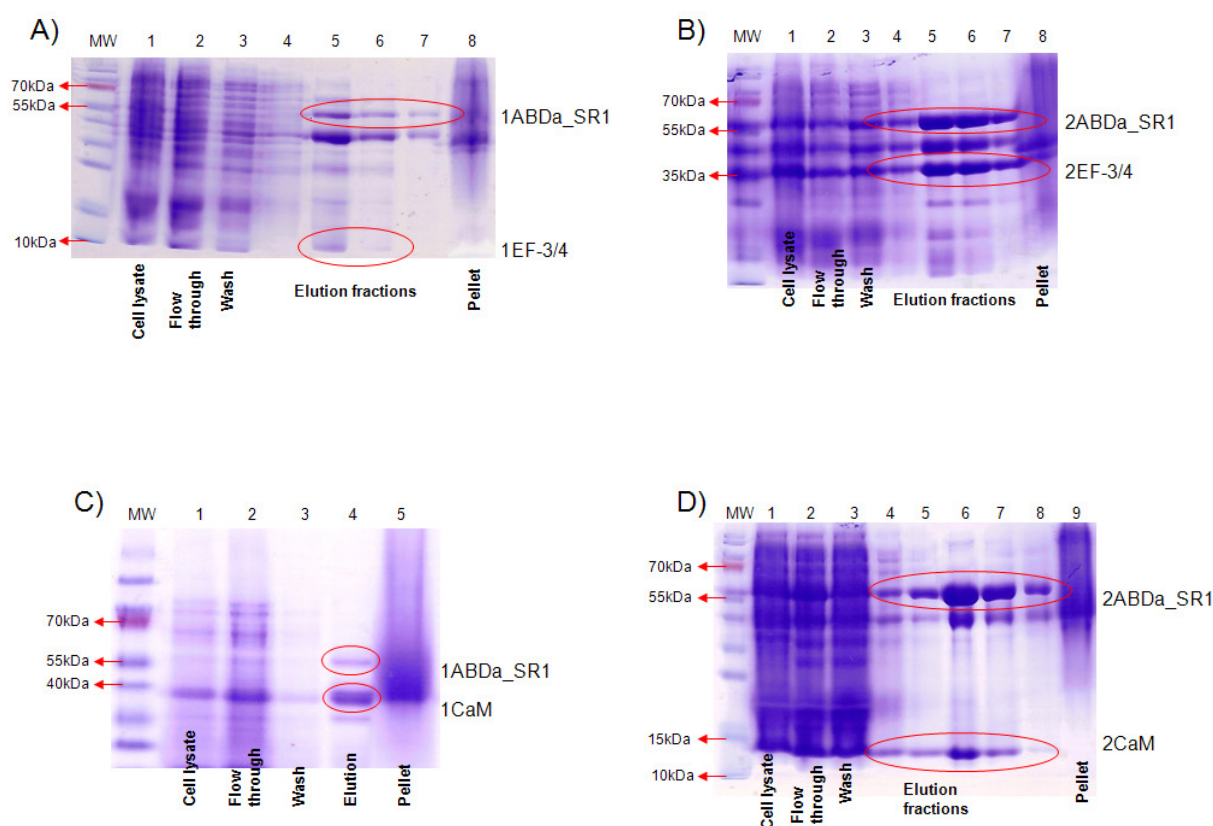


Figure 4.12 15% SDS-PAGE of fractions obtained from the co-purification experiments by gravity flow IMAC co-purification. **A)** 1ABDa_SR1 (His-tag + TrxA) + 1EF-3/4 (not tagged). Columns: 1- cell lysate, 2- flow through, 3- wash, 4, 5, 6, 7- elution fractions and 8- insoluble fraction of the cell lysate (pellet). **B)** 2ABDa_SR1 (His-tag + TrxA) + 2EF-3/4 (GST-tag). Columns: 1- cell lysate, 2- flow through, 3- wash, 4, 5, 6, 7- elution fractions and 8- insoluble fraction of the cell lysate (pellet). **C)** 1ABDa_SR1 (His-tag + TrxA) + 1CaM (GST-tag). Columns: 1- cell lysate, 2- flow through, 3- wash, 4- elution fractions and 5- insoluble fraction of the cell lysate (pellet). **D)** 2ABDa_SR1 (His-tag + TrxA) + 2CaM (not tagged). Columns: 1- cell lysate, 2- flow through, 3- wash, 4, 5, 6, 7, 8- elution fractions and 9- insoluble fraction of the cell lysate (pellet).

4.4.3.2 hd + PDZ domain of ZASP

To understand α -actinin regulation, experiments to form a complex between 2hd and PDZ in the presence and absence of the phospholipid LPA were carried out. The initial trial was performed by preparative size exclusion chromatography in the absence of LPA as a pilot experiment, resulting in a complex between PDZ (GST-tagged) and the excess of 6x His – SR3_SR4_CaM (Figure 4.13).

Analytical size exclusion chromatography was, subsequently, performed with non-tagged PDZ and 2hd without any excess of 6x His – SR3_SR4_CaM, in the absence and presence of different ratios of LPA. This analytical study was performed to verify whether the LPA would enhance complex formation (Figure 4.14). Experiments performed at molar ratios 1:1:3 and 1:1:5 of 2hd, PDZ and LPA show that no complex formation was detected under the condition used (20 mM Tris-HCl pH 7.6, 150 mM NaCl).

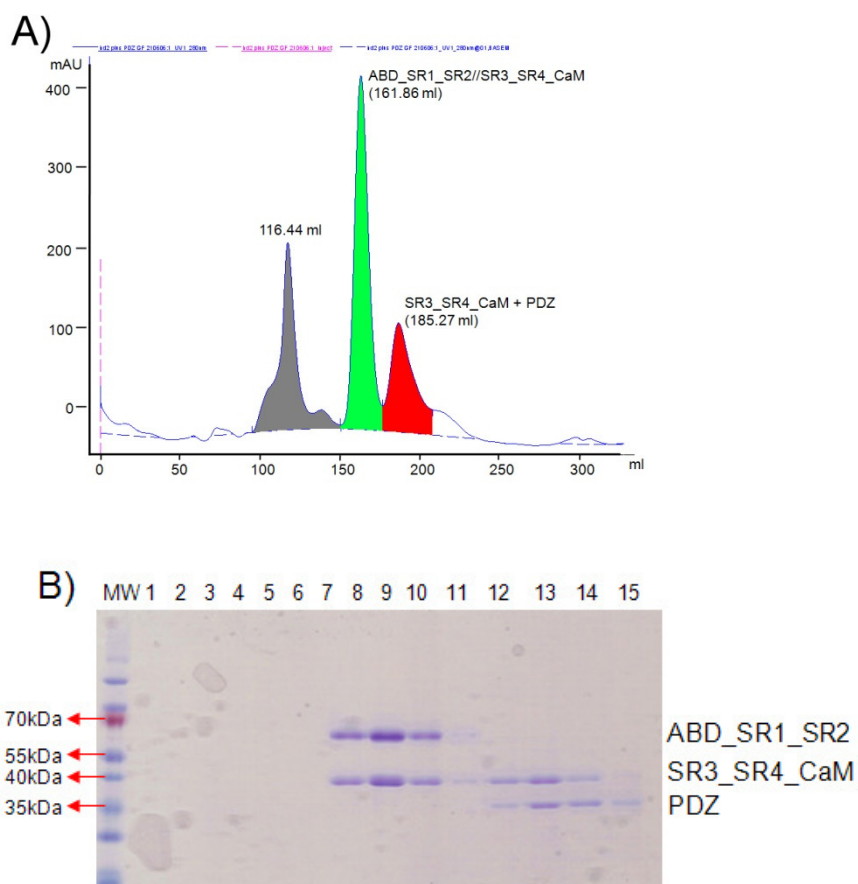


Figure 4.13 Formation of 2hd (his-tagged) and PDZ (GST-tagged) complex. **A)** Preparative SEC carried out in a Superdex200 HiLoad 26/60 column equilibrated with 20 mM Tris-HCl pH 7.6, 150 mM NaCl. **B)** 12% SDS-PAGE of fractions obtained from SEC. Columns: 1, 2, 3, 4, 5, 6 and 7- elution correspondent to the peak highlighted in gray (A); 8, 9, 10 and 11- elution correspondent to the peak highlighted in green (A, hd); 12, 13, 14 and 15- elution correspondent to peak highlighted in red (A, formation of PDZ (GST) and the excess of 6x His – SR3_SR4_CaM complex).

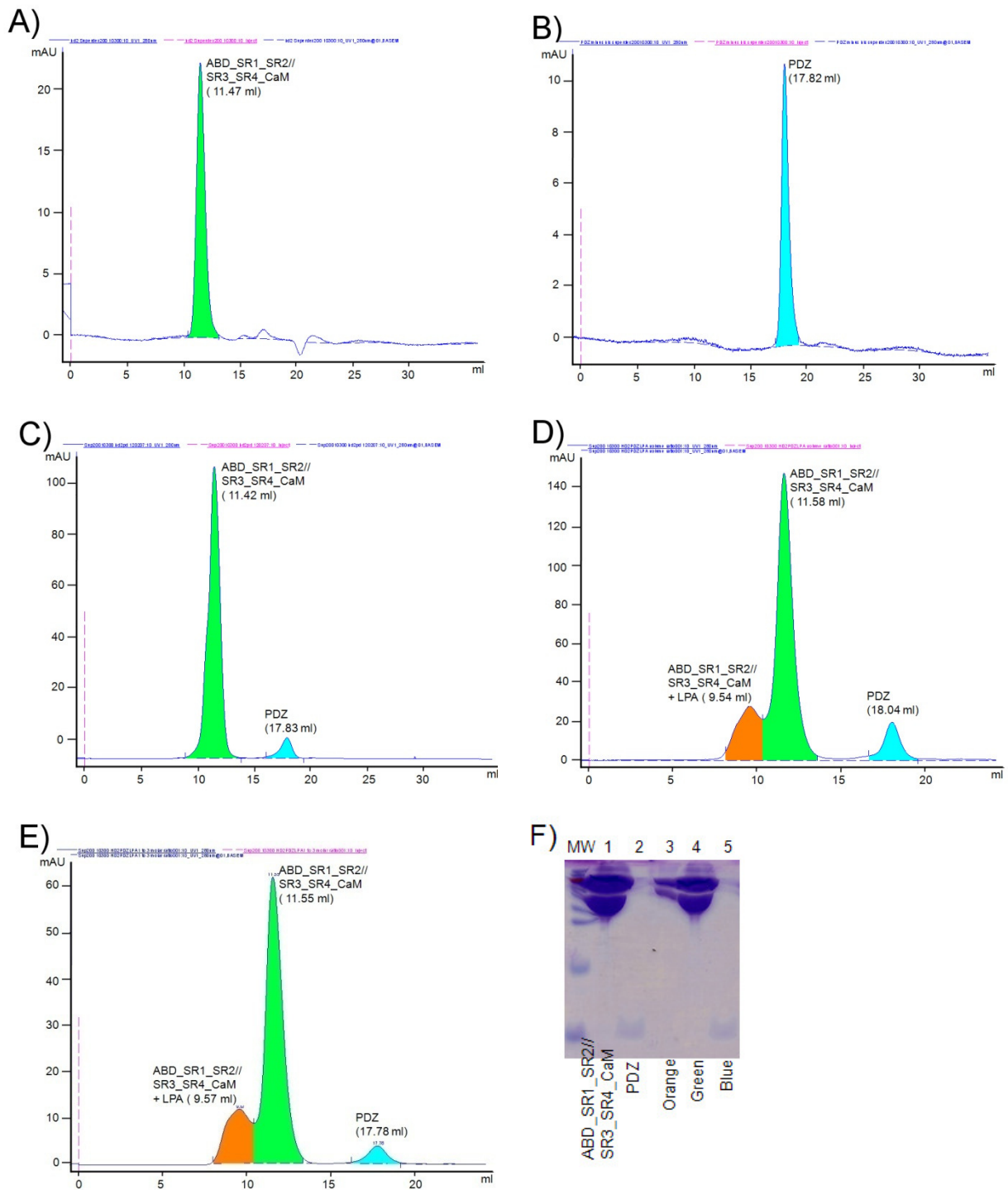


Figure 4.14 Analytical SEC of 2hd + PDZ (not tagged), carried out in a Superdex200 10/300 GL column equilibrated with 20 mM Tris-HCl pH 7.6, 150 mM NaCl. **A)** 2hd (peak highlighted in green). **B)** PDZ (peak highlighted in blue). **C)** a molar ratio 1:1 of 2hd and PDZ. **D)** a molar ratio 1:1:3 of 2hd, PDZ and LPA (formation of a new peak highlighted in orange). **E)** a molar ratio 1:1:5 of 2hd, PDZ and LPA. **F)** 15% SDS-PAGE of pooled fractions obtained from the analytical SEC of a molar ratio 1:1:3 experiment with the three components (D). Columns 1- 2hd (control); 2- PDZ (control); 3- elution correspondent to peak highlighted in orange; 4- elution correspondent to peak highlighted in green (hd), 5- elution correspondent to peak highlighted in blue (PDZ).

4.5 Dynamic light scattering (DLS)

DLS was used as a protein quality control before crystallization trials. All studied proteins presented low level of polydispersity (%Pd; Table 4.5).

Table 4.5 DLS measured in a DynaPro (Protein Solutions Inc.) at 22° C with 100 acquisitions at 1 s interval each. The table lists radius, %Pd and concentration data for each protein.

SAMPLE	R (nm)	%Pd	CONCENTRATION (mg/ml)
2ABDY	2.1	15.6	10.0
1AFL - EDTA	7.7	13.9	4.0
1AFL - CaCl ₂	8.1	13.5	5.0
6x His - Δ2AFLY	7.5	14.1	4.7
Δ2AFLY	7.8	15.1	4.7
1hd	5.4	13.1	10.0
2hd	5.5	13.4	4.0
2Eh	6.2	11.5	6.0

4.6 Crystallization trials and protein reductive methylation

After purification, all 6x His-tagged proteins (AFL, 2Eh, hd and ABD) were submitted to crystallization trials with methods and conditions described in the “materials and methods” section (Chapter 3).

Since no crystal hits were obtained, protein reductive methylation experiments was carried out, expecting that changes in the surface charges would enhance crystal formation. This resulted in crystal hits of Eh2 (6x His – 2Eh Met-K) and 2AFL (6x His – 2AFL Met-K).

Initial crystal hits of 6x His – 2Eh Met-K were obtained with protein concentration around 6.5 mg/ml and mother liquor conditions: A) 0.1 M Bis-tris propane pH 6.5, 0.2 M Na/K phosphate, 20% PEG 3350; B) 0.1 M Bis-tris pH 5.5, 0.2 M ammonium acetate, 25% PEG 3350; C) 0.1 M Bis-tris pH 6.5, 0.2 M ammonium acetate, 25% PEG 3350; D) 0.1 M Bis-tris pH 5.5, 0.2 M NaCl, 25% PEG 3350; E) 0.1 M Bis-tris pH 5.5, 0.2 M MgCl₂, 25% PEG 3350; F) 0.1 M Tris-HCl pH 8.5, 0.2 M MgCl₂, 25% PEG 3350 (Figure 4.15). These hits were obtained at 22° C and sitting drop vapour diffusion method. Optimization of crystallization conditions is in progress.

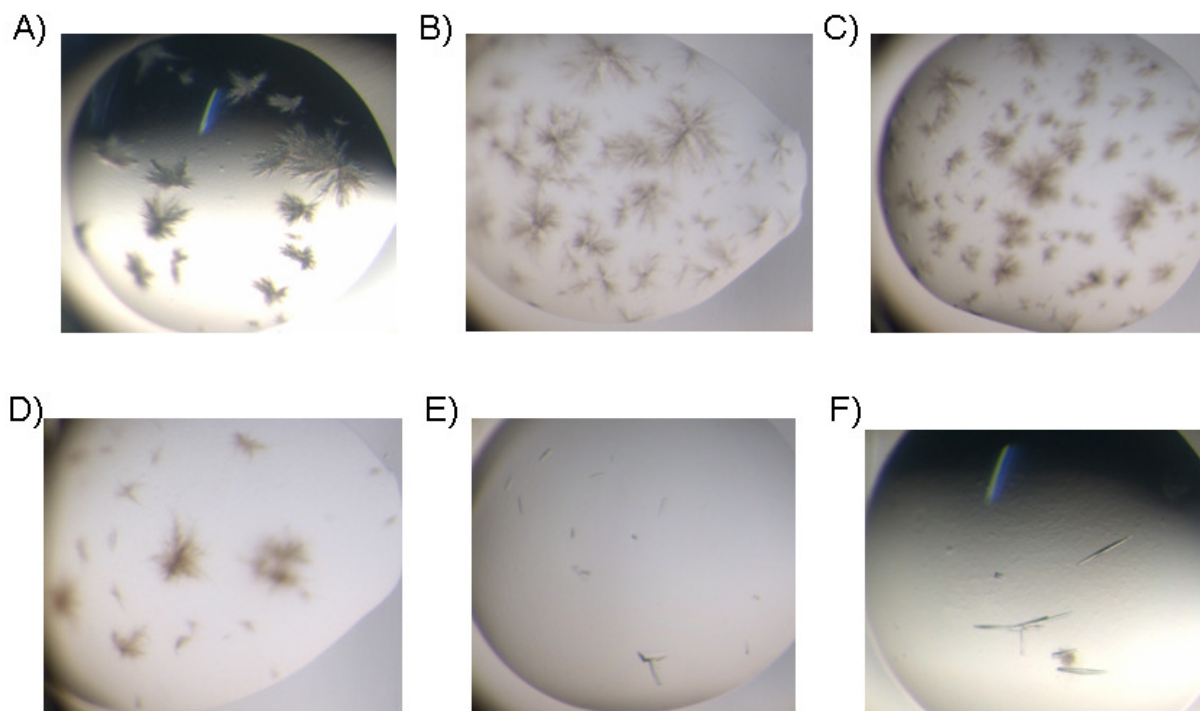


Figure 4.15 Crystal hits of 6x His - 2Eh Met-K. Protein concentration used was ~6.5 mg/ml in 20 mM Na cacodylate pH 6.5, 150 mM NaCl. Hits obtained after initial screen: **A)** 0.1 M Bis-tris propane pH 6.5, 0.2 M Na/K phosphate, 20% PEG 3350; **B)** 0.1 M Bis-tris pH 5.5, 0.2 M ammonium acetate, 25% PEG 3350; **C)** 0.1 M Bis-tris pH 6.5, 0.2 M ammonium acetate, 25% PEG 3350; **D)** 0.1 M Bis-tris pH 5.5, 0.2 M NaCl, 25% PEG 3350; **E)** 0.1 M Bis-tris pH 5.5, 0.2 M MgCl₂, 25% PEG 3350; **F)** 0.1 M Tris-HCl pH 8.5, 0.2 M MgCl₂, 25% PEG 3350.

The crystal hits of 6x His – 2AFL Met-K were obtained with protein concentration around 4.7 mg/ml. Initial hits were obtained in mother liquor conditions: A) 0.1 M Na thiocyanate, 20% PEG 3350; B) 0.1 M Bis-tris pH 5.5, 0.1 M ammonium acetate, 17% PEG 10000; C) 0.1 M MES pH 6.0, 10% PEG 6000. Optimization yielded improved crystal quality at 14° C in mother liquor conditions: D) 0.1 M Tris-HCl pH 7.4, 0.2 M Na thiocyanate, 20% PEG smear; E) 0.2M Na thiocyanate, 20% PEG smear; F) 0.2 M Na thiocyanate, 17% PEG 10000 (Figure 4.16) and hanging drop vapour diffusion method.

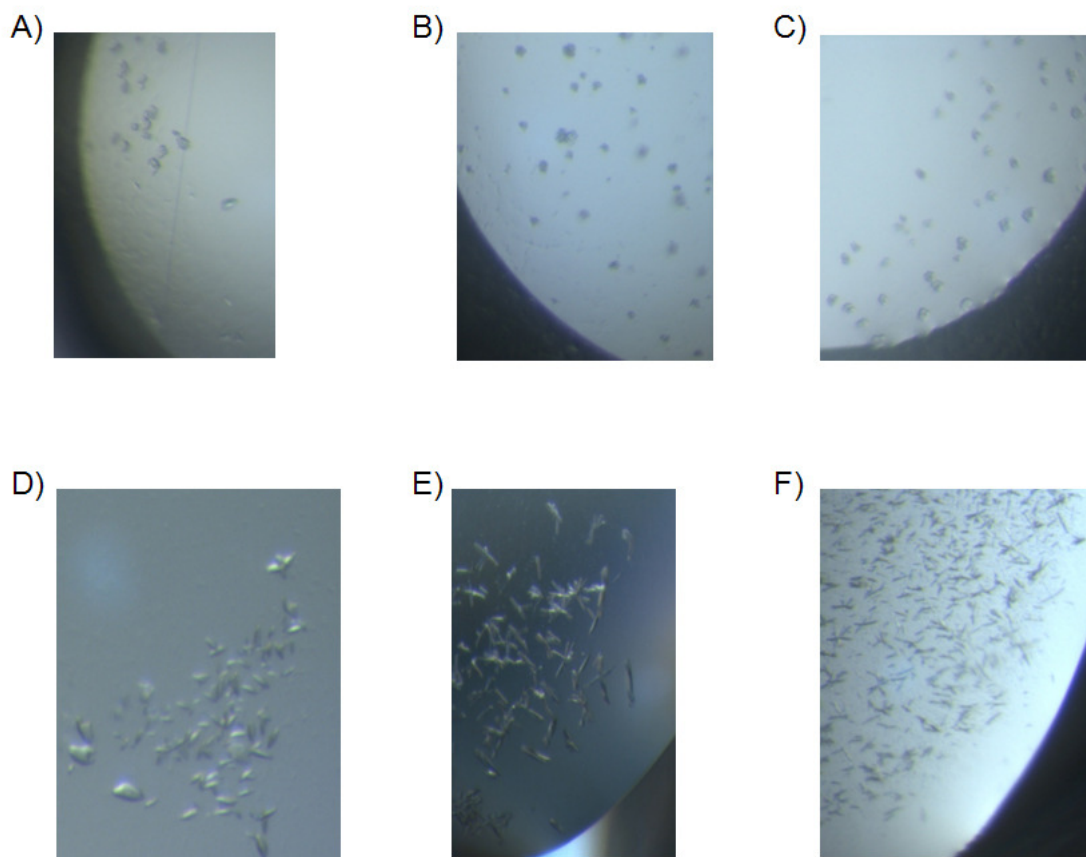


Figure 4.16 Crystal hits and further optimization hits of 6x His - 2AFL Met-K. Protein concentration was ~4.7 mg/ml in 20 mM Na cacodylate pH 6.5, 150 mM NaCl. Hits obtained after initial screen: **A)** 0.1 M Na thiocyanate, 20% PEG 3350; **B)** 0.1 M Bis-tris pH 5.5, 0.1 M ammonium acetate, 17% PEG 10000; **C)** 0.1 M MES pH 6.0, 10% PEG 6000. Hits obtained after optimization: **D)** 0.1 M Tris-HCl pH 7.4, 0.2 M Na thiocyanate, 20% PEG smear; **E)** 0.2 M Na thiocyanate, 20% PEG smear; **F)** 0.2 M Na thiocyanate, 17% PEG 10000.

4.7 Crystallization trials and protein surface entropy reduction (SER)

SER was used in an attempt to grow better crystals of 6x His – 2AFL.

The clusters for residue mutation suggested by the web site <http://nihserver.mbi.ucla.edu/SER/> were E23A/E24A/E25A, E149A/E150A, E260A/Q261A/E263A and E310A/K311A. Positive results were obtained with the triple-site mutant 6x His – Δ 2AFL E23A/E24A/E25A and the double-site mutant 6x His – Δ 2AFL E310A/K311A. These mutants were submitted to three-step protein purification and subsequent crystallization trials

Despite the attained high purity, the triple-site mutant presented a very low expression level. This proved insufficient for crystallization trials, as checked by PCT. On the other hand, the concentration obtained for the double-site mutant was enough to set up crystallization plates. Crystalline like structures were obtained in mother

liquor conditions: A) 0.1 M Tris-HCl pH 8.5, 0.2 M NaCl, 25% PEG 3350; B) 0.1 M Tris-HCl pH 8.5, 0.8 M K/Na tartrate, 0.5% PEG MME 5000 (Figure 4.17).

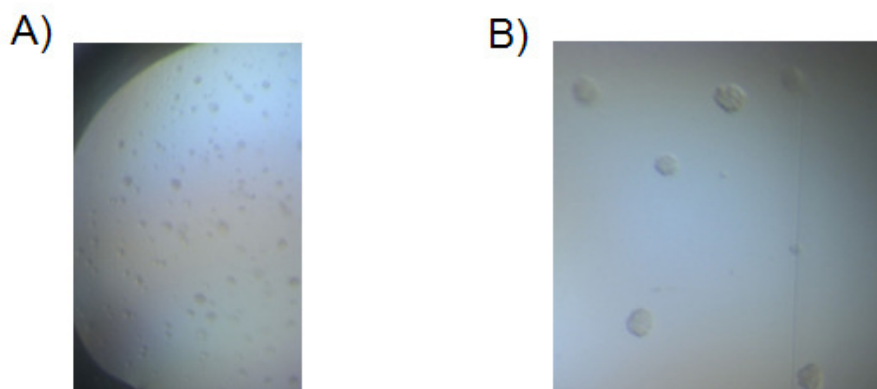


Figure 4.17 Initial crystalline hits of the double-site mutant 6x His - Δ 2AFL E310A/K311A. The protein concentration was \sim 4.7 mg/ml in 20mM Na cacodylate pH 6.5, 150 mM NaCl. Hits obtained after initial screen: **A)** 0.1 M Tris-HCl pH 8.5, 0.2 M NaCl, 25% PEG 3350; **B)** 0.1 M Tris-HCl pH 8.5, 0.8 M K/Na tartrate, 0.5% PEG MME 5000.

Since the optimization of initial crystal hits was unsuccessful, the 6x His – Δ 2AFL E310A/K311A was submitted to protein reductive methylation (6x His – Δ 2AFL Met-K). Needles about 100 – 120 μ m long and 10 – 20 μ m wide grew after optimization screens at 14° C in protein concentration around 4.7 mg/ml. The initial condition was 0.1 M Mg formate, 15% PEG 3350 and the best crystals were obtained by hanging drop diffusion method in mother liquor 0.2 M Na formate, 6% PEG smear (Figure 4.18).

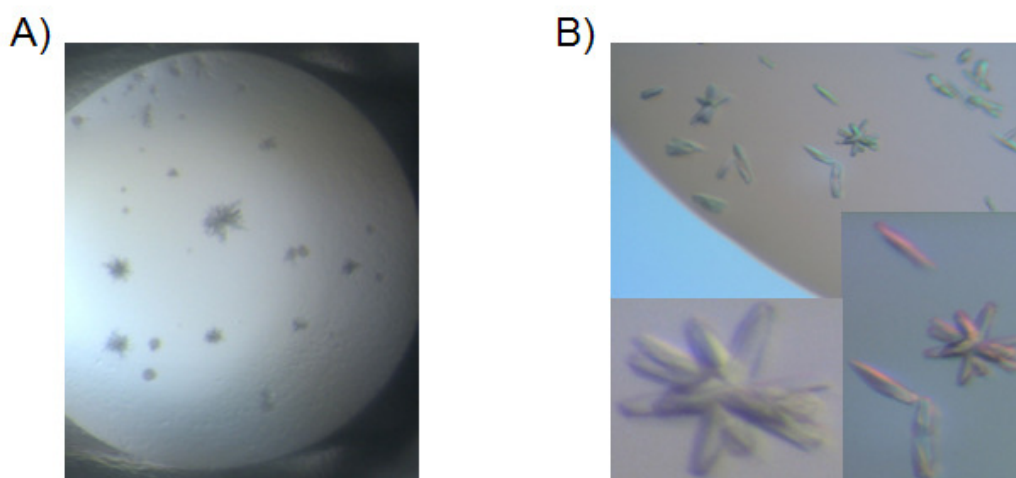


Figure 4.18 Crystal hits of 6x His - Δ 2AFL Met-K. The protein concentration was \sim 4.7 mg/ml in 20 mM Na cacodylate pH 6.5, 150 mM NaCl. **A)** Initial condition: 0.1 M Mg formate, 15% PEG 3350; **B)** Optimized condition: 0.2 M Na formate, 6% PEG smear.

4.7.1 Cleavage of the flexible N-terminal of Δ 2AFL E310A/K311A (Δ 2AFLY)

In order to decrease the flexibility of the α -actinin full length (AFL) and grow better crystals, a construct for 2AFL WT and mutants excluding the first eighteen amino acids was designed. DNA amplification (section 4.1.1), protein expression and purification (items 4.2.1 and 4.4.1) were shown previously. Positive results were obtained for the mutant Δ 2AFL E310A/K311A and after protein reductive methylation (6x His – Δ 2AFLY Met-K), tiny needles grew at 14° C (protein concentration around 4.7 mg/ml). The initial condition was the same as for the 6x His – Δ 2AFL Met-K (0.1 M Mg formate, 15% PEG 3350) but the best crystal hits were obtained in hanging drops in mother liquor 0.2 M Mg formate, 6% PEG smear, with and without 0.01 mM EDTA as additive (Figure 4.19).

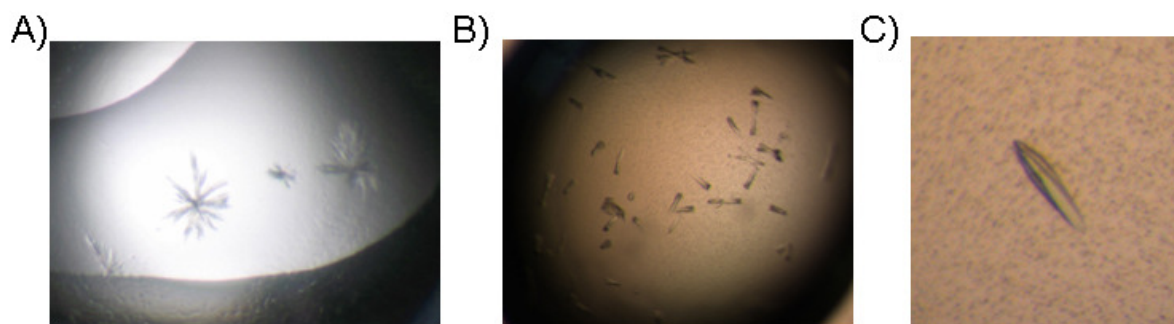


Figure 4.19 Crystal hits of 6x His - Δ 2AFLY Met-K. The protein concentration was ~4.7 mg/ml in 20 mM HEPES pH 8.0, 150 mM NaCl. Hit obtained after initial condition: **A)** 0.1 M Mg formate, 15% PEG 3350. Hits obtained after optimization: **B)** 0.2 M Mg formate, 6% PEG smear; **C)** 0.2 M Mg formate, 5% PEG smear, 0.01 M EDTA (as additive).

4.7.2 6x His - tag cleavage

Another strategy to grow better $\Delta 2$ AFLY crystals involved the 6x His tag cleavage. The $\Delta 2$ AFLY expression, purification, protein reductive methylation ($\Delta 2$ AFLY Met-K) and crystallization trials followed the same procedure established for 6x His – $\Delta 2$ AFLY Met-K. This resulted in crystals that were 250 – 300 μm long and 30 – 35 μm wide. Some of these crystals grew in different crystal forms when compared to 6x His – $\Delta 2$ AFLY Met-K. The initial condition was the same as for the 6x His – $\Delta 2$ AFL Met-K (0.1 M Mg formate, 15% PEG 3350) but the best crystals grew in 0.2 M Mg formate, 5% PEG smear and 0.01 mM EDTA as additive (Figure 4.20).

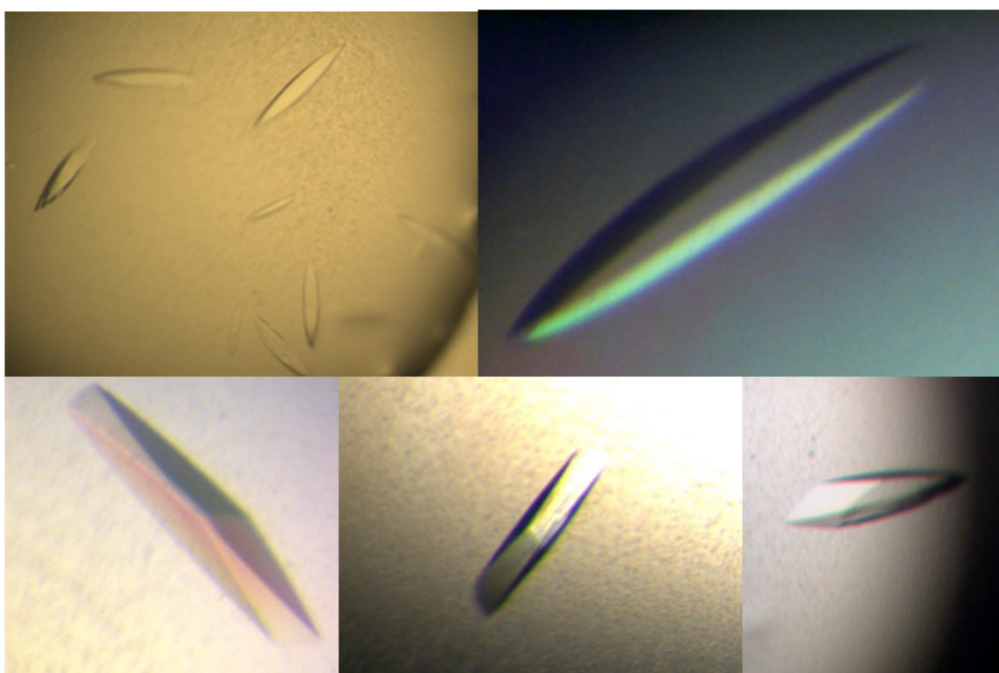


Figure 4.20 Crystal hits of $\Delta 2$ AFLY Met-K. The protein concentration was ~ 4.7 mg/ml in 20 mM HEPES pH 8.0, 150 mM NaCl. The crystals were obtained under the condition: 0.2 M Mg formate, 5% PEG smear, 0.01 M EDTA (as additive).

4.8 Preliminary data collection of AFL E310A/K311A

X-ray data for α -actinin AFL were collected on ID23-1 and ID23-2 ESRF beamlines, presenting a nice evolution of resolution according to the constructs. The 6x His - Δ 2AFL Met-K crystals were very small and diffracted to around 11 Å (Figure 4.21A) on beamline ID23-1. On the other hand, crystals of the truncated version of full length (6x His - Δ 2AFLY Met-K) yielded partial data-set to about 4 Å on the micro focus beamline ID23-2 (Figure 4.21B). Three data set were merged in the attempt to obtain one complete data; nevertheless, this approach was unsuccessful (Table 4.6).

The Δ 2AFLY Met-K crystals were of bigger size and generated data set to about around 4 Å on the beamline ID23-1 (Figure 4.21C). Data processing statistics are listed in Table 4.7.

Table 4.6 Merged scaling statistic of 6x His – Δ 2AFLY Met-K data sets. Values in brackets refer to the highest resolution shell.

Beamline	ID23-2
Wave length (Å)	0.87
Space group	P222
Unit cell parameters	a = 73.3 Å, b = 102.6 Å, c = 181.7 Å $\alpha = \beta = \gamma = 90^\circ$
Unique reflections	8601 (380)
Resolution (Å)	4.5
Completeness (%)	79.6 (61.6)
R-meas (%)	26.4 (68.4)

Table 4.7 Data collection and processing statistics of Δ 2AFLY Met-K. Values in brackets refer to the highest resolution shell.

Beamline	ID23-1
Wave length (Å)	0.97
Space group	P222
Unit cell parameters	a = 72.4 Å, b = 101.4 Å, c = 179.8 Å $\alpha = \beta = \gamma = 90^\circ$
Unique reflections	4352 (288)
Resolution (Å)	6.7
Completeness (%)	94.6 (87.8)
R-meas (%)	9.6 (40.3)

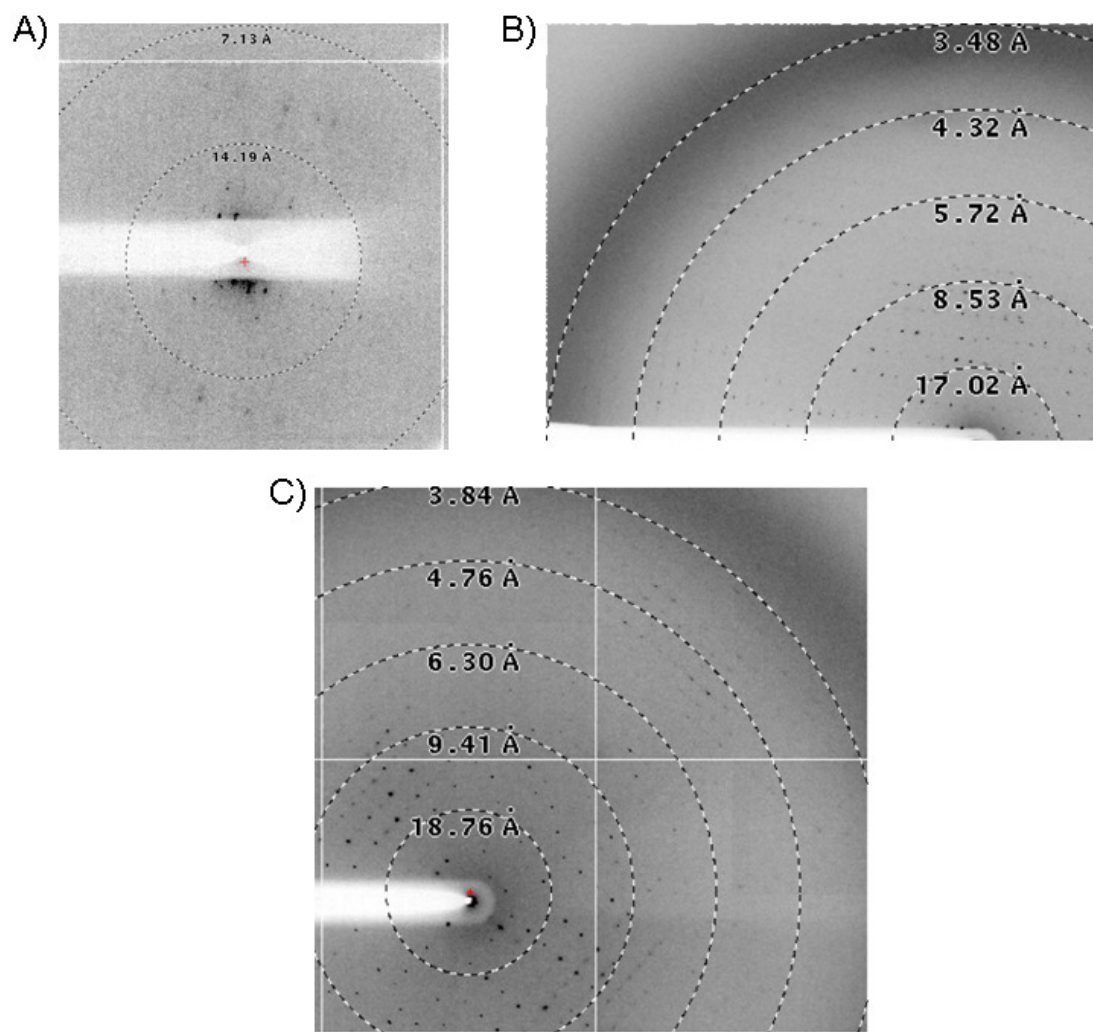


Figure 4.21 Diffraction patterns of $\Delta 2AFL$ and $\Delta 2AFly$ E310A/K311A Met-K collected at 100 K and displayed by ADXV software. **A)** 6x His - $\Delta 2AFL$ Met-K collected on ESRF beamline ID23-1 to a resolution ~ 11 Å, **B)** 6x His - $\Delta 2AFly$ Met-K collected on ESRF micro focus beamline ID23-2 to a resolution ~ 4 Å and **C)** $\Delta 2AFly$ Met-K collected on ESRF beamline ID23-1 to a resolution ~ 4 Å.

4.9 Actin binding domain (ABD): WT versus mutant

The single-site mutants ($\Delta 2ABDa$) designed for α -actinin isoform 2 to validate the proposed PIP2 binding site within the ABD (Franzot et al., 2005) were R163E, R169E and R192E. Positive results were obtained for $\Delta 2ABDa$ R169E and $\Delta 2ABDa$ R192E mutants. Expression and purification followed the protocol established for the ABDa WT (purification of WT is shown at Figure 4.10).

The major difference between the three samples was in the protein expression and purification yields. The mutant $\Delta 2ABDa$ R169E (yield per litre = 8 mg) is expressed in lower level than the WT (yield per litre = 12 mg) and the mutant $\Delta 2ABDa$ R192E (yield per litre = 18 mg). However, the expression of the mutant $\Delta 2ABDa$ R192E yielded increased amount of protein than the WT.

Binding of α -actinin 2ABDa WT and its mutants to different types of phosphoinositides was studied using different strategies. The first approach employed the PiP strips binding method, using as a negative control the protein chlorite dismutase (kindly provided by Julius Kostan). No significant binding was observed under the conditions used (Figure 4.22; N-terminal his-tagged proteins in 20 mM Tris-HCl pH 7.6 and 100 mM NaCl).

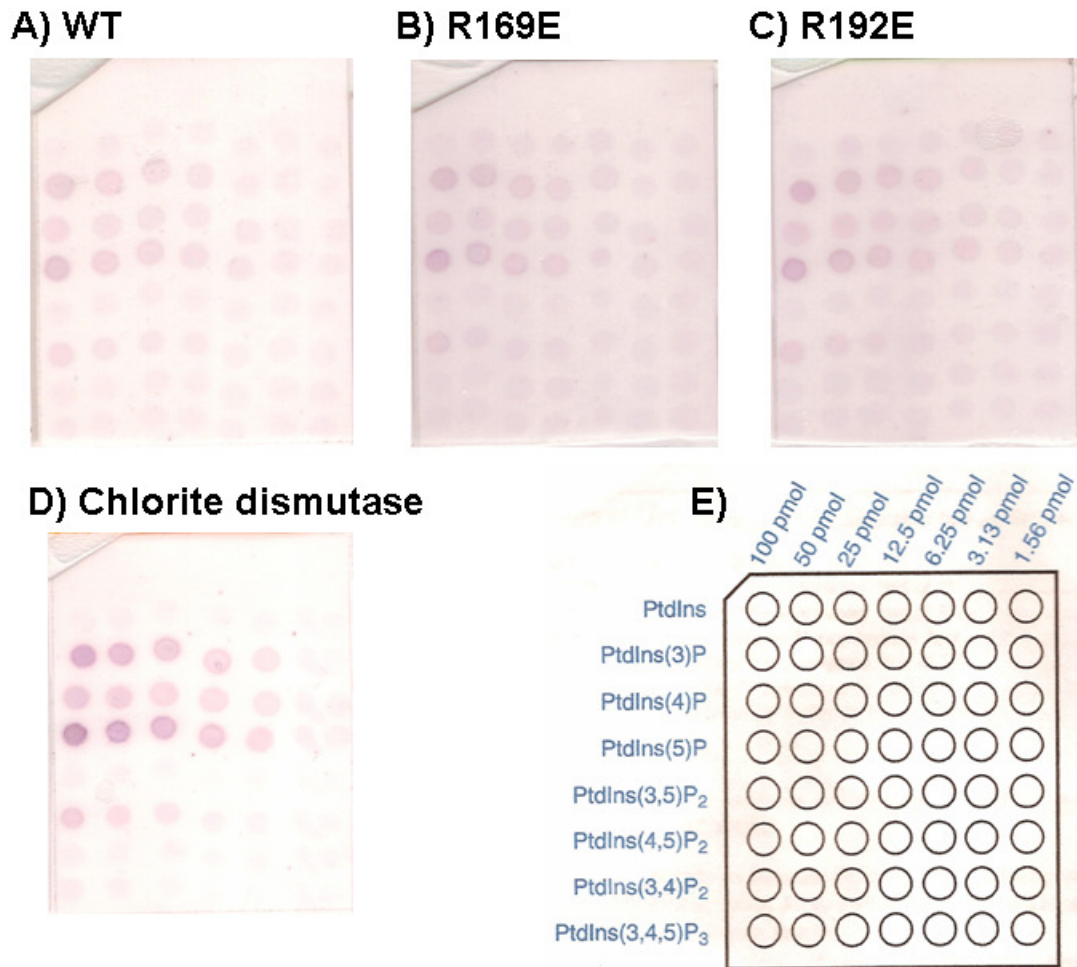


Figure 4.22 PiP strips binding assays for 2ABDa WT and the mutants Δ 2ABDa R169E, Δ 2ABDa R192E. **A)** 2ABDa WT, **B)** Δ 2ABDa R169E, **C)** Δ 2ABDa R192E, **D)** chlorite dismutase and **E)** illustration of a PiP strip showing the contents [phosphatidylinositol (PtdIns), phosphatidylinositol 3-phosphate (PtdIns(3)P), phosphatidylinositol 4-phosphate (PtdIns(4)P), phosphatidylinositol 5-phosphate (PtdIns(5)P), phosphatidylinositol 3,5-biphosphate (PtdIns(3,5)P₂), phosphatidylinositol 4,5-biphosphate (PtdIns(4,5)P₂), phosphatidylinositol 3,4-biphosphate (PtdIns(3,4)P₂), phosphatidylinositol 3,4,5-triphosphate (PtdIns(3,4,5)P₃)] and their concentrations.

4.9.1 Differential scanning fluorimetry (DSF)

DSF was used to study the binding of IP6 to 2ABDa WT. Increasing IP6 concentrations were used in an attempted to relate IP6 concentration and protein stability. Figure 4.23 shows a loss of protein stability at IP6 concentration of around 0.6 mM, which corresponds to a tenfold IP6 excess.

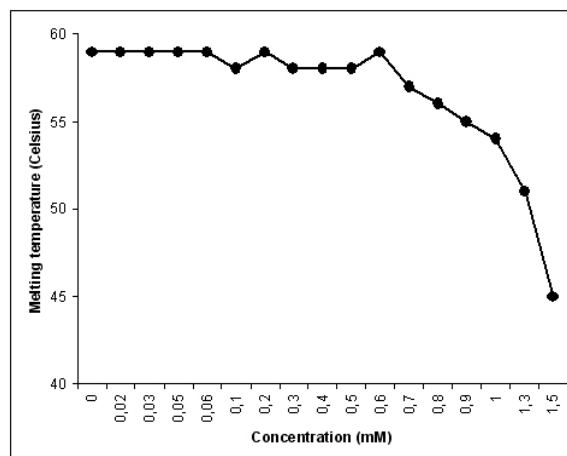


Figure 4.23 Stability of 2ABDa WT versus IP6 concentration. Y-axis corresponds to melting temperature in Celsius ($^{\circ}\text{C}$) and X-axis corresponds to IP6 concentration.

4.9.2 Circular dichroism (CD)

CD was performed at near-UV in order to follow the binding of 2ABDa WT and IP6. The protein to IP6 concentration ratio was 1:10 and the CD spectra show no tertiary conformational changes (Figure 4.24).

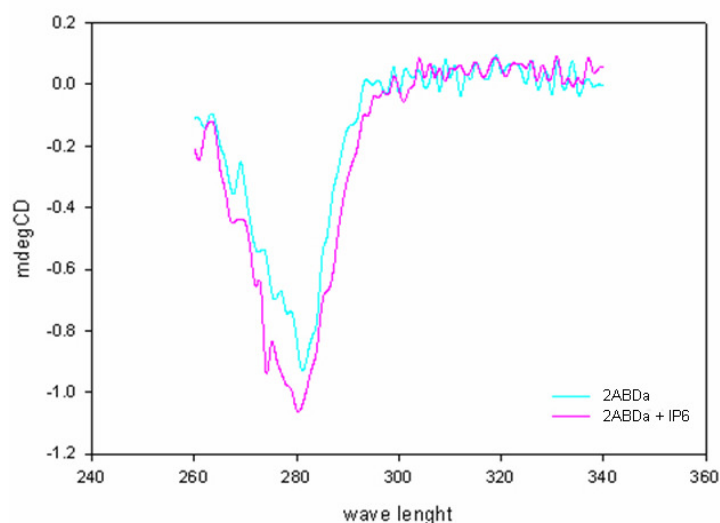


Figure 4.24 Near-UV CD spectra of 2ABDa WT and IP6 at protein:IP6 ratio 1:10. Y-axis corresponds to CD data (mdegCD) and X-axis corresponds to wave length (nm).

4.9.3 Nuclear magnetic resonance spectroscopy (NMR)

2D-NMR was performed to study the binding of 2ABDa WT and IP3. The spectrum shows small shifts in the signal of ^{15}N -2ABDa WT (Figure 4.25). Validation of these shifts was done through a selective T1 measurement with non-labelled 2ABDa WT and IP3. No difference in the relaxation time (T1) was observed.

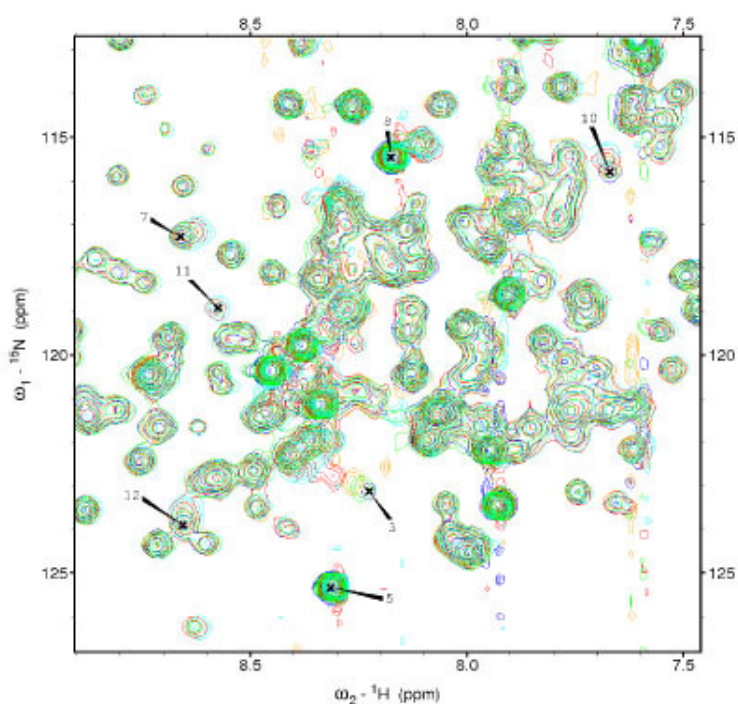


Figure 4.25 Part of the superposition HSQC spectra showing small shifts in the ^{15}N -2ABDa WT signal by increasing IP3 concentration. Blue: 1mM ^{15}N -2ABDa WT, green: protein and IP3 molar ratio 1:1 between protein and IP3, yellow: 1:2 molar ratio, red: 1:4 molar ratio and cyan: 1:6 molar ratio.

4.9.4 Isothermal titration calorimetry data (ITC)

ITC was applied to assess the binding of 2ABDa and IP3. 2ABDa WT and its mutants Δ 2ABDa R169E, Δ 2ABDa R192E were titrated with IP3 and the results are presented in Figure 4.26. Dissociation constants (K_d) were high: 1.8mM for 2ABDa WT, 1.2mM for Δ 2ABDa R169E and 2.8mM for Δ 2ABDa R192E (Table 4.8).

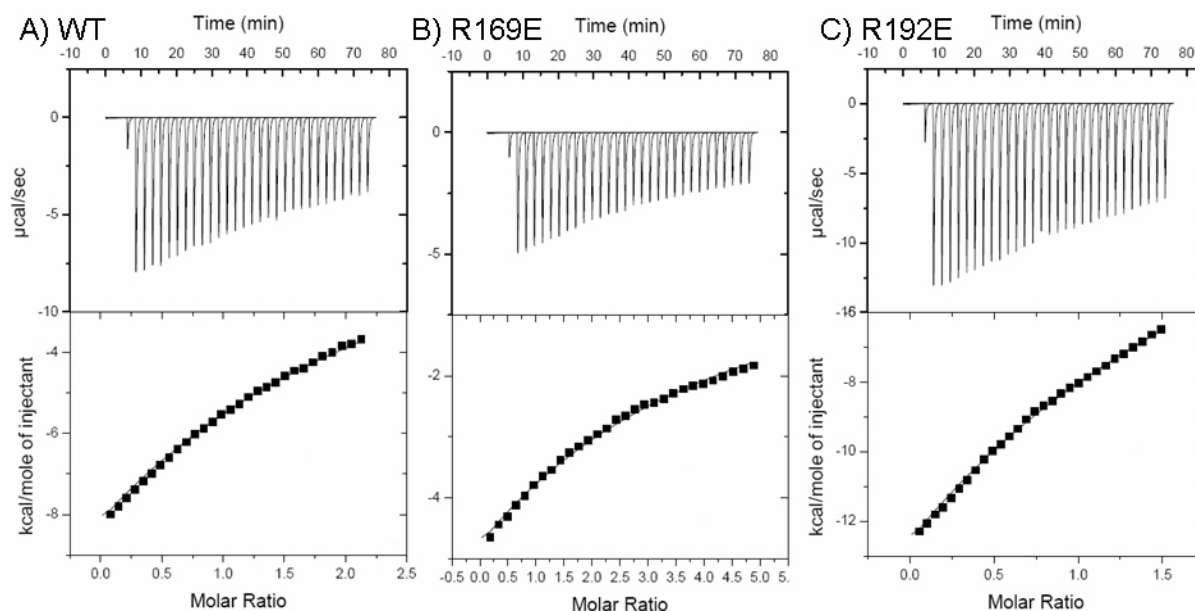


Figure 4.26 ITC data acquired at 25°C by titrating IP3 to 2ABDa WT and mutants. Representative raw ITC data (top) and integrated data fits (bottom) are shown for: **A)** 2ABDa WT, **B)** Δ 2ABDa R169E and **C)** Δ 2ABDa R192E.

Table 4.8 Isothermal titration analysis of 2ABDa WT and mutants.

Sample	ΔH (cal/mol)	ΔS (cal/mol/K)	$-T\Delta S$ (cal/mol)	ΔG (cal/mol)	K_a (M^{-1})	K_d (mM)
2ABDa WT	-61.2 ± 0.3	-193	57.9	-3.3	568 ± 36	1.8 ± 0.1
Δ 2ABDa R169E	-54.2 ± 0.9	-169	50.7	-3.5	813 ± 19	1.2 ± 0.03
Δ 2ABDa R192E	-104 ± 0.5	-337	101.1	-2.9	358 ± 20	2.8 ± 0.1

4.9.5 Protein crystallization: ABDa versus ABDY

With the aim to solve the structure of ABD in complex with IP3 or IP6, 2ABDa was submitted to crystallization trials. Since no crystals were obtained, an attempt was made to cleave the N-terminal 6x His-tag. This proved unsuccessful and a new construct based on the known structure of the human α -actinin ABD isoform 3 structure (Franzot et al., 2005) was designed. The first eighteen flexible residues (2ABDY) were excluded from the new construct and cloning, protein expression and purification followed the protocol established for 2ABDa (items 4.2.1 and 4.4.1).

After cleavage of the N-terminal 6x His-tag, crystal hits were obtained in different conditions (Figure 4.27) with a protein concentration around 10 mg/ml.

After optimization of selected hits, the crystals were soaked in cryo-solutions containing IP3 or IP6 in different concentrations prior to cryo-cooling in liquid nitrogen.

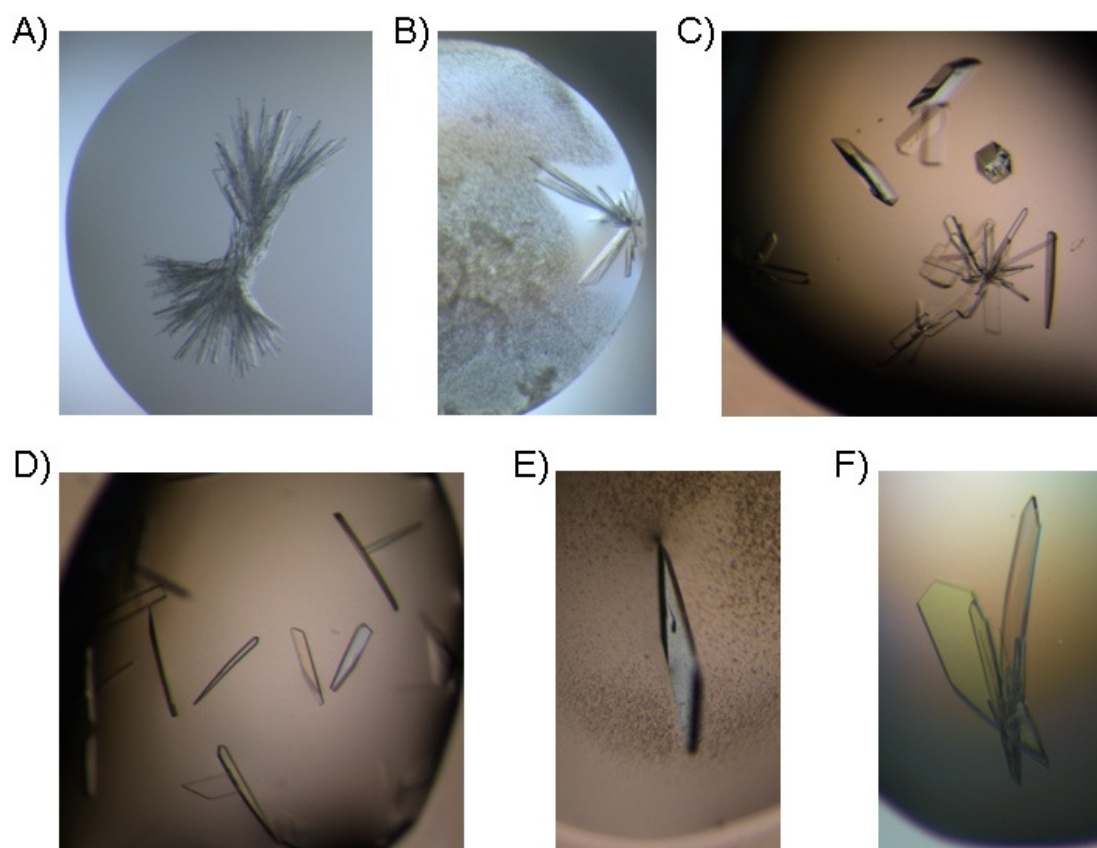


Figure 4.27 Crystal hits of 2ABDY used for soaking in IP3 or IP6. Protein concentration was ~10 mg/ml in 20 mM PIPES pH 7.5, 150 mM NaCl. Hits obtained after initial screening: **A)** 0.1 M MMT pH 6.0, 25% PEG 1500 in sitting drops, vapour diffusion method; **B)** 0.1 M MMT pH 5.0, 25% PEG 1500 and sitting drop vapour diffusion method. Hits obtained after optimization in hanging drops, vapour diffusion method: **C)** 0.1 M MMT pH 6.0, 25% PEG MME 2000; **D)** 0.1 M MMT pH 6.0, 25% PEG 1500; **E)** 0.1 M MMT pH 5.0, 25% PEG 3350 and **F)** 0.1 M Na acetate pH 5.6, 0.2 M ammonium acetate, 25% PEG 3350 + PEG 1500.

Some co-crystallization trials with IP3 were also performed, producing crystal hits in different conditions (Figure 4.28).

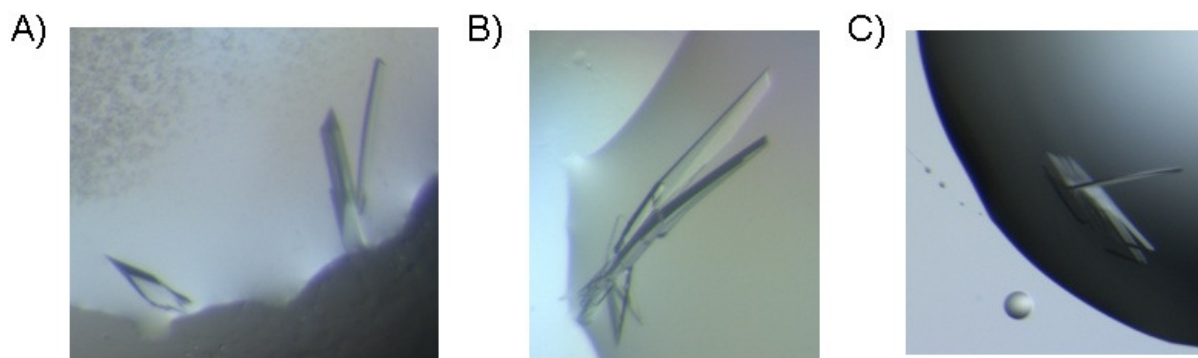


Figure 4.28 Crystals of 2ABDY + IP3. Protein concentration was ~10 mg/ml in 20 mM PIPES pH 7.5, 150 mM NaCl. The protein to IP3 molar ratio was 1:10. Hits obtained after initial screening: **A)** 0.1 M Bis-Tris pH 5.5, 25% PEG 3350; **B)** 0.1 M Bis-Tris pH 5.5, 0.2 M ammonium acetate, 25% PEG 3350. Hit obtained after optimization: **C)** 0.1 M Na acetate pH 5.5, 0.2 M ammonium acetate, 25% PEG 3350 + PEG 1500.

4.9.6 Data collection, processing and structure determination

Eight data sets for 2ABDY crystals soaked in or co-crystallized with IP3 or IP6 under different conditions were collected on beamline ESRF ID23-1. The crystals diffracted strongly and full data sets to a resolution around 1.8 Å were collected. Figure 4.29 shows the diffraction pattern of a 2ABDY crystal soaked in 12mM IP3.

The structure was solved by molecular replacement, using as search model the structure of α -actinin ABD isoform 3 [PDB entry 1WKU; (Franzot et al., 2005)]. All structures determined presented similar statistics and Table 4.9 shows a representative data collection, processing and refinement statistics. No IP3 or IP6 binding to the protein was detected in the difference electron density maps. The final structure of 2ABDY refined at 1.8 Å resolution is shown in Figure 4.30, after validation through MolProbity (Davis et al., 2004). Residues involved in the CH domains interactions (W136 and R243) are highlighted in the structure by sticks.

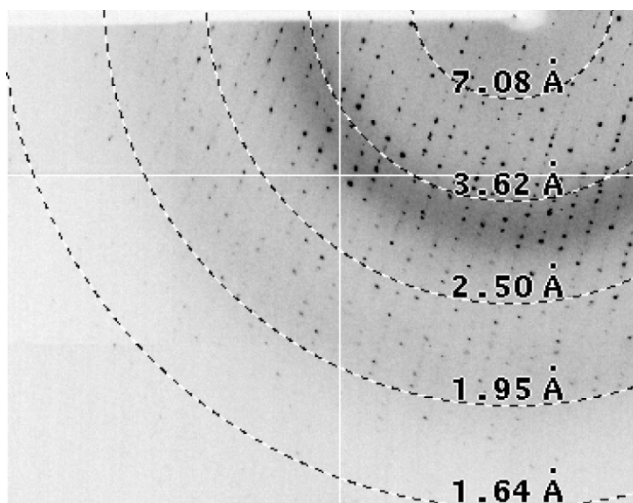


Figure 4.29 Diffraction pattern of 2ABDY collected at 100 K and displayed by ADXV software. This data set was collected from a 2ABDY crystal soaked in 12 mM IP3 on beamline ID23-1 to a resolution of 1.8Å.

Table 4.9 Data collection processing of 2ABDY: **(A)** and refinement **(B)** statistics.

A) Data collection	
Beamline	ID23-1
Wave length (Å)	1.07
Space group	P1
Unit cell parameters	a = 38.4 Å, b = 46.4 Å, c = 70.2 Å $\alpha = 73^\circ$, $\beta = 80^\circ$, $\gamma = 75^\circ$
Unique reflections	38623 (5672)
Resolution (Å)	1.8
Completeness (%)	93.1 (84.4)
R-meas (%)	6.9 (39.5)
B) Refinement	
No. Reflections	37719
Resolution (Å)	1.8
R _{factor} (%)	0.204
R _{free} (%)	0.237
No. protein atoms	7269
No. water molecules	476
r.m.s.d. Bond lengths (Å)	0.009
r.m.s.d. Bond angles (deg.)	1.119
Overall B-value (Å ²)	19.04

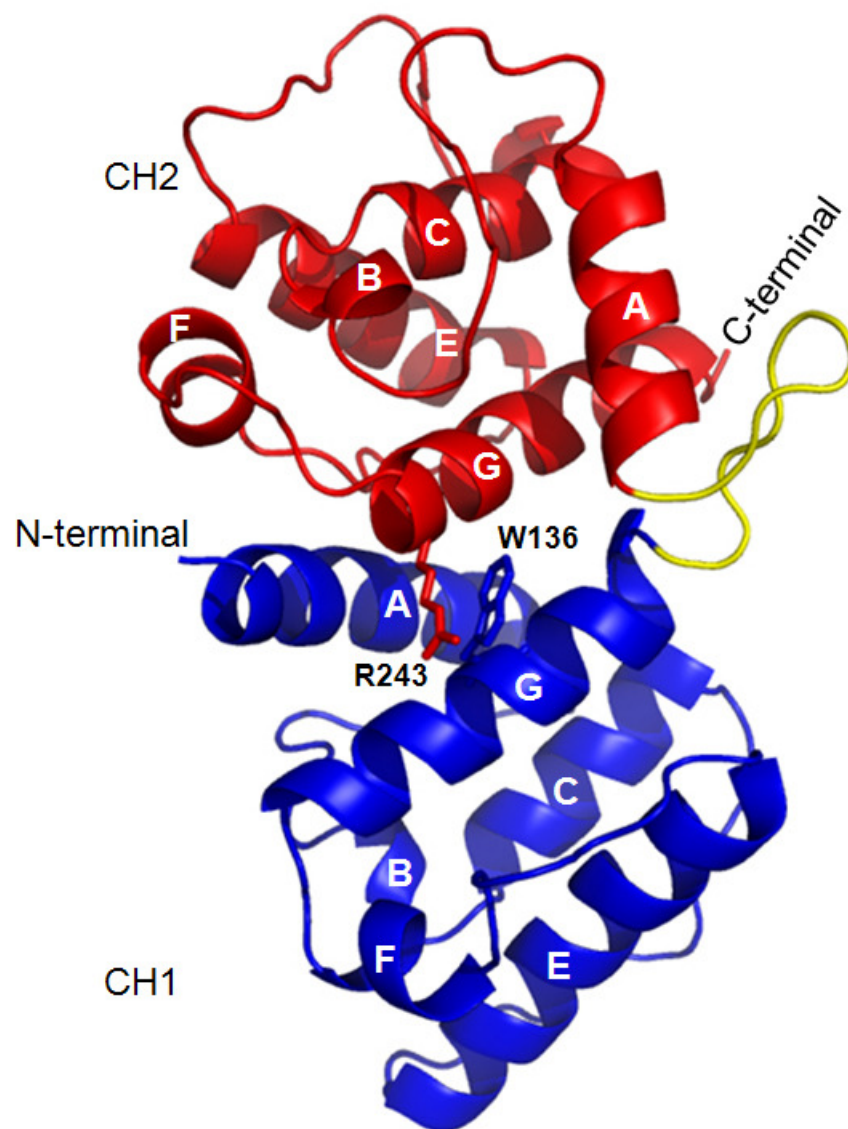


Figure 4.30 Overall structure of 2ABDY refined at 1.8 Å. The domain CH1 is coloured in blue, the CH2 is coloured in red and the α -helix are indicated by letters. The structure presents close conformation and the residues involved in the CH domains interactions are highlighted in sticks: W136 and R243. The picture was made using the program PyMOL (DeLano Scientific LLC), after validation through MolProbity (Davis et al., 2004).

4.10 Small angle X-ray scattering (SAXS): 2Eh, AFL and hd

The interaction of N-terminal and C-terminal ends of the α -actinin antiparallel dimer molecule was analyzed using SAXS. Data for human α -actinin both isoforms AFL, hd in different conditions ($\pm \text{Ca}^{2+}$ for isoform 1) and for *E. histolytica* α -actinin (2Eh) were collected on the X33 beamline (DESY, Hamburg).

Analysis of SAXS data presented maximum intramolecular distance for 2Eh ~ 240 Å, for 2hd ~ 190 Å and for 2AFL ~ 350 Å (Figure 4.31, inset). Additionally for 2AFL the distance distribution function presented a skewed appearance typical for elongated molecules. The low resolution molecular envelopes generated by SAXS data had expected sizes and shapes for all α -actinin constructs: 2Eh presented ~ 250 Å, 2hd ~ 194 Å and 2AFL ~ 365 Å, when compared to crystal structures of individual domains (central rod domain ~ 240 Å, ABD ~ 60 Å and EF-3/4 ~ 15 Å lengths).

Experimental X-ray scattering pattern for 2Eh, 2hd and 2AFL are shown in Figures 4.31. χ -values for fitting of *ab initio* models to experimental data are shown in Table 4.10.

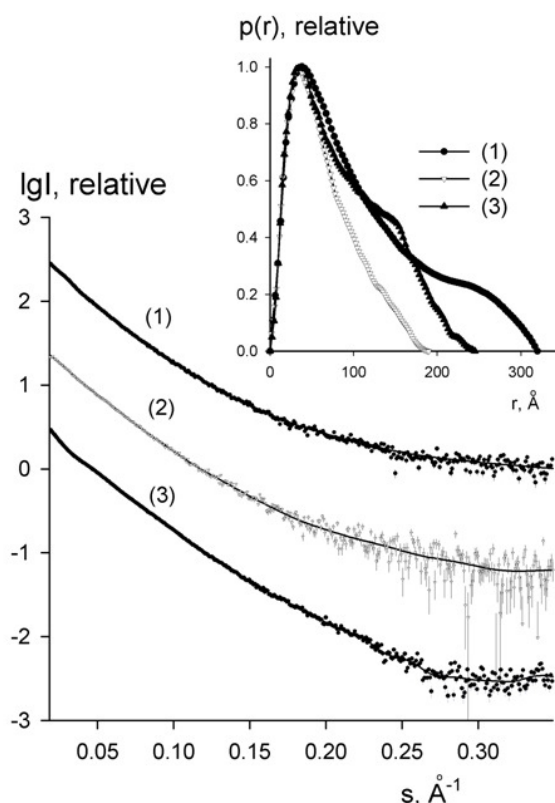


Figure 4.31 SAXS experimental X-ray scattering pattern for 2AFL (1), 2hd (2) and 2Eh (3) Full lines represent the scattering computed from a typical *ab initio* model. Distance distribution functions are displayed in the inset: 1- 2AFL, 2- 2hd and 3- 2Eh.

Table 4.10 SAXS χ -values for fitting of ab initio models to experimental data.

Sample	χ-value
1AFL	1.65
1hd	1.36
2AFL	1.86
2hd	1.24
2Eh	2.4

The molecular envelope of 2Eh, 2hd and 2AFL were fit with the structure of the individual domains by rigid body modelling. Models together with molecular envelopes are shown in Figure 4.32. χ -values for fitting of rigid body modelling to experimental data are shown in Table 4.11.

Table 4.11 SAXS χ -values for fitting of rigid body modelling to experimental data rigid body modelling χ -values.

Sample	χ-value
2AFL	2.40
2hd	1.65
2Eh	2.60

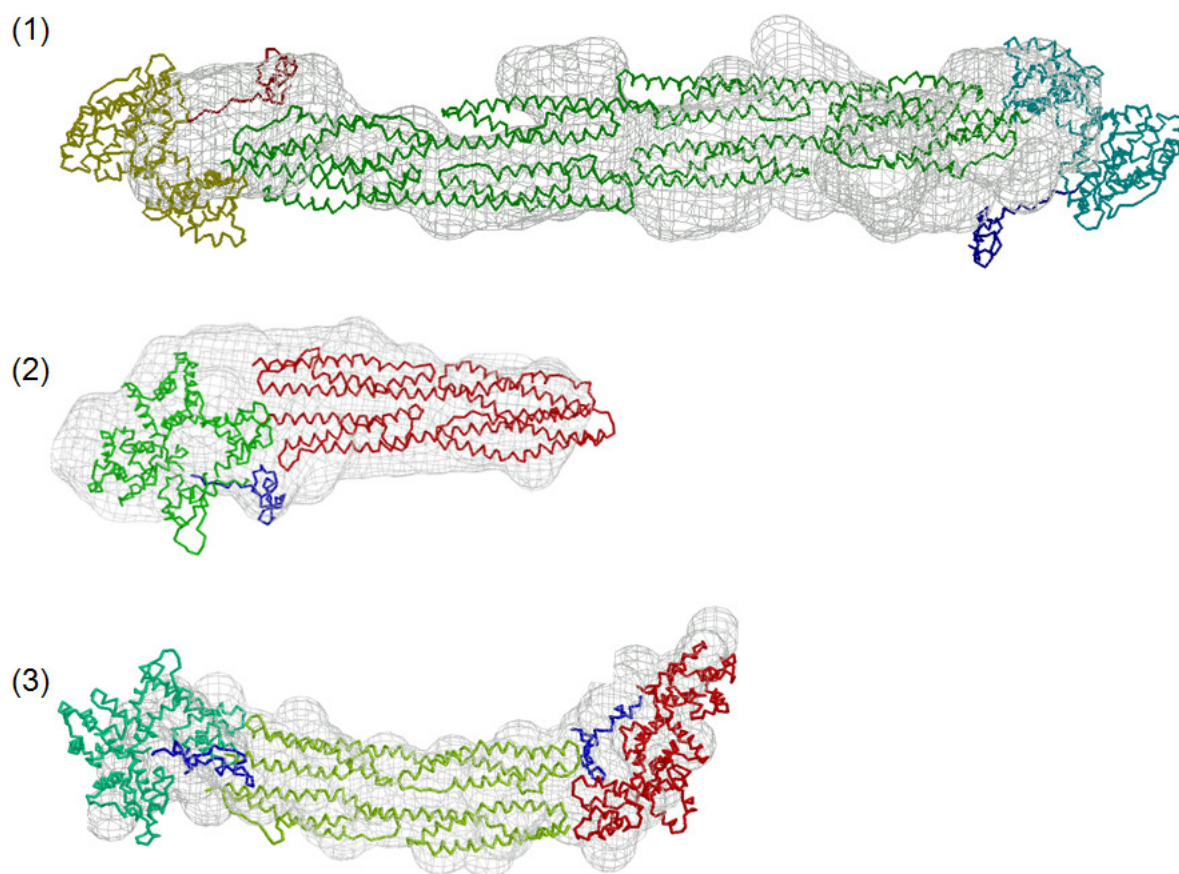


Figure 4.32 SAXS rigid body models for 2AFL (1), 2hd (2) and 2Eh (3) calculated using the program BUNCH (Petoukhov and Svergun, 2005). Molecular envelopes are represented with grey mesh and missing residues modelled as dummy atoms are represented as blue links.

5. DISCUSSION AND PERSPECTIVES

5.1 Cloning of α -actinin domains

The pETM system plasmids have the NcoI recognition site (5' C ∇ CATGG 3') immediately after the TEV cleavage site. This is the best approach for further structural studies since it involves addition of only one residue to the protein sequence. Given that α -actinin DNA has several NcoI recognition sites within its sequence, a strategy that would allow cloning these fragments into the pETM plasmids was necessary.

It involved the design of the forward oligonucleotides with a BsaI recognition site (5' GGTCTC(N)₁ ∇ 3') since it creates compatible ends to NcoI (Figure 5.1). This approach resulted, after TEV cleavage, in the addition of one glycine or alanine at the N-terminus (before the first residue of the protein).

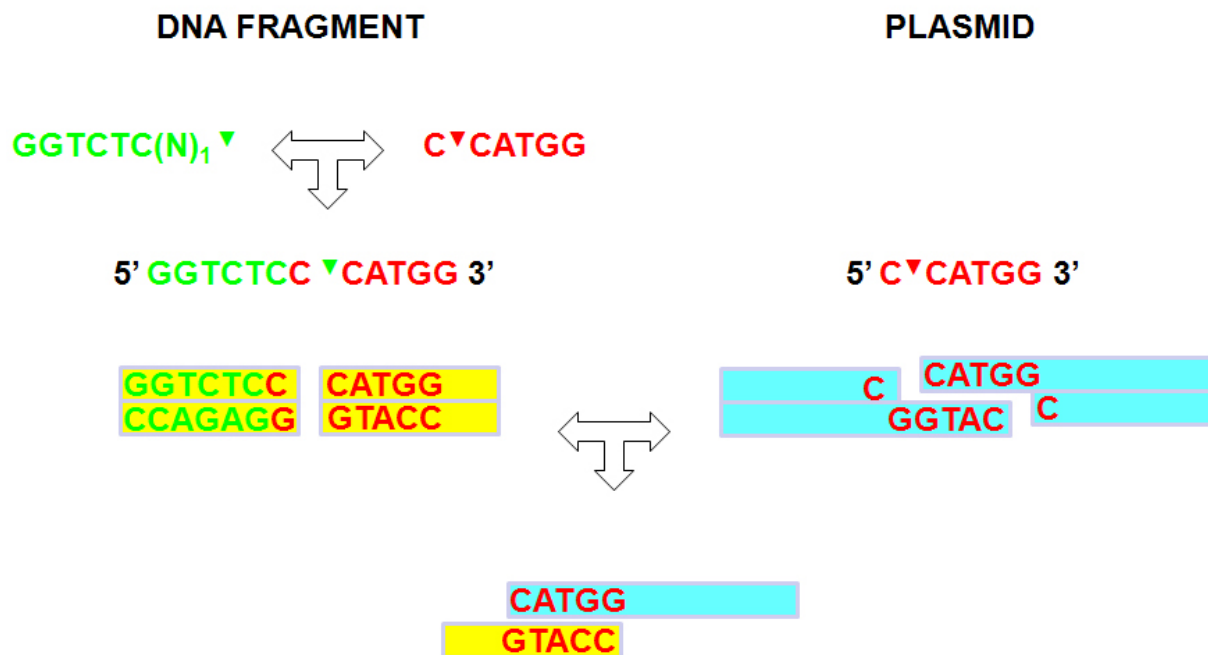


Figure 5.1 Schematic view of BsaI (green) and NcoI (red) compatible ends for cloning of human α -actinin inserts (yellow) into pETM expression plasmids (blue).

5.2 Actin binding domain (2ABD)

Series of binding studies were performed to validate the putative PiP2 binding site within the ABD (Franzot et al., 2005). Three single-site mutants (Δ 2ABDa R163E, Δ 2ABDa R169E and Δ 2ABDa R192E) were designed with this purpose (Figure 5.2). Arginine (R) residues were mutated to glutamate (E) to validate the predicted PiP2 binding residues since the repulsion between the negatively charged residue E and the PiP2 head group (inositols) would hinder PiP2 and ABD interaction.

The ABD of α -actinin isoform 2 construct (2ABDa WT) was designed starting at residue A35 (number corresponding to α -actinin isoform 2) exactly at the beginning of the actin-binding domain (Figure 3.1), according to the crystallographic structure of ABD isoform 3 (Franzot et al., 2005). Two out of three single-site mutants were successfully cloned, expressed and purified to homogeneity: Δ 2ABDa R169E and Δ 2ABDa R192E.

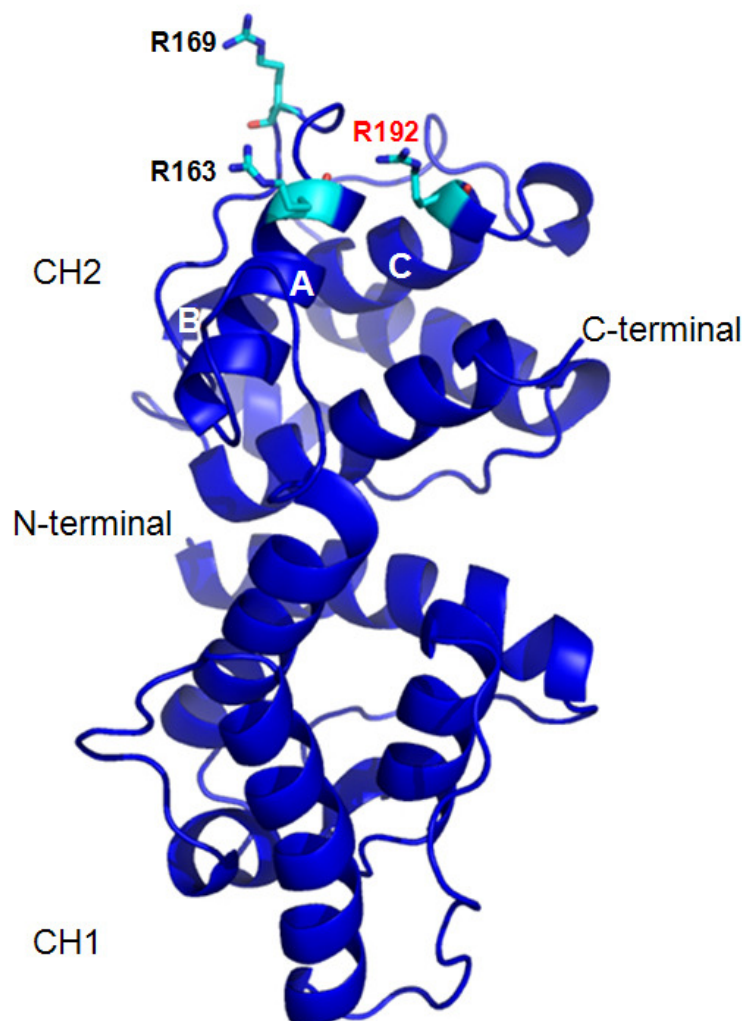


Figure 5.2 Putative PiP2 binding residues of 2ABD, residues involved are highlighted in sticks. The positive single-site mutants used on this work were Δ 2ABDa R169E and Δ 2ABDa R192E.

The initial binding study consisted of assays to assess the ability of the 2ABDa WT and mutants to bind different phosphoinositides. The experiments were carried out using PiP strips and no binding was observed with any of the ABD samples (Figure 4.22A - C). On the other hand, the chlorite dismutase from *Nitrospira* used as negative control showed binding to several phosphoinositides, including PiP2 (Figure 4.22D). Given that the control experiment was not reliable, these results were not taken in further consideration and alternative approaches were consequently employed to characterize the WT and the mutants.

Subsequent experiments involved use of inositols IP3 or IP6 as a substitute of PiP2 to avoid the interference of the hydrophobic tail in the binding studies or in further crystallization trails of the complex. IP3 is the soluble head group of PiP2, with three phosphates, while IP6 has six phosphates.

In an attempt to relate phosphoinositides influence on 2ABDa WT stability, we employed differential scanning fluorimetry (DSF). Results showed 2ABDa WT is stable with increasing IP6 concentration up to tenfold molar excess, when the melting temperature decreases (Figure 4.23), indicating protein destabilization. This could be caused by either by IP6 binding or most probably by protein aggregation upon increased amount of IP6, which could generate changes in pH and ionic strength of the sample.

Near-UV CD experiments were carried out to monitor potential protein tertiary conformational changes upon binding of IP6. 2ABDa WT to IP6 molar ratio was 1:10 to guarantee binding and no notable changes in tertiary structure were detected (Figure 4.24). This is in line with observations on other phosphoinositides binding domain, PH domain, which also do not undergo considerable structural changes upon ligand binding (Baraldi et al., 1999; Thomas et al., 2002).

Since IP6 carrying six phosphate groups might not be the highest affinity binder of α -actinin ABD, IP3 was used as ligand in all subsequent experiments.

2D-NMR experiments were carried out using the ^{15}N -labeled 2ABDa WT at different IP3 concentrations. Very small protein signal shifts were observed (Figure 4.25), preventing the determination of K_d from this titration experiment. Thus, a selective T1 measurement on the ligand IP3 was designed to validate the small protein shifts. No differences in the relaxation time (T1) of the ligand were observed, indicating inexistent or very weak binding under experimental conditions.

Quantitative characterization of 2ABDa WT and mutants binding to IP3 was performed through ITC. Data were acquired titrating IP3 to mutants Δ 2ABDa R169E, Δ 2ABDa R192E and to wild type 2ABDa WT (Figure 4.26). Data analysis (Table 4.7) showed an exothermic reaction, with low affinity, consequently K_d in the mM range. Although the dissociation constant of Δ 2ABDa R169E (1.8 ± 0.1 mM) and the WT (1.2 ± 0.03 mM) is 50% different, it suggests that this arginine residue R169 is probably not involved in binding of PiP2. On the contrary, the mutant Δ 2ABDa R192E (2.8 ± 0.1 mM) presents more than twofold difference in dissociation constant compared to the WT, indicating that this arginine residue R192, which is mapped to the end of α -helix C of CH2 domain (Figure 5.2), might play a role within the PiP2 interaction site: R163, R169 and R192 according to studies on ABD crystal structure [numbers according α -actinin isoform 2; (Franzot et al., 2005)].

Nevertheless, more accurate data need to be measured with the optimal protein concentration, a more suitable IP3 concentration and the ideal salt concentration (especially relevant in low affinity binding). Protein concentrations used in ITC experiments to verify reaction behaviour were based on the maximum concentration achievable for 2 ml of sample (technique limitation). With access to the new ITC machine (ITC200, MicroCal) in our laboratory, it will become possible to increase protein concentration easily, with a required sample volume ten times smaller (200 μ l).

In addition to these binding studies, crystal soaking of ABD into IP3 or IP6 and co-crystallization of ABD with IP3 were set up in order to validate the proposed PiP2 binding site within the ABD (Franzot et al., 2005). 6x His - 2ABDa WT was submitted to crystallization trials but since no crystal hits were obtained, the sample was subsequently submitted to TEV cleavage. The reaction was unsuccessful, possibly due to the fact that the TEV recognition site was not accessible to protease after the folding process.

A new ABD construct was, therefore, designed (2ABDY; Figure 5.3) based on the construct used to determine the crystal structure of α -actinin ABD isoform 3, which included the sixteen residues that precede the actin-binding domain of the ABDa construct (numbering according to α -actinin isoform 2). This construct initiates at the residue Y19, corresponding to the start of the first α -helix according to the secondary structure prediction (Figure 5.4).

The 6x Histag was cleaved successfully and crystal hits on 2ABDY were readily obtained in several different conditions (Figures 4.27 and 4.28).

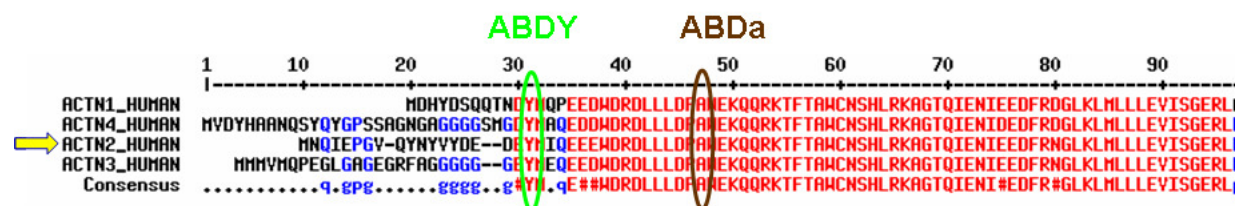


Figure 5.3 Alignment of the four human α -actinin isoforms, showing the difference between constructs. The ABDa starts at the beginning of the actin-binding domain (ABD), while the ABDY construct is longer and based on the structure of human ABD isoform 3. The 2FLY construct starts at the same tyrosine residue (Y19) as for ABDY (Figure 3.1). The alignment was performed using the Multiple Sequence Alignment software (Corpet, 1988).



Figure 5.4 N-terminal secondary structure prediction of 2ABD calculated by the software PSIPRED (Jones, 1999). **C** represents coil and **H** represents α -helix, which are also represented in green. In blue is represented the prediction confidence.

Soaking and co-crystallization experiments were set up using different IP3 or IP6 concentrations, in an attempt to obtain the protein-ligand complex under the crystallization process. Eight structures of 2ABDY were solved and analysed for the presence of the ligand, which was not found bound to ABD (section 4.9.6). The absence of bound ligand in the crystal structure might be due pH and precipitant agents concentrations used for crystallization that decrease the efficiency of binding, coupled to low intrinsic affinity as indicated by NMR and ITC experiments.

The 2ABDY crystal structure (Figure 4.30) was determined by molecular replacement using as a search model the structure of α -actinin ABD isoform 3 [PDB entry 1WKU; (Franzot et al., 2005)], which shares around 95% of identity with ABD isoform 2. As indicated from solvent content of 45% (Matthews B. W., 1968), two molecules in the asymmetric unit were searched for molecular replacement. Refinement and model statistics were very good already after a few cycles of refinement (Table 4.9).

2ABDY presented closed conformation of the two CH domains as observed for the ABD structure of other actin-binding proteins such as *S. pombe* fimbrin, utrophin, dystrophin, human and mouse plectin, as well as the other isoforms of α -actinin. However in utrophin and dystrophin structures, the closed conformation is attained *via* a domain swapping between two molecules, a crystal artefact observed and recognized in macromolecular crystallography. ABD open conformation was observed in *Arabidopsis thaliana* fimbrin (Borrego-Diaz et al., 2006; Franzot et al., 2005; Garcia-Alvarez et al., 2003; Goldsmith et al., 1997; Keep et al., 1999; Klein et al., 2004; Lee et al., 2008; Liu and Eisenberg, 2002; Sevcik et al., 2004). Comparison of 2ABDY refined structure with α -actinin isoforms 1, 3 and 4 (Figure 5.5) showed no significant differences in the overall structure, as indicated by r.m.s.d. after superposition of equivalent C α atoms ranging from 0.34 to 0.46 Å. Although the interaction between CH1 and CH2 domains of ABD is maintained by the residues K and W in α -actinin isoforms 1, 3 and 4; this interaction is maintained by residues R243 and W136 in isoform 2 (Figure 5.5), where the aliphatic part of R246 side chain is involved in hydrophobic interaction with W136 side chain.

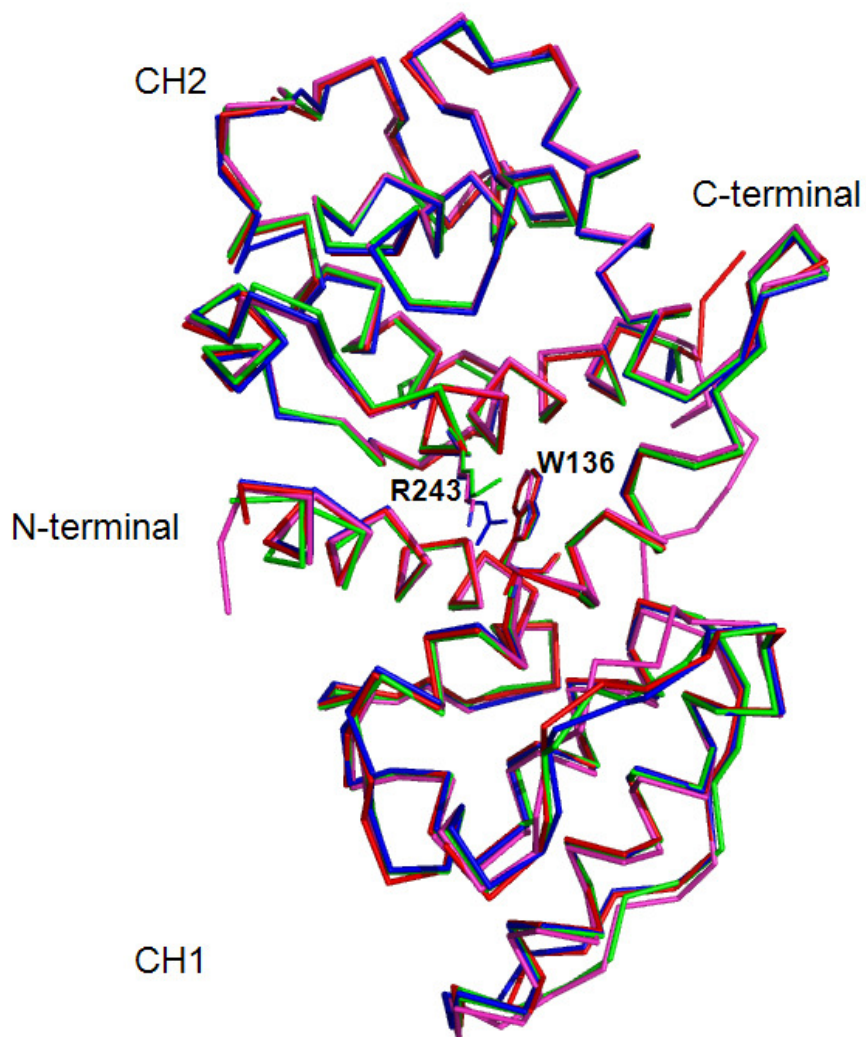


Figure 5.5 Structure superposition of human α -actinin ABD isoforms: 1 [pink; (Borrego-Diaz et al., 2006)], 2 (blue, Figure 4.30); 3 [green; (Franzot et al., 2005)] and 4 [red; (Lee et al., 2008)]. Residues involved in the CH1 and CH2 domains interactions are highlighted in lines: residues W are conserved in all four isoforms; residues K are found in isoforms 1, 3 and 4, while R is found in isoform 2 (numbers according to isoform 2).

5.3 Full length α -actinin

5.3.1 *Entamoeba histolytica* α -actinin (2Eh)

E. histolytica α -actinin isoform 2 is smaller than its human equivalent, presenting only two spectrin-like repeats instead of four as found in α -actinins from higher phyla. The structural studies on *E. histolytica* isoform 2 were undertaken, as it was therefore believed to be less flexible and more prone to crystallize.

Several commercial screens, different crystallization temperatures and protein conditions (tagged, non-tagged and at different concentrations) were used for crystallization trials that did not result in crystal hits. DSF and protein reductive methylation were consequently carried out in the attempt to enhance protein stability

in solution (DSF, Table 4.3) and the crystal packing by changing surface properties (Walter et al., 2006). These strategies resulted in crystal hits in several different conditions (Figure 4.15) and the optimization is in progress.

5.3.2 Human α -actinin isoform (2AFL)

Human α -actinin isoform 2 (2AFL) was submitted to crystallization trials using several commercial screens, different crystallization temperatures and protein conditions (tagged, non-tagged and in different concentrations). No crystal hits were obtained.

In order to increase protein stability in solution, DSF was employed to determine optimal buffer conditions. Crystallization trials were repeated with the identified optimal buffer (Table 4.3), but they proved unsuccessful.

Protein reductive methylation resulted in initial crystalline hits, which could be optimized to clusters of tiny needles (6x His - 2AFL Met-K, Figure 4.16), which in turn could not be refined to larger single crystals.

Rational surface engineering was therefore used, applying the methodology of surface entropy reduction (SER) mutation, which can enhance formation of crystal contacts (Derewenda, 2004b). Two mutants were successfully produced: the triple-site mutant 6x His – Δ 2AFL E23A/E24A/E25A and the double-site mutant 6x His – Δ 2AFL E310A/K311A. According to protein expression and purification yields (section 4.7), the double-site mutant (6x His-tag Δ 2AFL) was selected for further crystallization trials. The low protein yield observed for the triple mutant might be related to the importance of the N-terminal in protein folding or stability, since constructs with intact N-terminal (full length α -actinin, double-site mutant) do not show protein yield or stability problems.

Initial crystallization screens of the double-site mutant 6x His-tag Δ 2AFL yielded crystalline hits (Figure 4.17), which were difficult to optimize. Protein reductive methylation (6x His-tag Δ 2AFL Met-K) resulted in optimized single needles (Figure 4.18) that showed diffraction to resolution of 11 Å at ESRF beamline ID23-1.

In order to improve crystal quality and increase resolution limits, N-terminally truncated construct was designed (2AFLY), based on the same idea of keeping the integrity of the first α -helix used to design the construct 2ABDY (section 5.2; Figures 5.3 and 5.4). In this case, the first eighteen residues were excluded from the

construct, which also started at residue 19Y (numbering according to α -actinin isoform 2).

Full length α -actinin WT and both SER mutants (6x His – Δ 2AFL E23A/E24A/E25A and 6x His – Δ 2AFL E310A/K311A) were submitted to DNA amplification and cloning with primers designed for the N-terminally truncated construct, following the same methodology (section 3.2). Successfully cloning, protein expression and purification were obtained only for the SER double-site mutant (Δ 2AFLY): 6x His – Δ 2AFLY E310A/K311A. Crystallization trials for the new construct, Δ 2AFLY, resulted in single needles after reductive methylation. The needles obtained for 6x His - Δ 2AFLY Met-K (Figure 4.19) were notably bigger than those obtained for 6x His - Δ 2AFL Met-K and a partial data set to resolution around 4 Å was collected at the micro focus beamline ID23-2 (ESRF).

Three partial data sets were collected and merged during scaling, in an attempt to obtain a complete data set. Data were indexed and integrated in orthorhombic space group P222 but data quality and limited resolution prevented from discerning the real space groups P222₁, P2₁2₁2 and P2₁2₁2₁ through analysis of systematic absences. The merged data were not of sufficient quality to solve the structure (Table 4.6).

Subsequently, the tag from 6x His - Δ 2AFLY was cleaved and single crystals were obtained in different crystal forms after protein reductive methylation (Δ 2AFLY Met-K; Figure 4.20). X-ray data were collected at beamline ID23-1 (ESRF). Extensive screens of diffraction capacity of crystals (on average of ~ 80 crystals diffracted X-ray) yielded diffraction data from one Δ 2AFLY crystal to a resolution of around 4 Å. Higher resolution data were, however, of poor quality and a resolution cut-off at 6.7 Å was necessary to produce a complete data set with acceptable data statistics (Table 4.7). The data were integrated on space group orthorhombic (P222) and as in the case of the tagged construct 6x His - Δ 2AFLY Met-K, the real space group was not assigned due to the absence of high resolution data.

According to Matthews coefficient calculations [$V_M = 3.30 \text{ \AA}^3 \cdot \text{Da}^{-1}$; (Matthews B. W., 1968)], the asymmetric unit of Δ 2AFLY crystal could accommodate either one half dimer molecule (hd) or one full monomer. Considering α -actinin molecular architecture where two subunits are related by a twofold axis perpendicular to the central rod domain axis and the fact that the expected length of the full monomer (~ 400 Å) is too long to fit in the asymmetric unit ($a = 72.4 \text{ \AA}$, $b = 101.4 \text{ \AA}$, $c = 179.8 \text{ \AA}$

and $\alpha = \beta = \gamma = 90^\circ$; Table 4.7), the unit cell packing accommodating the half dimer molecule is believed to be the most probable.

Improvement of crystal diffraction quality due to surface engineering plus design of an N-terminal truncated version of 2AFL is shown Figure 4.21. Protein surface charges might be affecting crystal packing, therefore, changes in surface properties induced by protein reductive methylation combined with SER mutation strategies enhanced crystallization propensity of $\Delta 2AFLY$, resulting in crystal hits. Further experimental optimizations are necessary to obtain diffraction data to higher resolution and quality. Two approaches combined with massive screening of crystals could be employed: protein reductive cyclic pentylation of free amines by glutaraldehyde (Vetting et al., 2009) and post-crystallization treatments, including crystal dehydration [reviewed by (Heras and Martin, 2005)].

5.4 Protein-protein complex: α -actinin half dimer (hd) and PDZ domain of ZASP

It is known that the PDZ domain of ZASP interacts with the C-terminal region (EF-3/4) of α -actinin isoform 2 (Faulkner et al., 1999). This complex was used as a model to validate the regulation of α -actinin upon phosphatidylinositol (4, 5)-biphosphate (PiP2) binding, in the context of antiparallel dimer where functional domains (ABD and CaM) are juxtaposed. Protein components of the complex formation were the half dimer of α -actinin isoform 2 (2hd) and the PDZ domain of ZASP. Lysophosphatidic acid (LPA) was used to check if it could enhance the complex formation, since it is more soluble than PiP2 and contains the same hydrophobic tail as PiP2 molecule. Therefore, LPA hydrophobic tail could disturb the interaction of N-terminal and C-terminal of α -actinin antiparallel subunits.

Complex formation studies were carried out by preparative and analytical size exclusion chromatography. The preparative size exclusion chromatography was used as a pilot experiment and resulted, in the absence of LPA, in a complex formation between the tagged PDZ and the excess of tagged α -actinin C-terminal part of the dimer (6x His – R3_SR4_CaM, Figure 4.13). Consequently, analytical size exclusion chromatography studies were performed to verify whether the LPA would enhance complex formation without any excess of 6x His – SR3_SR4_CaM.

Different 2hd, PDZ and LPA molar ratios were prepared for the analytical studies. As can be seen in Figure 4.14 (D and E), a formation of a new peak is observed in the size exclusion chromatography elution profile in the presence of LPA.

This peak contains the 2hd molecule alone (Figure 4.14F), indicating that either the 2hd is aggregating in the presence of LPA due to alterations in pH or 2hd is interacting with LPA. If the latter case occurred, it shows that although 2hd and LPA interact, no complex between α -actinin and PDZ domain of ZASP is formed under conditions used.

Since the binding affinity between the PDZ domain of ZASP and α -actinin EF-3/4 is relatively weak [$K_d = 35.6 \mu\text{M}$; (Au et al., 2004)] the experimental condition used for SEC could have hindered binding or disturbed the complex formation. Another explanation could be that the head of LPA is not interacting properly with ABD, since it is considerably different from PiP2 soluble head, resulting in the tail not being positioned correctly to interfere with the binding of CaM domain of one subunit to the neck of the other subunit.

5.5 Other constructs

5.5.1 α -actinin domains complex

In order to understand the molecular architecture of α -actinin and the structural mechanisms underlying its regulation, the production of different complexes involving shorter N-terminal and C-terminal regions of α -actinin composed of only one or two consecutive domains (ABDa_SR1 and SR4_CaM, CaM or EF-3/4; Figure 3.1) was attempted for structural studies. Two different approaches were employed: co-expression (Figure 4.3 and Table 4.2) and co-purification experiments (Figure 4.12), which both resulted in similar results: low purity, low concentration and insolubility issues (Figures 4.3 and 4.12), which made crystallization trials impossible.

5.5.1.1 Co-expression

For co-expression experiments, complexes formation was attempted between tagged and/or non-tagged domains of α -actinin isoforms 1 and 2 (Figure 4.3 and Table 4.2). Different approaches to achieve high-level expression of the recombinant proteins were used, such as transforming several *E. coli* hosts with plasmids, cloning the fragments into different plasmids and over-expressing the recombinant protein at different temperatures [reviewed by (Makrides, 1996)].

N-terminal and C-terminal constructs used were: the N-terminal part ABDa_SR1 (actinin binding domain plus spectrin-like repeat 1) and C-terminal part SR4_CaM (spectrin-like repeat 4 plus calmodulin like domain), CaM (calmodulin like

domain with 4 EF hands) or EF-3/4 (the last part of the calmodulin like domain with EF hands 3 and 4). Generally, a soluble C-terminal component and an insoluble N-terminal component (Figure 4.3) were obtained. Since protein solubility was checked after a small scale over-expression assay and the protein yield was not high, the most promising soluble complex ABDa_SR1 (6x His-tag + TrxA tagged) and SR4_CaM (non-tagged) of α -actinin isoform 2 (Sample 15 in Figure 4.3) was selected for scale-up. Large scale over-expression experiment (Figure 4.11A, B) resulted in a complex of 2ABDa_SR1 + 2SR4_CaM complex (Figure 4.11C), which was neither sufficiently pure nor concentrated to allow for crystallization trials.

Over-expression of another protein of a molecular weight around 40 kDa was present in almost all tested conditions. It was speculated that it could be a product of ABDa_SR1 degradation, but since this protein is present even in the presence of protease inhibitors during cell lysis as well as when the protein expression is induced at 20°C. We believe that it could be one of the classical *E. coli* contaminants - chaperone protein DnaJ, which can be co-purified by IMAC, binding either to the recombinant protein or directly to the resin (Graslund et al., 2008).

5.5.1.2 Co-purification

Co-purification experiments were carried out in attempt to obtain complexes of tagged and/or non-tagged domains of α -actinin isoforms 1 and 2. The components used in this study were ABDa_SR1 (6x His-tag + TrxA tagged) with CaM or EF-3/4, either tagged or non-tagged (Figure 3.1, Table 4.1). Results of gravity flow IMAC (Figure 4.12) show a low protein yield and purity and confirm the presence of the additional protein with a molecular weight around 40 kDa as obtained in the co-expression experiments.

Another approach used to form a complex of α -actinin N-terminal and C-terminal domains was based on purification of individual domains and subsequent complex formation after purification steps. TEV cleavage of the tag from 6x His - ABDa_SR1 resulted in protein aggregation, caused due to the hydrophobic patches found at the spectrin-like repeat 1 [SR1;(Ylanne et al., 2001a)] or not optimal cleavage conditions. Additionally, this aggregation could as well be a result of the absence of the N-terminal, which might be involved in protein folding or stability. As already mentioned, according to the secondary structure prediction (Figure 5.4), a construct starting at residue 35 (number corresponds to α -actinin isoform 2) is lacking

part of the first α -helix, which is probably disturbing the structural integrity of the protein.

5.5.2 α -Actinin half dimer (*hd*)

The approach of generating α -actinin half of the dimer unit *via* bicistronic vector where the N-terminal is not tagged (ABD_SR1_SR2) and the C-terminal is tagged (6x His - SR3_SR4_CaM) proved to be the best way to purify a smaller version than α -actinin full length (AFL) homodimer (Figure 4.9). The stability of *hd* is comparable to the AFL dimer along the lines that the SR stabilize the dimer formation.

5.5.3 Crystallization of other α -actinin constructs

Crystallization trails for α -actinin half dimer of both isoforms and the full length of isoform 1 were unsuccessful, even after protein reductive methylation. Strategies to obtain diffraction quality crystal will probably require involvement of surface engineering similar to what was applied to 2AFL, since protein reductive methylation alone did not yield crystal hits.

5.6 Small angle X-ray scattering (SAXS): 2Eh, AFL and *hd*

SAXS derived molecular envelopes for human α -actinin full length and half dimers as well as on *E. histolytica* α -actinin (Figures 4.32 and 4.33) presented the expected sizes as estimated from structural information on individual domains: ABD (Franzot et al., 2005), central rod domain (Ylanne et al., 2001a) and EF-3/4 (Atkinson et al., 2001) and rigid body fitting, both presenting very good χ -values (around 1; Tables 4.10 and 4.11).

The molecular envelopes in all cases showed CaM in the proximity of ABD in close conformation (as observed in the ABD crystal structure, Figure 4.30). This structural information on α -actinin in solution sheds additional light on the question of open/closed conformation of ABD in α -actinin cryo EM study of frozen hydrated 2-D arrays of α -actinin rabbit muscle isoform showing ABD in open conformation (Tang et al., 2001) and 3-D reconstruction of chicken gizzard α -actinin in lipid layers revealed ABD in both open and closed conformation (Liu et al., 2004).

At the available SAXS data resolution (~ 20 Å), it was not possible to observe conformational changes in α -actinin N-terminal or C-terminal ends, when Ca^{2+} was

added to the sample, given that the expected changes are localized in the C-terminal calcium binding domain (CaM), which represents only ~ 7% of the scattering mass of entire dimer. Another reason for no observed conformational changes could be in the protein preparation, in what concerns the presence and absence of Ca^{2+} ions: if they were present from the starting point, changes upon addition of Ca^{2+} could not be triggered. New samples of full length α -actinin isoform 1 (Ca^{2+} sensitive) were, subsequently, prepared in a buffer containing Ca^{2+} (20 mM Tris-HCl pH 7.6, 150 mM NaCl, 2 mM CaCl_2) or in a buffer excluding Ca^{2+} (20 mM Tris-HCl pH 7.6, 150 mM NaCl, 5 mM EDTA). Ca^{2+} ion chelating agent (EDTA) was added to insure that the α -actinin sample was Ca^{2+} ion free. SAXS data from the two samples were collected and analysis is ongoing in collaboration with the SAXS group of EMBL-Hamburg (DESY).

6. CONCLUSIONS

6.1 Actin binding domain (2ABD)

Validation of the putative PiP2 binding site involved binding studies IP3 or IP6 (phosphoinositides head group with three and six phosphates respectively) with ABD WT, PiP2 single-site mutants (two out of three residues predicted to be involved in PiP2 interaction mutated: Δ R169E and Δ R192E).

Among all experiments performed to characterise the interaction (DSF, CD, NMR and ITC), ITC was the only that clearly showed binding, albeit weak. These results indicate that ABD and IP3 are low affinity binders in general and that residue 192 (R192) might be an important player in this interaction, as the mutant Δ R192E showed a significantly lower affinity constant to IP3.

Besides these binding studies, crystallization trials were carried out in the presence of IP3 or IP6 by crystal soaking or co-crystallization. Crystal hits were obtained in several conditions and eight crystal structures could be determined to a resolution of 1.8 Å and analysed for ligand binding. No IP3 or IP6 were found bound to ABD and the absence of ligand in the structure could be attributed to the low affinity as seen in the binding studies, combined with crystallization conditions, which might not be optimal for binding.

6.2 Full length α -actinin

Due to its size and flexibility, full length α -actinin has been considered a recalcitrant protein to crystallization for a long time. Automation of crystallization procedures through implementation of robotics, able to set thousands of different conditions in a short time, and improvement of protein surface engineering methodologies have provided the necessary tools for α -actinin crystallization.

Successful enhancement of crystal contacts and induced crystal growth were achieved through protein surface engineering methodologies (protein reductive methylation and surface entropy reduction - SER), giving these techniques an outstanding relevance for the results described in this thesis.

Although *E. histolytica* α -actinin is a smaller version and distantly related to the human isoforms, crystal hits were obtained only after protein reductive methylation. For human α -actinin isoform 2, besides reductive methylation, SER mutations had to

be performed in order to obtain crystal hits, demonstrating critical interference of surface charges on the crystal packing process.

Improvement of crystal diffraction quality for human α -actinin SER mutant (Δ 2AFL) correlated with employed strategies, becoming better with the truncated version SER mutant (Δ 2AFLY), after reductive methylation and His-tag cleavage. Nevertheless, these crystals diffracted to low resolution, making structure determination not amenable.

6.3 Protein-protein complex: α -actinin half dimer (hd) and PDZ domain of ZASP

Binding studies were performed to verify whether the hydrophobic tail of PiP2 is able to enhance complex formation of ZASP and α -actinin. These studies were carried out using LPA since it contains the same hydrophobic tail as PiP2. No binding between α -actinin hd and PDZ domain of ZASP was observed under the experimental conditions used. The polar head of LPA might not interact strongly enough with ABD to bring about the hydrophobic tail, which hinders binding of α -actinin N-terminal and C-terminal ends. Additionally, due to the low affinity constant of PDZ domain of ZASP and α -actinin EF-3/4, size exclusion chromatography might not be the best way to study this interaction.

6.4 Final remark

Several questions concerning α -actinin regulation and its overall molecular architecture remain open, but the work described here contributed to bringing us closer than ever to answering them.

7. REFERENCES

- Araki, N., Hatae, T., Yamada, T., and Hirohashi, S. (2000). Actinin-4 is preferentially involved in circular ruffling and macropinocytosis in mouse macrophages: analysis by fluorescence ratio imaging. *J Cell Sci* *113* (Pt 18), 3329-3340.
- Arimura, C., Suzuki, T., Yanagisawa, M., Imamura, M., Hamada, Y., and Masaki, T. (1988). Primary structure of chicken skeletal muscle and fibroblast alpha-actinins deduced from cDNA sequences. *Eur J Biochem* *177*, 649-655.
- Atkinson, R.A., Joseph, C., Kelly, G., Muskett, F.W., Frenkiel, T.A., Nietlispach, D., and Pastore, A. (2001). Ca²⁺-independent binding of an EF-hand domain to a novel motif in the alpha-actinin-titin complex. *Nat Struct Biol* *8*, 853-857.
- Au, Y., Atkinson, R.A., Guerrini, R., Kelly, G., Joseph, C., Martin, S.R., Muskett, F.W., Pallavicini, A., Faulkner, G., and Pastore, A. (2004). Solution structure of ZASP PDZ domain; implications for sarcomere ultrastructure and enigma family redundancy. *Structure* *12*, 611-622.
- Baines, A.J. (2003). Comprehensive analysis of all triple helical repeats in beta-spectrins reveals patterns of selective evolutionary conservation. *Cell Mol Biol Lett* *8*, 195-214.
- Banuelos, S., Saraste, M., and Djinovic-Carugo, K. (1998). Structural comparisons of calponin homology domains: implications for actin binding. *Structure* *6*, 1419-1431.
- Baraldi, E., Djinovic Carugo, K., Hyvonen, M., Surdo, P.L., Riley, A.M., Potter, B.V., O'Brien, R., Ladbury, J.E., and Saraste, M. (1999). Structure of the PH domain from Bruton's tyrosine kinase in complex with inositol 1,3,4,5-tetrakisphosphate. *Structure* *7*, 449-460.
- Barstead, R.J., Kleiman, L., and Waterston, R.H. (1991). Cloning, sequencing, and mapping of an alpha-actinin gene from the nematode *Caenorhabditis elegans*. *Cell Motil Cytoskeleton* *20*, 69-78.
- Beggs, A.H., Byers, T.J., Knoll, J.H., Boyce, F.M., Bruns, G.A., and Kunkel, L.M. (1992). Cloning and characterization of two human skeletal muscle alpha-actinin genes located on chromosomes 1 and 11. *J Biol Chem* *267*, 9281-9288.
- Blanchard, A., Ohanian, V., and Critchley, D. (1989). The structure and function of alpha-actinin. *J Muscle Res Cell Motil* *10*, 280-289.
- Borgstahl, G.E. (2007). How to use dynamic light scattering to improve the likelihood of growing macromolecular crystals. *Methods Mol Biol* *363*, 109-129.
- Borrego-Diaz, E., Kerff, F., Lee, S.H., Ferron, F., Li, Y., and Dominguez, R. (2006). Crystal structure of the actin-binding domain of alpha-actinin 1: evaluating two competing actin-binding models. *J Struct Biol* *155*, 230-238.

- Brenman, J.E., Chao, D.S., Gee, S.H., McGee, A.W., Craven, S.E., Santillano, D.R., Wu, Z., Huang, F., Xia, H., Peters, M.F., *et al.* (1996). Interaction of nitric oxide synthase with the postsynaptic density protein PSD-95 and alpha1-syntrophin mediated by PDZ domains. *Cell* *84*, 757-767.
- Bresnick, A.R., Janmey, P.A., and Condeelis, J. (1991). Evidence that a 27-residue sequence is the actin-binding site of ABP-120. *J Biol Chem* *266*, 12989-12993.
- Bresnick, A.R., Warren, V., and Condeelis, J. (1990). Identification of a short sequence essential for actin binding by Dictyostelium ABP-120. *J Biol Chem* *265*, 9236-9240.
- Bricheux, G., Coffe, G., Pradel, N., and Bruggerolle, G. (1998). Evidence for an uncommon alpha-actinin protein in *Trichomonas vaginalis*. *Mol Biochem Parasitol* *95*, 241-249.
- Broderick, M.J., and Winder, S.J. (2005). Spectrin, alpha-actinin, and dystrophin. *Adv Protein Chem* *70*, 203-246.
- Burridge, K., and Feramisco, J.R. (1981). Non-muscle alpha actinins are calcium-sensitive actin-binding proteins. *Nature* *294*, 565-567.
- Castresana, J., and Saraste, M. (1995). Does Vav bind to F-actin through a CH domain? *FEBS Lett* *374*, 149-151.
- Clark, K.A., McElhinny, A.S., Beckerle, M.C., and Gregorio, C.C. (2002). Striated muscle cytoarchitecture: an intricate web of form and function. *Annu Rev Cell Dev Biol* *18*, 637-706.
- Condeelis, J., and Vahey, M. (1982). A calcium- and pH-regulated protein from Dictyostelium discoideum that cross-links actin filaments. *J Cell Biol* *94*, 466-471.
- Corgan, A.M., Singleton, C., Santoso, C.B., and Greenwood, J.A. (2004). Phosphoinositides differentially regulate alpha-actinin flexibility and function. *Biochem J* *378*, 1067-1072.
- Corpet, F. (1988). Multiple sequence alignment with hierarchical clustering. *Nucleic Acids Res* *16*, 10881-10890.
- Corrado, K., Mills, P.L., and Chamberlain, J.S. (1994). Deletion analysis of the dystrophin-actin binding domain. *FEBS Lett* *344*, 255-260.
- Crowley, P.B., and Golovin, A. (2005). Cation-pi interactions in protein-protein interfaces. *Proteins* *59*, 231-239.

- Cuppen, E., Gerrits, H., Pepers, B., Wieringa, B., and Hendriks, W. (1998). PDZ motifs in PTP-BL and RIL bind to internal protein segments in the LIM domain protein RIL. *Mol Biol Cell* *9*, 671-683.
- D'Arcy, A. (1994). Crystallizing proteins - a rational approach? *Acta Crystallogr D Biol Crystallogr* *50*, 469-471.
- Davis, I.W., Murray, L.W., Richardson, J.S., and Richardson, D.C. (2004). MOLPROBITY: structure validation and all-atom contact analysis for nucleic acids and their complexes. *Nucleic Acids Res* *32*, W615-619.
- Davison, M.D., and Critchley, D.R. (1988). alpha-Actinins and the DMD protein contain spectrin-like repeats. *Cell* *52*, 159-160.
- Derewenda, Z.S. (2004a). Rational protein crystallization by mutational surface engineering. *Structure* *12*, 529-535.
- Derewenda, Z.S. (2004b). The use of recombinant methods and molecular engineering in protein crystallization. *Methods* *34*, 354-363.
- Djinovic-Carugo, K., Gautel, M., Ylanne, J., and Young, P. (2002). The spectrin repeat: a structural platform for cytoskeletal protein assemblies. *FEBS Lett* *513*, 119-123.
- Djinovic-Carugo, K., Young, P., Gautel, M., and Saraste, M. (1999). Structure of the alpha-actinin rod: molecular basis for cross-linking of actin filaments. *Cell* *98*, 537-546.
- Edlund, M., Lotano, M.A., and Otey, C.A. (2001). Dynamics of alpha-actinin in focal adhesions and stress fibers visualized with alpha-actinin-green fluorescent protein. *Cell Motil Cytoskeleton* *48*, 190-200.
- Emsley, P., and Cowtan, K. (2004). Coot: model-building tools for molecular graphics. *Acta Crystallogr D Biol Crystallogr* *60*, 2126-2132.
- Ericsson, U.B., Hallberg, B.M., Detitta, G.T., Dekker, N., and Nordlund, P. (2006). Thermofluor-based high-throughput stability optimization of proteins for structural studies. *Anal Biochem* *357*, 289-298.
- Ervasti, J.M. (2003). Costameres: the Achilles' heel of Herculean muscle. *J Biol Chem* *278*, 13591-13594.
- Fabbrizio, E., Bonet-Kerrache, A., Leger, J.J., and Mornet, D. (1993). Actin-dystrophin interface. *Biochemistry* *32*, 10457-10463.
- Faulkner, G., Lanfranchi, G., and Valle, G. (2001). Telethonin and other new proteins of the Z-disc of skeletal muscle. *IUBMB Life* *51*, 275-282.

- Faulkner, G., Pallavicini, A., Formentin, E., Comelli, A., Ievolella, C., Trevisan, S., Bortoletto, G., Scannapieco, P., Salamon, M., Mouly, V., *et al.* (1999). ZASP: a new Z-band alternatively spliced PDZ-motif protein. *J Cell Biol* *146*, 465-475.
- Fechheimer, M., Brier, J., and Rockwell, M. (1982). A calcium- and pH-regulated actin binding protein from *D. discoideum* *Cell Motility* *2*, 287-308.
- Flood, G., Kahana, E., Gilmore, A.P., Rowe, A.J., Gratzer, W.B., and Critchley, D.R. (1995). Association of structural repeats in the alpha-actinin rod domain. Alignment of inter-subunit interactions. *J Mol Biol* *252*, 227-234.
- Flood, G., Rowe, A.J., Critchley, D.R., and Gratzer, W.B. (1997). Further analysis of the role of spectrin repeat motifs in alpha-actinin dimer formation. *Eur Biophys J* *25*, 431-435.
- Fraley, T.S., Tran, T.C., Corgan, A.M., Nash, C.A., Hao, J., Critchley, D.R., and Greenwood, J.A. (2003). Phosphoinositide binding inhibits alpha-actinin bundling activity. *J Biol Chem* *278*, 24039-24045.
- Franco, S., Perrin, B., and Huttenlocher, A. (2004). Isoform specific function of calpain 2 in regulating membrane protrusion. *Exp Cell Res* *299*, 179-187.
- Franzot, G., Sjoblom, B., Gautel, M., and Djinovic Carugo, K. (2005). The crystal structure of the actin binding domain from alpha-actinin in its closed conformation: structural insight into phospholipid regulation of alpha-actinin. *J Mol Biol* *348*, 151-165.
- Frixione, E. (2000). Recurring views on the structure and function of the cytoskeleton: a 300-year epic. *Cell Motil Cytoskeleton* *46*, 73-94.
- Fukami, K., Furuhashi, K., Inagaki, M., Endo, T., Hatano, S., and Takenawa, T. (1992). Requirement of phosphatidylinositol 4,5-bisphosphate for alpha-actinin function. *Nature* *359*, 150-152.
- Fukami, K., Sawada, N., Endo, T., and Takenawa, T. (1996). Identification of a phosphatidylinositol 4,5-bisphosphate-binding site in chicken skeletal muscle alpha-actinin. *J Biol Chem* *271*, 2646-2650.
- Full, S.J., Deinzer, M.L., Ho, P.S., and Greenwood, J.A. (2007). Phosphoinositide binding regulates alpha-actinin CH2 domain structure: analysis by hydrogen/deuterium exchange mass spectrometry. *Protein Sci* *16*, 2597-2604.
- Fyrberg, E., Kelly, M., Ball, E., Fyrberg, C., and Reedy, M.C. (1990). Molecular genetics of *Drosophila* alpha-actinin: mutant alleles disrupt Z disc integrity and muscle insertions. *J Cell Biol* *110*, 1999-2011.

- Garcia-Alvarez, B., Bobkov, A., Sonnenberg, A., and de Pereda, J.M. (2003). Structural and functional analysis of the actin binding domain of plectin suggests alternative mechanisms for binding to F-actin and integrin beta4. *Structure* *11*, 615-625.
- Gimona, M., Djinovic-Carugo, K., Kranewitter, W.J., and Winder, S.J. (2002). Functional plasticity of CH domains. *FEBS Lett* *513*, 98-106.
- Gimona, M., and Winder, S.J. (1998). Single calponin homology domains are not actin-binding domains. *Curr Biol* *8*, R674-675.
- Goldschmidt, L., Cooper, D.R., Derewenda, Z.S., and Eisenberg, D. (2007). Toward rational protein crystallization: A Web server for the design of crystallizable protein variants. *Protein Sci* *16*, 1569-1576.
- Goldsmith, S.C., Pokala, N., Shen, W., Fedorov, A.A., Matsudaira, P., and Almo, S.C. (1997). The structure of an actin-crosslinking domain from human fimbrin. *Nat Struct Biol* *4*, 708-712.
- Granzier, H., and Labeit, S. (2007). Structure-function relations of the giant elastic protein titin in striated and smooth muscle cells. *Muscle Nerve* *36*, 740-755.
- Granzier, H.L., and Labeit, S. (2005). Titin and its associated proteins: the third myofilament system of the sarcomere. *Adv Protein Chem* *71*, 89-119.
- Graslund, S., Nordlund, P., Weigelt, J., Hallberg, B.M., Bray, J., Gileadi, O., Knapp, S., Oppermann, U., Arrowsmith, C., Hui, R., *et al.* (2008). Protein production and purification. *Nat Methods* *5*, 135-146.
- Greenwood, J.A., Theibert, A.B., Prestwich, G.D., and Murphy-Ullrich, J.E. (2000). Restructuring of focal adhesion plaques by PI 3-kinase. Regulation by PtdIns (3,4,5)-p(3) binding to alpha-actinin. *J Cell Biol* *150*, 627-642.
- Grum, V.L., Li, D., MacDonald, R.I., and Mondragon, A. (1999). Structures of two repeats of spectrin suggest models of flexibility. *Cell* *98*, 523-535.
- Hanahan, D. (1983). Studies on transformation of *Escherichia coli* with plasmids. *J Mol Biol* *166*, 557-580.
- Hemmings, L., Kuhlman, P.A., and Critchley, D.R. (1992). Analysis of the actin-binding domain of alpha-actinin by mutagenesis and demonstration that dystrophin contains a functionally homologous domain. *J Cell Biol* *116*, 1369-1380.
- Heras, B., and Martin, J.L. (2005). Post-crystallization treatments for improving diffraction quality of protein crystals. *Acta Crystallogr D Biol Crystallogr* *61*, 1173-1180.

- Honda, K., Yamada, T., Endo, R., Ino, Y., Gotoh, M., Tsuda, H., Yamada, Y., Chiba, H., and Hirohashi, S. (1998). Actinin-4, a novel actin-bundling protein associated with cell motility and cancer invasion. *J Cell Biol* 140, 1383-1393.
- Hung, A.Y., and Sheng, M. (2002). PDZ domains: structural modules for protein complex assembly. *J Biol Chem* 277, 5699-5702.
- Ikura, M. (1996). Calcium binding and conformational response in EF-hand proteins. *Trends Biochem Sci* 21, 14-17.
- Izaguirre, G., Aguirre, L., Hu, Y.P., Lee, H.Y., Schlaepfer, D.D., Aneskievich, B.J., and Haimovich, B. (2001). The cytoskeletal/non-muscle isoform of alpha-actinin is phosphorylated on its actin-binding domain by the focal adhesion kinase. *J Biol Chem* 276, 28676-28685.
- Jones, D.T. (1999). Protein secondary structure prediction based on position-specific scoring matrices. *J Mol Biol* 292, 195-202.
- Joseph, C., Stier, G., O'Brien, R., Politou, A.S., Atkinson, R.A., Bianco, A., Ladbury, J.E., Martin, S.R., and Pastore, A. (2001). A structural characterization of the interactions between titin Z-repeats and the alpha-actinin C-terminal domain. *Biochemistry* 40, 4957-4965.
- Kabsch, W. (1993). Automatic processing of rotation diffraction data from crystals of initially unknown symmetry and cell constants. *JApplCryst* 26, 795-800.
- Kaplan, J.M., Kim, S.H., North, K.N., Rennke, H., Correia, L.A., Tong, H.Q., Mathis, B.J., Rodriguez-Perez, J.C., Allen, P.G., Beggs, A.H., *et al.* (2000). Mutations in ACTN4, encoding alpha-actinin-4, cause familial focal segmental glomerulosclerosis. *Nat Genet* 24, 251-256.
- Keep, N.H., Winder, S.J., Moores, C.A., Walke, S., Norwood, F.L., and Kendrick-Jones, J. (1999). Crystal structure of the actin-binding region of utrophin reveals a head-to-tail dimer. *Structure* 7, 1539-1546.
- Kelly, S.M., and Price, N.C. (2000). The use of circular dichroism in the investigation of protein structure and function. *Curr Protein Pept Sci* 1, 349-384.
- Klein, M.G., Shi, W., Ramagopal, U., Tseng, Y., Wirtz, D., Kovar, D.R., Staiger, C.J., and Almo, S.C. (2004). Structure of the actin crosslinking core of fimbrin. *Structure* 12, 999-1013.
- Kliche, W., Fujita-Becker, S., Kollmar, M., Manstein, D.J., and Kull, F.J. (2001). Structure of a genetically engineered molecular motor. *Embo J* 20, 40-46.

- Kornau, H.C., Schenker, L.T., Kennedy, M.B., and Seeburg, P.H. (1995). Domain interaction between NMDA receptor subunits and the postsynaptic density protein PSD-95. *Science* *269*, 1737-1740.
- Kuhlman, P.A., Hemmings, L., and Critchley, D.R. (1992). The identification and characterisation of an actin-binding site in alpha-actinin by mutagenesis. *FEBS Lett* *304*, 201-206.
- Kusunoki, H., MacDonald, R.I., and Mondragon, A. (2004a). Structural insights into the stability and flexibility of unusual erythroid spectrin repeats. *Structure* *12*, 645-656.
- Kusunoki, H., Minasov, G., Macdonald, R.I., and Mondragon, A. (2004b). Independent movement, dimerization and stability of tandem repeats of chicken brain alpha-spectrin. *J Mol Biol* *344*, 495-511.
- Laemmli, U.K. (1970). Cleavage of structural proteins during the assembly of the head of bacteriophage T4. *Nature* *227*, 680-685.
- Lan, S., Wang, H., Jiang, H., Mao, H., Liu, X., Zhang, X., Hu, Y., Xiang, L., and Yuan, Z. (2003). Direct interaction between alpha-actinin and hepatitis C virus NS5B. *FEBS Lett* *554*, 289-294.
- Lebart, M.C., and Benyamin, Y. (2006). Calpain involvement in the remodeling of cytoskeletal anchorage complexes. *FEBS J* *273*, 3415-3426.
- Lee, S.H., Weins, A., Hayes, D.B., Pollak, M.R., and Dominguez, R. (2008). Crystal structure of the actin-binding domain of alpha-actinin-4 Lys255Glu mutant implicated in focal segmental glomerulosclerosis. *J Mol Biol* *376*, 317-324.
- Levine, B.A., Moir, A.J., Patchell, V.B., and Perry, S.V. (1990). The interaction of actin with dystrophin. *FEBS Lett* *263*, 159-162.
- Levine, B.A., Moir, A.J., Patchell, V.B., and Perry, S.V. (1992). Binding sites involved in the interaction of actin with the N-terminal region of dystrophin. *FEBS Lett* *298*, 44-48.
- Lewis, E.A., and Murphy, K.P. (2005). Isothermal titration calorimetry. *Methods Mol Biol* *305*, 1-16.
- Lewit-Bentley, A., and Rety, S. (2000). EF-hand calcium-binding proteins. *Curr Opin Struct Biol* *10*, 637-643.
- Liu, J., Taylor, D.W., and Taylor, K.A. (2004). A 3-D reconstruction of smooth muscle alpha-actinin by CryoEm reveals two different conformations at the actin-binding region. *J Mol Biol* *338*, 115-125.

- Liu, Y., and Eisenberg, D. (2002). 3D domain swapping: as domains continue to swap. *Protein Sci* *11*, 1285-1299.
- MacArthur, D.G., and North, K.N. (2004). A gene for speed? The evolution and function of alpha-actinin-3. *Bioessays* *26*, 786-795.
- Makrides, S.C. (1996). Strategies for achieving high-level expression of genes in *Escherichia coli*. *Microbiol Rev* *60*, 512-538.
- Maruyama, K. (1997). Connectin/titin, giant elastic protein of muscle. *Faseb J* *11*, 341-345.
- Masaki, T., Endo, M., and Ebashi, S. (1967). Localization of 6S component of a alpha-actinin at Z-band. *J Biochem* *62*, 630-632.
- Michie, K.A., and Lowe, J. (2006). Dynamic filaments of the bacterial cytoskeleton. *Annu Rev Biochem* *75*, 467-492.
- Mills, M., Yang, N., Weinberger, R., Vander Woude, D.L., Beggs, A.H., Eastal, S., and North, K. (2001). Differential expression of the actin-binding proteins, alpha-actinin-2 and -3, in different species: implications for the evolution of functional redundancy. *Hum Mol Genet* *10*, 1335-1346.
- Murshudov, G.N., Vagin, A.A., and Dodson, E.J. (1997). Refinement of Macromolecular Structures by the Maximum-Likelihood method. *Acta Cryst D* *53*, 240-255.
- Nakayama, S., and Kretsinger, R.H. (1994). Evolution of the EF-hand family of proteins. *Annu Rev Biophys Biomol Struct* *23*, 473-507.
- Nikolopoulos, S.N., Spengler, B.A., Kisselbach, K., Evans, A.E., Biedler, J.L., and Ross, R.A. (2000). The human non-muscle alpha-actinin protein encoded by the ACTN4 gene suppresses tumorigenicity of human neuroblastoma cells. *Oncogene* *19*, 380-386.
- Noegel, A., Witke, W., and Schleicher, M. (1987). Calcium-sensitive non-muscle alpha-actinin contains EF-hand structures and highly conserved regions. *FEBS Lett* *221*, 391-396.
- Norwood, F.L., Sutherland-Smith, A.J., Keep, N.H., and Kendrick-Jones, J. (2000). The structure of the N-terminal actin-binding domain of human dystrophin and how mutations in this domain may cause Duchenne or Becker muscular dystrophy. *Structure* *8*, 481-491.
- Ohtsuka, H., Yajima, H., Maruyama, K., and Kimura, S. (1997). Binding of the N-terminal 63 kDa portion of connectin/titin to alpha-actinin as revealed by the yeast two-hybrid system. *FEBS Lett* *401*, 65-67.

- Otey, C.A., and Carpen, O. (2004). Alpha-actinin revisited: a fresh look at an old player. *Cell Motil Cytoskeleton* *58*, 104-111.
- Otto, J.J. (1994). Actin-bundling proteins. *Curr Opin Cell Biol* *6*, 105-109.
- Pascual, J., Pfuhl, M., Walther, D., Saraste, M., and Nilges, M. (1997). Solution structure of the spectrin repeat: a left-handed antiparallel triple-helical coiled-coil. *J Mol Biol* *273*, 740-751.
- Pavalko, F.M., and Burridge, K. (1991). Disruption of the actin cytoskeleton after microinjection of proteolytic fragments of alpha-actinin. *J Cell Biol* *114*, 481-491.
- Petoukhov, M.V., and Svergun, D.I. (2005). Global rigid body modeling of macromolecular complexes against small-angle scattering data. *Biophys J* *89*, 1237-1250.
- Rossmann, M.G. (1990). The molecular replacement method. *Acta Cryst A* *46*, 73-82.
- Rossmann, M.G., and Blow, D.M. (1962). The detection of sub-units with the crystallographic asymmetric unit. *Acta Cryst* *15*, 24-31.
- Saido, T.C., Nagao, S., Shiramine, M., Tsukaguchi, M., Sorimachi, H., Murofushi, H., Tsuchiya, T., Ito, H., and Suzuki, K. (1992). Autolytic transition of mu-calpain upon activation as resolved by antibodies distinguishing between the pre- and post-autolysis forms. *J Biochem* *111*, 81-86.
- Sato, T., Irie, S., Kitada, S., and Reed, J.C. (1995). FAP-1: a protein tyrosine phosphatase that associates with Fas. *Science* *268*, 411-415.
- Sevcik, J., Urbanikova, L., Kost'an, J., Janda, L., and Wiche, G. (2004). Actin-binding domain of mouse plectin. Crystal structure and binding to vimentin. *Eur J Biochem* *271*, 1873-1884.
- Sheikh, F., Bang, M.L., Lange, S., and Chen, J. (2007). "Z"eroing in on the role of Cypher in striated muscle function, signaling, and human disease. *Trends Cardiovasc Med* *17*, 258-262.
- Sheterline, P., Clayton, J., and Sparrow, J. (1995). Actin. *Protein Profile* *2*, 1-103.
- Shieh, B.H., and Zhu, M.Y. (1996). Regulation of the TRP Ca²⁺ channel by INAD in *Drosophila* photoreceptors. *Neuron* *16*, 991-998.
- Shih, Y.L., and Rothfield, L. (2006). The bacterial cytoskeleton. *Microbiol Mol Biol Rev* *70*, 729-754.
- Sjoblom, B., Salmazo, A., and Djinovic-Carugo, K. (2008a). Alpha-actinin structure and regulation. *Cell Mol Life Sci* *65*, 2688-2701.

- Sjoblom, B., Ylanne, J., and Djinovic-Carugo, K. (2008b). Novel structural insights into F-actin-binding and novel functions of calponin homology domains. *Curr Opin Struct Biol* *18*, 702-708.
- Sorimachi, H., Freiburg, A., Kolmerer, B., Ishiura, S., Stier, G., Gregorio, C.C., Labeit, D., Linke, W.A., Suzuki, K., and Labeit, S. (1997). Tissue-specific expression and alpha-actinin binding properties of the Z-disc titin: implications for the nature of vertebrate Z-discs. *J Mol Biol* *270*, 688-695.
- Speicher, D.W., and Marchesi, V.T. (1984). Erythrocyte spectrin is comprised of many homologous triple helical segments. *Nature* *311*, 177-180.
- Sprague, C.R., Fraley, T.S., Jang, H.S., Lal, S., and Greenwood, J.A. (2008). Phosphoinositide binding to the substrate regulates susceptibility to proteolysis by calpain. *J Biol Chem*.
- Squire, J.M. (1997). Architecture and function in the muscle sarcomere. *Curr Opin Struct Biol* *7*, 247-257.
- Squire, J.M., Al-Khayat, H.A., Knupp, C., and Luther, P.K. (2005). Molecular architecture in muscle contractile assemblies. *Adv Protein Chem* *71*, 17-87.
- Stout, A.L., Wang, J., Sanger, J.M., and Sanger, J.W. (2008). Tracking changes in Z-band organization during myofibrillogenesis with FRET imaging. *Cell Motil Cytoskeleton* *65*, 353-367.
- Svergun, D.I. (1992). Determination of the regularization parameter in indirect-transform methods using perceptual criteria. *J Appl Cryst* *25*, 495-503.
- Svergun, D.I. (1999). Restoring low resolution structure of biological macromolecules from solution scattering using simulated annealing. *Biophys J* *76*, 2879-2886.
- Tang, J., Taylor, D.W., and Taylor, K.A. (2001). The three-dimensional structure of alpha-actinin obtained by cryoelectron microscopy suggests a model for Ca(2+)-dependent actin binding. *J Mol Biol* *310*, 845-858.
- Thomas, C.C., Deak, M., Alessi, D.R., and van Aalten, D.M. (2002). High-resolution structure of the pleckstrin homology domain of protein kinase b/akt bound to phosphatidylinositol (3,4,5)-trisphosphate. *Curr Biol* *12*, 1256-1262.
- Thomas, G.H., Newbern, E.C., Korte, C.C., Bales, M.A., Muse, S.V., Clark, A.G., and Kiehart, D.P. (1997). Intragenic duplication and divergence in the spectrin superfamily of proteins. *Mol Biol Evol* *14*, 1285-1295.
- Trave, G., Pastore, A., Hyvonen, M., and Saraste, M. (1995). The C-terminal domain of alpha-spectrin is structurally related to calmodulin. *Eur J Biochem* *227*, 35-42.

- Trinick, J. (1996). Titin as a scaffold and spring. *Cytoskeleton. Curr Biol* 6, 258-260.
- Vagin, A., and Teplyakov, A. (1997). MOLREP: an Automated Program for Molecular Replacement. *J Appl Cryst* 30, 1022-1025.
- Vetting, M.W., Hegde, S.S., and Blanchard, J.S. (2009). Crystallization of a pentapeptide-repeat protein by reductive cyclic pentylation of free amines with glutaraldehyde. *Acta Crystallogr D Biol Crystallogr* 65, 462-469.
- Viel, A. (1999). Alpha-actinin and spectrin structures: an unfolding family story. *FEBS Lett* 460, 391-394.
- Virel, A., Addario, B., and Backman, L. (2007). Characterization of *Entamoeba histolytica* alpha-actinin2. *Mol Biochem Parasitol* 154, 82-89.
- Virel, A., and Backman, L. (2004). Molecular evolution and structure of alpha-actinin. *Mol Biol Evol* 21, 1024-1031.
- Virel, A., and Backman, L. (2006). Characterization of *Entamoeba histolytica* alpha-actinin. *Mol Biochem Parasitol* 145, 11-17.
- Virel, A., and Backman, L. (2007). A comparative and phylogenetic analysis of the alpha-actinin rod domain. *Mol Biol Evol* 24, 2254-2265.
- Walter, T.S., Meier, C., Assenberg, R., Au, K.F., Ren, J., Verma, A., Nettleship, J.E., Owens, R.J., Stuart, D.I., and Grimes, J.M. (2006). Lysine methylation as a routine rescue strategy for protein crystallization. *Structure* 14, 1617-1622.
- Wang, J., Shaner, N., Mittal, B., Zhou, Q., Chen, J., Sanger, J.M., and Sanger, J.W. (2005). Dynamics of Z-band based proteins in developing skeletal muscle cells. *Cell Motil Cytoskeleton* 61, 34-48.
- Way, M., Pope, B., and Weeds, A.G. (1992). Evidence for functional homology in the F-actin binding domains of gelsolin and alpha-actinin: implications for the requirements of severing and capping. *J Cell Biol* 119, 835-842.
- Winder, S.J. (1997). The membrane-cytoskeleton interface: the role of dystrophin and utrophin. *J Muscle Res Cell Motil* 18, 617-629.
- Winder, S.J., Hemmings, L., Maciver, S.K., Bolton, S.J., Tinsley, J.M., Davies, K.E., Critchley, D.R., and Kendrick-Jones, J. (1995). Utrophin actin binding domain: analysis of actin binding and cellular targeting. *J Cell Sci* 108 (Pt 1), 63-71.
- Winkelmann, J.C., and Forget, B.G. (1993). Erythroid and nonerythroid spectrins. *Blood* 81, 3173-3185.

- Witke, W., Hofmann, A., Koppel, B., Schleicher, M., and Noegel, A.A. (1993). The Ca(2+)-binding domains in non-muscle type alpha-actinin: biochemical and genetic analysis. *J Cell Biol* 121, 599-606.
- Wu, J.Q., Bahler, J., and Pringle, J.R. (2001). Roles of a fimbrin and an alpha-actinin-like protein in fission yeast cell polarization and cytokinesis. *Mol Biol Cell* 12, 1061-1077.
- Xia, H., Winokur, S.T., Kuo, W.L., Altherr, M.R., and Bredt, D.S. (1997). Actinin-associated LIM protein: identification of a domain interaction between PDZ and spectrin-like repeat motifs. *J Cell Biol* 139, 507-515.
- Xu, J., Wirtz, D., and Pollard, T.D. (1998). Dynamic cross-linking by alpha-actinin determines the mechanical properties of actin filament networks. *J Biol Chem* 273, 9570-9576.
- Yan, Y., Winograd, E., Viel, A., Cronin, T., Harrison, S.C., and Branton, D. (1993). Crystal structure of the repetitive segments of spectrin. *Science* 262, 2027-2030.
- Ylanne, J., Scheffzek, K., Young, P., and Saraste, M. (2001a). Crystal structure of the alpha-actinin rod reveals an extensive torsional twist. *Structure* 9, 597-604.
- Ylanne, J., Scheffzek, K., Young, P., and Saraste, M. (2001b). Crystal Structure of the alpha-Actinin Rod: Four Spectrin Repeats Forming a Thight Dimer. *Cell Mol Biol Lett* 6, 234.
- Young, P., Ferguson, C., Banuelos, S., and Gautel, M. (1998). Molecular structure of the sarcomeric Z-disk: two types of titin interactions lead to an asymmetrical sorting of alpha-actinin. *Embo J* 17, 1614-1624.
- Young, P., and Gautel, M. (2000). The interaction of titin and alpha-actinin is controlled by a phospholipid-regulated intramolecular pseudoligand mechanism. *Embo J* 19, 6331-6340.
- Zamir, E., and Geiger, B. (2001). Molecular complexity and dynamics of cell-matrix adhesions. *J Cell Sci* 114, 3583-3590.
- Zhou, Q., Chu, P.H., Huang, C., Cheng, C.F., Martone, M.E., Knoll, G., Shelton, G.D., Evans, S., and Chen, J. (2001). Ablation of Cypher, a PDZ-LIM domain Z-line protein, causes a severe form of congenital myopathy. *J Cell Biol* 155, 605-612.

CURRICULUM VITAE

PERSONAL PROFILE

Name: Testa Salmazo
First Name: Anita Paula
Date of birth: 2nd Sep 1977
Nationality: Brazilian
Marital status: married to Roberto Lacerda de Orio
Children: not yet

EDUCATION

- 05/2005:** PhD position at Max Perutz F. Laboratories, University of Vienna, Austria.
Subject: Structural and functional studies of α -actinin.
Supervisor: Dr. Kristina Djinović-Carugo.
Techniques: PCR; cloning; directed-site mutagenesis; prokaryotic protein expression; affinity, ionic and size exclusion chromatography; differential scanning fluorimetry (DSF); dynamic light scattering (DLS); isothermal titration calorimetry (ITC); protein reductive methylation; surface reduction entropy mutations; protein crystallization; X-ray crystallography and molecular replacement (MR).
- 09/2004 – 04/2005:** Trainee at the EMBL Hamburg Outstation in the group of Dr. Matthias Wilmanns.
Subject: Structural studies on HDAC-6.
Supervisor: Dr. Inari Kursula.
Techniques: PCR; cloning, prokaryotic and eukaryotic protein expression; affinity and size exclusion chromatography; protein crystallization; X-ray crystallography; molecular replacement (MR).
- 03/2002 – 07/2004:** Master's degree at the Brazilian National Synchrotron Radiation Laboratory (LNLS) in Campinas, São Paulo, Brazil.
Subject: Studies on structure and function of proteins from the bacterium *Xylella fastidiosa*, involved in pathogenicity and adaptation.
Supervisor: Dr. Francisco Javier Medrano Martín.
Techniques: PCR; cloning; DNA sequencing; prokaryotic protein expression; affinity chromatography; circular dichroism spectroscopy (CD) and protein modelling.
- 01/2000 – 02/2002:** Junior Research in Molecular Biology at the State University of Campinas (UNICAMP), Campinas, São Paulo, Brazil.
Subject: Cloning and Characterization of the gene *SWI3* from the yeast *Hansenula polymorpha* and the study of its influence in the transcription of the *MOX* gene".
Supervisor: Dr. Goncalo A.G. Pereira.
Techniques: PCR; DNA sequencing; homology recombination and viability assays.
- 02/1998 – 12/2001:** Biologist graduated at Catholic University of Campinas, Brazil.

COURSES ATTENDED

10/2006: BioCrys 2006 course on the "Fundamentals of Modern Methods in Biocrystallography" which took place in Oeiras, Portugal.

05/2006: EMBO practical course on the "Structural Characterization of Macromolecular Complexes" which took place in Grenoble, France.

SCIENTIFIC MEETINGS

09/2008: 11th Heart of Europe Bio-Crystallography meeting, Greifswald, Germany.

08/2008: XXI Congress of the International Union of Crystallography (IUCr 2008), Osaka, Japan. Poster: "**Crystallization and SAXS studies of α -actinin 2**"

01/2007: Vienna Workshop on muscle cytoskeleton, Vienna, Austria. Talk: "**Towards understanding the molecular architecture of α -actinin**".

09/2006: 9th Heart of Europe Bio-Crystallography meeting, Teistungenburg, Germany. Talk: "**Structural base for α -actinin regulation**".

06/2006: Workshop on the definition of protein domains and their likelihood of crystallization, Vienna, Austria.

03/2006: Winter School on Soft X-Rays in Macromolecular, Seefeld, Austria.

09/2005: 8th Heart of Europe Bio-Crystallography meeting, Karlovy Vary, Czech Republic.

09/2004: International conference at EMBL-Hamburg entitled: Structural Biology at Crossroads: from biological molecules to biological systems.

05/2004: XXXIII SBBq – Annual meeting of Biochemistry and Molecular Biology Brazilian Society. Poster: "**Expression, purification and modelling of *Xylella fastidiosa* response regulator (PhoP) protein**"

PUBLICATIONS

Björn Sjöblom, Anita Salmazo, Kristina Djinović-Carugo (2008). " **α -actinin structure and regulation**". *Cellular and Molecular Life Sciences* 65, 2688 - 2701.

ADDITIONAL INFORMATION

Languages:

Portuguese – mother tongue
English – fluent
German – intermediate level